A STUDY OF THE SOLUBILITY AND SEPARATION OF ALKANETHIOL STABILIZED GOLD NANOPARTICLES IN SUPERCRITICAL FLUIDS

Thesis submitted in accordance with the requirements of the University of Liverpool for the degree of Doctor in Philosophy

by

Dylan Powell Williams

February 2008

ABSTRACT

This thesis is a record of a series of studies into the solubility of alkanethiol stabilized gold nanoparticles of various sizes in supercritical ethane at a range of pressures. In order to perform this study it was first necessary to discover a simple synthetic technique for the preparation of gold nanoparticles that disperse easily in supercritical ethane. In order to do this a number of different stabilizing ligands were tested, it was found that dodecanethiol stabilised gold nanoparticles purified by Soxhlet extraction were most suitable due to compatibility with the fluid (supercritical ethane) and the excellent stability of these nanoparticles.

The dodecanethiol stabilized gold nanoparticles prepared for the first part of the study were found to be rather polydisperse from TEM measurements. It was shown that selectively dissolving certain sizes in supercritical ethane (by variation of fluid pressure) resulted in the isolation of small quantities of more monodisperse size fractions from the sample. Further study of this technique is required for a more accurate 'fractionation' process.

Monodisperse dodecanethiol stabilised gold nanoparticles were prepared by synthesising gold nanoparticles functionalized by a thioether terminated polymer followed by a simple ligand exchange reaction with dodecanethiol. Some of these samples were then used in simple solubility tests in supercritical ethane. A quantitative consideration of the solubility behaviour of these particles shows that they behave in a similar manner to other solids in supercritical fluids at low mole fractions. The calculation of accurate theoretical Henry's Law constants for the nanoparticles was impossible; this is believed to be due to differences between the solubility behaviour of nanoparticles dissolved in supercritical fluids and the solubility behaviour of gases dissolved in fluids. The pressure dependent solubility of gold nanoparticles in the 2-4 nm size range was found to be in the region of $3.5\text{-}5 \times 10^{-18}$ mol.bar^{-1}.

CONTENTS

ACKNOWLEDGMENTS

I would like to thank all members of the University of Liverpool Centre or Nanoscale Science, especially Dr. John Satherley and Professor Mathias Brust for all of their support and guidance. I would also like to thank all of the technical staff at the university, particularly Miss Cornelia Muncke at the Liverpool Electron Micsoscopy Unit and Mr. Alan Mills at the Department of Chemistry.

Without the support of my friends and family none of the work that went into the research in this project and the writing of this thesis would have been possible. I would also like to thank all members of the Cooper group – past and present – for their support and friendship.

Finally, I would like to thank all the staff at the University of Leicester Departments of Chemistry and Physics & Astronomy who have made my transition from research to teaching (as well as from the North West to the East Midlands) a smooth one.

GLOSSARY

This is a glossary of the units, terms, symbols and contractions used in this thesis.

EXPERIMENTAL TECHNIQUES

TEM	Transmission Electron Microscopy
DLS	Dynamic Light Scattering
MALDI-TOF	Matrix Assisted Lased Desorption/Ionization – Time of Flight Mass Spectrometry
TOF	Time of Flight
MS	Mass Spectrometry
UV-Vis.	Ultraviolet-Visible
HPLC	High Performance Liquid Chromatography

UNITS AND SYMBOLS

nm	Nanometre
meV	Millielectron-Volts
K	Kelvin
T	Temperature
bar	bar (Pressure unit)
Pa	Pascal (Pressure unit)
E_f	Fermi Energy
n	Number of Valence Electrons
δ	Kubo gap energy
k	Boltzmann constant
SC	Supercritical
T_C	Critical Temperature
P_C	Critical Pressure
C	Critical Point
ρ	Number density of a fluid
N	Number of moles of fluid molecules
V	Volume of fluid
r	Radius of cavity produced by a solute in a fluid
W	Reversible work needed to produce a cavity of radius r
$\rho_0(r,\rho)$	Probability of such a cavity existing
σ_1	Hard sphere solvent diameter
σ_2	Hard sphere solute diameter

W	Interaction energy between molecules
D	Separation between particles
$V_S\ V_A\ V_R\ V_T$	Potential energy due to: $_S$ – Solvent, $_A$ – Attractive Forces and $_R$ – Repulsive Forces. V_T is the total potential energy
A	Hamaker constant.
ξ	Zeta potential
κ	A function of the ionic composition (DLVO)
Π	Solvent permeability (DLVO)
ε	Dielectric constant
DLVO	Derjaguin, Landau, Verwey and Overbeek (Theory)
MPEG	Methoxypolyethylene Glycol
m/z	Mass to charge ratio
mM	Milli molar
k_B	Boltzmann Constant
C_s	Cunningham Correction Factor
η	Solvent Viscosity
α_S	Polarizability of a spherical particle
R	Radius of a spherical nanoparticle
D	Average core diameter of a metal nanoparticle established from TEM.
N	The average number of gold atoms per nanoparticle (Extinction coefficient calculation).
N_A	Avagadro's Number
V	Volume of reaction solution
ε	Molar extinction coefficient (Units = $M^{-1}cm^{-1}$)

POLYMERS & ALKANETHIOLS

PVDF	Poly(vinylidene fluoride)
POEM	Poly(oxyethylene methacrylate)
PMAA	Poly(methacrylic acid)
PAA	Poly(acrylic acid)
PTMP	Pentaerythritol tetramercaptopropionate
DDT	Dodecanethiol

Chapter One

Introduction

Chapter 1 Introduction

1.1 Aims of the Project

Although synthetic techniques which allow the preparation of alkanethiol stabilized metal nanoparticles exist [1-4], there is a large variation in the degrees of polydispersity present in nanoparticles prepared by these various processes. In order to make use of the unique electronic and optical properties [5-18] of these nanoparticles in potential applications a high degree of monodispersity and size control is essential. This concern is of particular relevance to this project.

One of the aims of this study was to determine solubility data for samples of alkanethiol stabilized gold nanoparticles in supercritical ethane and the effect of modifying the functionalities and core diameters on these solubilities. In order to achieve this aim another study would have to be conducted into the suitability of different samples of gold nanoparticles (prepared by a variety of technique and with a range of different functionalities) in supercritical ethane. This part of the project involved some fundamental synthetic research into gold nanoparticle synthesis as well as a study into the effect of using a new purification technique on the solubility of gold nanoparticles in supercritical fluids.

Further aims were developed during the course of the project; these included an analysis of the separation of samples of polydisperse gold nanoparticles in supercritical ethane as well as a study into novel synthetic procedures used to obtain highly monodisperse samples of metal nanoparticles. This work followed on from an earlier project in which supercritical fluids were used to separate a bimodal mixture of two different size samples of gold nanoparticles [19]. This study aimed to show that a similar technique could be used in separations of nanoparticles much closer in size (ie. the individual size fractions from a polydisperse sample of gold nanoparticles with an initial polydispersity under ± 3 nm). The use

of polymer stabilizing ligands in the synthesis of a range of different metal nanoparticles was investigated and the effects of the polymer on the polydispersity of samples recorded.

The analysis of the synthesis of metal nanoparticles and the separation and solubility studies of these particles made use of several common analytical techniques such as UV-Visible absorption spectroscopy and Transmission Electron Microscopy (TEM). Several less common techniques were also used including Dynamic Light Scattering (DLS) and Matrix Assisted Laser Desorption Ionization Time of Flight (MALDI-TOF) Mass Spectrometry. All analysis was performed by myself apart from Mass Spectrometry

1.2 Historical Background

The study of metal nanoparticles is a common subject to anyone familiar with today's leading materials, inorganic and physical chemistry journals. For reasons that will be discussed shortly, many of the most important breakthroughs in the field have been made in the last twenty years, but the earliest recorded evidence of the identification and application of colloidal gold date back to Ancient Roman, Egyptian and Chinese societies [20] (The 5^{th} century Roman Lycurgus Chalice is possibly the oldest object containing nanoparticles, see Figure 1). Initially the main application of these colloidal solutions was in colouring glass [21] and ceramics. There were few advances in the field until the nineteenth century when Faraday reported [22] the synthesis of red solutions of colloidal gold by the reduction of tetrachloroaurate. Faraday also demonstrated the variation of the optical properties of these solutions depending on the size of the particles present. The optical properties were explained in more detail by Mie when he solved Maxwell's equations for the absorption and scattering of electromagnetic radiation by spherical metal particles [23].

Figure 1. The Lycurgus chalice. On the left the chalice appears green; however, when illuminated from within (the image on the right), it appears red due to the plasmon band absorption in the visible region of the electromagnetic spectrum [24].

Major developments in the field were inhibited by the inherent instability of metal nanoparticles in colloidal solutions prepared by pre-20th century synthetic techniques. The synthesis of ligand stabilized gold nanoparticles was described by Turkevich [1] (and later developed by Frens [2]) in the mid-twentieth century. Turkevich demonstrated the reduction of gold (III) ions in aqueous solution by reflux in a solution of sodium citrate. The resulting nanoparticles were stabilized by a loosely bound layer of citrate ligands and were therefore hydrophilic. This technique remains a popular way of producing nanoparticles of 10 nm and above, partly due to its versatility. The average core diameter of the nanoparticles produced may be controlled, to an extent, by modifying the ratio of gold to reducing agent. The technique may also be modified by co-functionalizing the particles with another stabilizing ligand during the reduction step. This was

a landmark in the development of metal nanoparticles as this process yielded stable metal nanoparticles which could be studied under laboratory conditions.

In the late twentieth century several publications [4, 25, 26] detailed synthetic techniques which led to the preparation of ligand stabilized metal nanoparticles in the size range 1-10 nm. This size range is of particular interest to contemporary research as it is at these sizes that metal clusters exhibit unique electronic properties between those of bulk materials and those of individual molecules. In 1981 Schmid *et al.* [3] reported the formation of a stable phosphine functionalized gold cluster with an average core diameter well below 2 nm. In the early 1990's a series of papers led to the development of a simple, controllable technique to produce stable gold clusters in the size range of 1-10 nm. The two-phase reduction of aqueous hydrogen tetrachloroaurate by sodium borohydride (using tetraoctylammoniumhalide as a phase transfer agent) allows the addition of a wide range of alkanethiols to the gold cluster resulting in the formation of hydrophobic gold nanoparticles. The strong nature of the Au-S bond means particles of this type are very stable; they can be stored in non-polar solvents as well as in their solid state without aggregation [4].

Since then the two-phase synthesis has become established as the main route for preparing small nanoparticles, a number of modifications to the technique have arisen [25-27]. It was soon discovered that increasing the thiol:gold ratio led to the formation of nanoparticles with a smaller average core diameter. Introducing the reducing agent quickly, quenching the reaction mixture and using sterically bulky ligands have been shown to lead to the production of smaller and more monodisperse nanoparticles [27-31]. Another interesting modification is the use of polymer groups to modify the particles. Solutions of hydrogen tetrachloroaurate mixed together with dodecanethiol terminated polymethacrylic acid have been reduced by sodium borohydride to produce polymer stabilized nanoparticles [32, 33]. These particles can be further modified by reaction

with an ethanolic solution of dodecanethiol which leads to ligand exchange with the alkanethiol. The most interesting feature of this synthesis is the highly monodisperse nature of these nanoparticles. Another very useful feature is the ability to control the average core diameter of the produced particles by varying the concentration of the polymer added at the first stage of the synthesis. The alkanethiol stabilized nanoparticles may be further modified by simple ligand place-exchange reactions which change the nature of the stabilizing ligands allowing modifications to some of the nanoparticle's physical properties (such as solubility, hydrophobicity/hydrophilicity, reactivity, etc.) [34, 35].

1.3 Electronic Structure and Properties

The electronic properties of metal nanoparticles can differ greatly from those of the bulk metal [8, 14, 17, 18, 36]. Nanoparticles can exhibit electronic behaviour of zero-dimensional quantum dots when the de Broglie wavelength of valence electrons is similar to the dimensions of the nanoparticle itself. This behaviour results in the existence of an energy gap between the valence and conduction bands of metal nanoparticles which does not exist in the bulk form. This gap produces a size dependent metal-insulator transition. Quantization of the electrons into discrete energy levels occurs below 20 nm and leads to a number of unique properties [37, 38].

The electronic properties of metal nanoparticles are heavily dependent on their size. In small particles, the electronic states exist as a series of discrete states rather than a continuous band as a consequence of the confinement of the electron wavefunction. The average spacing between these states is known as the Kubo gap (δ) and is given by equation 1 [39]:

$$\delta = 4E_f/3n \qquad \textbf{(1)}$$

In equation 1 E_f represents the Fermi energy of the bulk metal and n is the number of valence electrons in the nanoparticle (usually taken as its nuclearity). If we consider a silver nanoparticle with a diameter of 3 nm containing ~10^3 atoms, the value of δ would be 5-10 meV. At room temperature kT = 25 meV, therefore, the nanoparticle, in this case, would behave as a metal (the thermal energy of the electrons is greater than the Kubo gap). At low temperatures the energy level spacings (especially for small nanoparticles) become close to kT, and the particles would become non-metallic. The Kubo gap results in quantum size effects for many properties, including electrical conductivity and magnetic susceptibility. The discrete nature of the energy levels can influence spectral features, particularly those related to the valence band.

One of the most identifiable properties of solutions of gold nanoparticles are their colourful solutions [22, 37, 40], these colours are absent from solutions of the bulk forms of the same materials and also from individual atoms. The characteristic red colour of solutions of gold nanoparticles occurs as a consequence of the surface plasmon band of particles of certain sizes. This occurs due to the confinement of the electron gas within these small particles and results in the collective oscillation of the free conduction electrons when induced by an interacting electromagnetic field (Ultraviolet and Visible light in this case) [40].

The surface plasmon resonance does not occur in the bulk form of the metal or in nanoparticles of core diameter below around 2 nm (solutions of these nanoparticles appear brown, see Figure 2). The reason for this lack of plasmon resonance in small nanoparticles is the increasing importance of quantum size effects in small particles [41, 42]. The Plasmon band appears as a broad band at a wavelength of around 520 nm in water which allows the use of UV-visible absorption spectroscopy in the detection of the wavelength of this band and therefore the nature of the nanoparticles. The band appears at progressively higher wavelengths as the core diameter of the nanoparticle increases. The nature of the surface

Plasmon band can also be affected by the refractive index of the solvent and the nature of the interaction between the gold atoms and the stabilizing ligands.

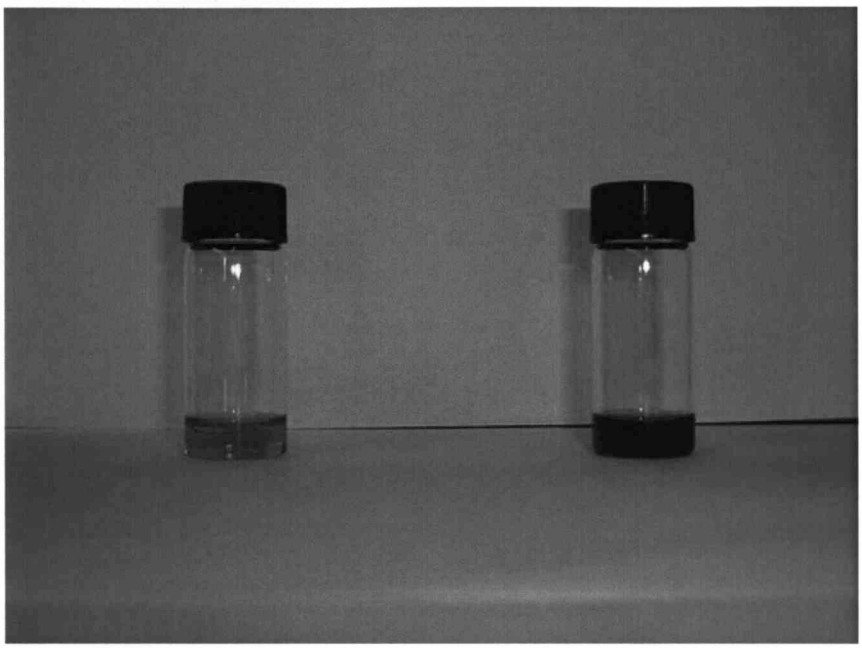

Figure 2. An image illustrating the difference in plasmon band absorption for gold nanoparticles in the size range 1-10 nm. The sample of particles on the left exhibits a plasmon band resonance which manifests itself in a pink-red colour solution. The sample on the right contains smaller nanoparticles in which the electronic structure can no longer be described as a continuous 'band', therefore, plasmon absorption does not occur for this sample.

Gold nanoparticles form stable structural arrangements, the number of atoms present in these structures often adhering to a 'magic number' of core atoms. It has been observed that structures containing these numbers of atoms exhibit enhanced stability (Figure 3). It has been proposed that this process occurs during the growth stage of the cluster, when the cluster reaches a magic number size the structure gains additional thermodynamic stability due to the fact that each surface metal atom has the maximum

number of metal-metal bonds. This additional stability results in the particles growing more slowly whereas non magic number nanoparticles will continue to grow.

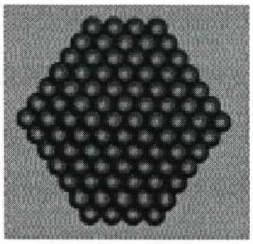

Figure 3. A 'magic number' gold nanoparticle consisting of a truncated octahedral array of gold atoms [43].

1.4 Closing Remarks

Metal nanoparticles in the size range 1 – 100 nm have a range of unique physical properties which make them ideal subjects for further study. The development of techniques used to stabilize these nanoparticles has led to increased study of applications of these nanoparticles in research various research areas, bio-sciences and electronics in particular (applications will be discussed in more detail in the following chapter) [17, 44-47].

One of the main issues concerning the development of applications based upon metal nanoparticles is the necessity to perfect preparative techniques in order to obtain highly monodisperse (i.e. samples with a homogenous core size) samples of nanoparticles. This study attempts to address this problem and investigate other associated synthetic issues.

Chapter Two

The Preparation of Monodisperse Gold Nanoparticles: From Separation To Synthesis

Chapter 2 The Preparation of Monodisperse Gold Nanoparticles: From Separation to Synthesis

2.1.1 Introduction

The following chapter includes a review of several of the techniques used to obtain monodisperse samples of metal nanoparticles as well as a discussion of the role of stabilizing ligands in metal nanoparticles. This chapter also presents an introduction to the mathematical model used for the determination of the solubility of small particles which will be used to a greater extent in later chapters.

2.1.2 Separation Techniques

Although many synthetic approaches result in good degrees of monodispersity (see Chapter 2.2), a deviation from the average core diameter remains with most techniques. One of the most commonly employed techniques to obtain monodisperse samples therefore is the fractionation of samples with some degree of polydispersity. This sub-chapter aims to provide a short review of some of the more useful separation techniques.

One of the earliest published examples of effective fractionation of polydisperse samples of metal nanoparticles was published by Whetten *et. al.* [125]. In this publication the fractional crystallisation of samples from solution was performed by the addition of varying concentrations of an anti-solvent (acetone in this case), each step was monitored by mass spectrometry. It was found that at the lowest concentrations of acetone only the largest size fractions precipitated. This was due to the fact that the attractive interaction between these particles is greater than it is for smaller particles so they require a greater degree of solubilisation.

One of the most promising new separation techniques involves the use of CO_2 gas expanded liquids to obtain several fractions of well defined core diameters from a polydisperse sample of alkanethiol stabilized nanoparticles. McLeod *et. al.* [48] demonstrated a simple technique which effectively separated such a sample using a novel piece of glassware (Figure. 4).

It has been observed that by expanding CO_2 pressurized over a liquid solvent causes an expansion of the liquid. The pressure of the gas controls the fraction of liquid CO_2 and this produces the gas expanded liquid. This allows the solubility of the expanded liquid to be varied between that of the original liquid and that of pure liquid CO_2. By increasing the pressure of CO_2 the solvent strength is progressively decreased and at a certain point will drop below the minimum point which allows the stabilization of particles of a certain size so particles of that core diameter will precipitate out of solution above that pressure.

In order to precipitate different fractions from the same sample a unique piece of glassware was placed into a high pressure vessel. This apparatus was an open ended glass vial which incorporated a spiral channel running through the length of the vial (similar to a corkscrew, Figure 4). The polydisperse sample was placed in the first groove and the system pressurized to the point which allowed precipitation of the first fraction of nanoparticles. After this had been achieved the vial was rotated which allowed the still dissolved nanoparticles to pass into the next groove. At this point the pressure of CO_2 was increased to a certain point which resulted in the precipitation of the next fraction. This procedure was repeated for all grooves until each contained a different size fraction, each one of progressively smaller core diameter. The larger particles precipitated out of solution first as due to the decreased solvent-ligand interactions which are weakest for larger nanoparticles. The precipitated samples were then analysed by TEM and UV-visible absorption spectroscopy.

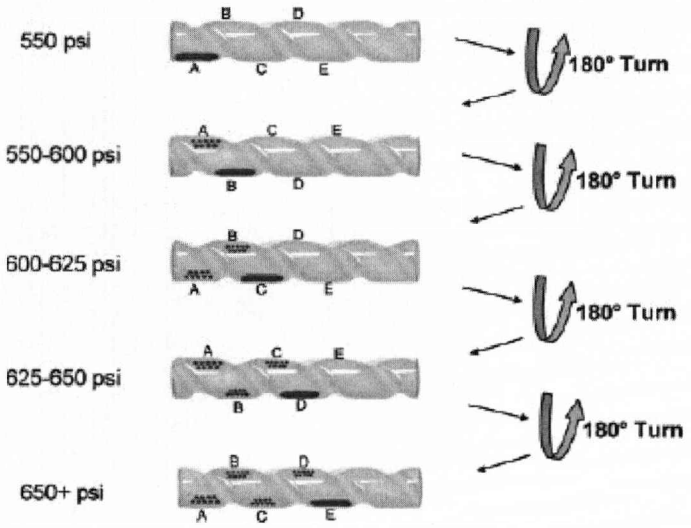

Figure 4 (previous page). Diagrammatic representation of the spiral precipitation apparatus used by McLeod *et. al.* during their study into the separation of a polydisperse sample of metal nanoparticles by precipitation in CO_2 expanded solvent at a range of pressures [48].

The gas-expanded liquid technique has many advantages, of which the simplicity of the system remains one of the most important. Each of the fractions can be precipitated in a single experimental run unlike most of the preceding experimental set-ups [19, 49]. Relatively low pressures (550-600 psi) are needed to allow the precipitation of alkanethiol stabilized nanoparticles, this is due to the fact that alkanethiol stabilized particles are so insoluble in CO_2 in both its liquid and gaseous states. There are also environmental advantages to this technique. The use of CO_2 eliminates the need for organic solvents for separations which are difficult to dispose of. It is possible that further study of this technique could lead to a refinement of the monodispersity of the nanoparticles obtained by each precipitation as a small degree of polydispersity is observed in the analysis of the TEM images of these fractions. Another interesting observation of this study was the finding that dodecanethiol stabilized gold nanoparticles are most suitable to this type of size-selective fractionation.

Another recently reported separation technique involved the synthesis of DNA functionalized gold nanoparticles and the size-dependent melting temperature of these particles. Mirkin *et al.* [50] presented a technique for the separation of DNA modified particles. Gold nanoparticles were functionalized by 5'-thiol-functionalized oligonucleotides under buffered conditions. Two samples of nanoparticles of the same size were modified by two different sequences of DNA. These samples were then combined and heated for ten minutes to allow hybridization. Melting analysis of these colloids was performed by following the change of extinction in the UV-visible absorption spectrum at 260 nm every 0.2 °C at a rate of 1 °C min^{-1}. The melting temperatures were derived from the maximum of the first derivative of the melting transition.

The above procedure was then used to separate binary and ternary mixtures of different size nanoparticles. The testing of the melting temperatures of the single component samples showed that the melting temperature increases significantly with increasing particle size. As the difference between the melting temperature for different size nanoparticles was significant, the separation of particles from mixtures was also achieved when the mixture was heated to a temperature between the melting temperatures of the two components. The smaller nanoparticles would melt and at the end of the experiment would only be found dispersed in the supernatant whereas aggregates of the larger nanoparticles were still detected.

Another unique technique used to separate gold nanoparticles by size involves the use of diafiltration. Hutchison *et. al.* [51] demonstrated a technique for the size selective separation of water soluble, thiol stabilized gold nanoparticles. The purification of water soluble particles is particularly difficult due to the similar solubility behaviour of nanoparticles across a range of sizes.

Initially two samples of water soluble, thiol stabilized gold nanoparticles were prepared and purified by a number of techniques. When

investigating the effect of purifying these nanoparticles using a 70 kDa diafiltration membrane it was found that those particles which passed through the membrane displayed a much higher degree of monodispersity than the initial sample when studied by TEM. In order to test this technique a bimodal mixture of nanoparticles with different average core sizes was passed through a membrane. Comparisons of the UV-visible absorption spectra of the permeate and retentate fractions along with those of the components of the mixture and that of the mixture itself were made. It was clearly seen from this comparison that the two components had been effectively separated during diafiltration, this result was confirmed by TEM.

As a follow up the fractionation of a polydisperse sample of gold nanoparticles using this technique was attempted. The aim of the attempt was to reduce the range of average core diameters present in samples prepared by standard synthetic techniques. The process was achieved by diafiltration through a 70 nm membrane to remove the largest fraction of nanoparticles. Successive diafiltrations using progressively smaller pore size membranes allowed the isolation of smaller core size particles. A variation of colours in the fractions was observed which was a clear indication of the effective fractionation of the polydisperse sample. This result has been verified by recording the UV-visible absorption spectra of each fraction and by analysing TEM images of all fractions. It has been shown that the average core diameter of the particles separated from the sample does decrease as the process progresses and successive diafiltration cycles have been achieved.

This study has shown that diafiltration is capable of separating gold nanoparticles but in order to improve this technique better membranes must be developed which allow a greater selectivity during the successive diafiltration cycles which, therefore result in more monodisperse fractions.

A technique similar to diafiltration has been demonstrated by Mayes et. al. [52] Membrane Filtration was used to isolate desired size

fractions from sample of simple alkanethiol stabilized gold nanoparticles. The size dependent diffusivity of several sample of gold nanoparticles through nanofiltration membranes (consisting of a self-assembling graft copolymer with a hydrophilic poly(vinylidene fluoride) (PVDF) backbone and hydrophilic poly(oxyethylene methacrylate) (POEM) side chains) which create nanosize channels (due to the formation of a bicontinuous structure with uniformly sized nanoscale channels of poly(ethylene oxide) created by the phase separation of the backbone and side chain). As a result of this structure, only nanoparticles up to a certain 'cutoff' size can pass through the membrane. Larger nanoparticles are not able to pass through the membrane and do not appear in the solution which permeates through the membrane. The separation process was tuned by using different alkanethiol ligand chain lengths, different solvents and varying the time allowed for the solution to permeate through the membrane. This technique allows the isolation of a fraction of a sample of gold nanoparticles up to a certain size but no discussion of recovery of the fraction of larger nanoparticles (i.e. those with a larger core diameter than the channel) was made, presumably these nanoparticles could be recovered once all of the smaller fractions had been filtered off. Additionally there is no discussion of varying the channel size to allow different fractions to pass through the membrane for a single sample of nanoparticles; a simple chemical modification to the membrane would be desirable as this would allow a continuous isolation of different fractions from the same sample.

Chromatography has also been used to separate polydisperse nanoparticles, HPLC [53, 54] and size exclusion chromatography [55, 56] have been used to this end. This is a basic summary of some of the more useful, recently developed separation techniques. The next sub-chapter reviews the preparation of near monodisperse samples of metal nanoparticles by manipulation of synthesis conditions.

2.1.3 Synthetic Techniques

The techniques commonly used to synthesize stable metal nanoparticles result in products with varying degrees of monodispersity. This sub-chapter looks at ways of modifying these basic techniques in order to control the monodispersity of products.

One of the most effective synthetic techniques used to prepare near-monodisperse metal nanoparticles is the reduction of a gold salt in the presence of a stabilizing polymer. This technique allows precise control of the core diameter of the nanoparticles produced by variation of the reaction conditions.

A study by Hussain *et. al.* [57] showed that by reducing a solution of aqueous hydrogen tetrachloroaurate premixed with an aqueous solution of a polymer – dodecanethiol (DDT) end terminated poly(methacrylic acid) (PMAA) – highly monodisperse, water soluble gold nanoparticles were produced. Additionally it was discovered that variation of the gold:polymer ratio in the initial solution had a direct effect on the core diameter and polydispersity of the nanoparticles produced. It was found that increasing the concentration of polymer in that initial solution (at a fixed concentration of gold) resulted in products with a lower average core diameter. The highly monodisperse nature of the products was detected by UV-visible absorption spectroscopy and analysis of TEM images of the samples.

In order to make hydrophobic nanoparticles, a simple ligand transformation was performed which involved adding an ethanolic solution of alkanethiol to the aqueous solution of polymer stabilized nanoparticles. This solution was allowed to react overnight, after which the hydrophobic alkanethiol stabilized nanoparticles were extracted in organic solvent. Excess polymer and alkanethiol were then removed by washing in water and ethanol respectively. The technique produces highly monodisperse nanoparticles with either hydrophilic or hydrophobic ligands.

It has been proposed that the monodispersity of the products occurs as a consequence of the creation of a hydrophilic protective shell by the polymer, around the growing metal nuclei. That shell is permeable to tetrachloroaurate ions but prevents the fusion of two or more metal particles due to the steric and electrostatic stabilization provided by the polymer bound to the surface of the particles.

In a follow up paper by Hussain *et. al.* [33] a one step aqueous preparation of highly monodisperse metal nanoparticles using thioether and thiol-functionalized polymers has been described. It was found that the particle size and size distribution was controlled by subtle variation of the polymer structure and the initial concentration of the polymer. The previously mentioned dodecanethiol terminated PMAA as well as dodecanethiol terminated PAA (poly(acrylic acid)) were identified as the most effective stabilizing polymers studied and lower molar mass polymer ligands (around 2500 g/mol) gave rise to the narrowest particle size distribution. The effect of the hydrophobicity of the end-group of the stabilizing ligand attached to the metal core of the nanoparticles was shown to affect the degree of monodispersity of the particles produced as well as the chemical stability of the particles (tested by decreasing the pH of the solution by the addition of acid).

Several of the observations recorded in the first paper were expanded upon in this publication. This included the conclusion that at a given concentration of dodecanethiol terminated polymer, (DDT)-PMAA, the core diameter of the gold nanoparticles produced decreases and the degree of monodispersity within a sample increases as the molar mass of the polymer is decreased. The monodispersity of gold nanoparticles produced in this way was also found to increase with an increasingly hydrophobic end-group on the polymer; this was shown to be the case for octadecane terminated PMAA. When PMAA functionalized with free thiol groups was used in the synthesis of gold nanoparticles it was found to stabilize gold nanoparticles with the monodispersity observed with

alkanethiol terminated PMAA. The use of multidentate ligands such as DDT-PTMP (dodecanethiol terminated Pentaerythritol tetramercaptopropionate, a tetrathiol functionalized form of the polymer) resulted in the smallest and most monodisperse gold nanoparticles identified by this study to date. By using the observations of this study as a guide, a versatile range of monodisperse gold nanoparticles may be synthesized.

It has been proposed that the enhanced monodispersity of nanoparticles stabilized with DDT-PAA and DDT-PMAA is due to the presence of the carboxylic acid group in these polymers which allows stabilization of metal nanoparticles by a combination of electrostatic and steric mechanisms. Metal nanoparticles stabilized by PAA and PMAA based polymers have been previously described and often exhibit similarly impressive degrees of monodispersity. It has been proposed by Shimmin *et. al.* [58] that in the small particle limit a weak increase in particle size will be observed for larger passivant molecules (which may be interpreted as corresponding to higher M_W polymers in this case) as they need more time to diffuse and passivate growing metal nanoparticles. Another theory proposed by the same group was that heteroatom containing polymers may act as a 'net' for the distribution of gold atoms to small, unstable clusters faster than to other clusters during the particle nucleation stage. It was also proposed that the effect of hydrophobicity of the end group of the polymer may be a direct result of stronger physisorption of these molecules to the growing gold particles compared to other stabilizing molecules.

2.1.4 Supercritical Fluid Separations

Supercritical fluids provide a potentially useful medium for the fractionation of polydisperse metal nanoparticles. Due to the nature of these fluids, the solubilising properties can be tuned by variation of the pressure. The variation of pressure can, therefore, provide a simple means

to affect the interaction between the nanoparticles (or, more specifically, the ligands) and the solvent. Using supercritical fluids to achieve the separation of such a sample would have several advantages including the easy recovery of both the dissolved and undissolved fractions, the isolation of pure fractions and the lack of organic solvents makes the process more environmentally friendly.

Supercritical fluids were first identified by the French engineer and physicist Baron Cagniard de la Tour in 1822 [59], during a fascinating experiment in which he listened for discontinuities in the sound of a flint ball rolling in a sealed cannon, which was filled with fluids at a range of temperatures. During this experiment he discovered that above a particular temperature the densities of both the liquid and vapour phases were equal so the phase boundary between them disappears, effectively leaving a single phase.

This research was used as the basis of new projects by a number of groups and the supercritical phase of various pure components, as well as mixtures, were investigated. It was soon discovered that the solubilization properties of the fluids were directly related to their pressures. This has been attributed to the supercritical fluid density and the solid sublimation density of the solute.

Supercritical fluids exhibit a unique combination of physical properties usually observed separately in liquids and gases. The density properties of these fluids are similar to those of liquids whereas the viscosity properties resemble those of gases.

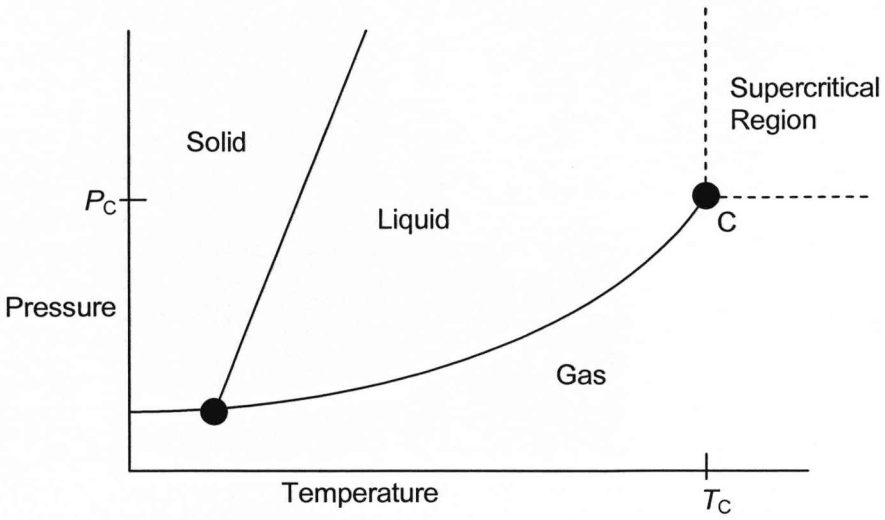

Figure 5. Phase diagram for a pure substance showing the supercritical phase.

Figure 5 shows a generic phase diagram for a pure substance. A supercritical fluid exists above the critical temperature (T_C, this corresponds to the temperature at point C) and critical pressure (P_C, this corresponds to the pressure at point C) of a substance. The line that separates the gaseous and liquid phases is known as the boiling line; this ceases at the critical point (shown as point C in Figure 5). At this point the densities of the gas and liquid phases are equal, resulting in the formation of a single, supercritical phase. Above the critical point there is a very large variation in physical properties for a relatively small variation of pressure. The critical temperature and pressure for ethane are: $T_C = 305$ K $P_C = 4.9 \times 10^5$ Pa.

In recent years supercritical fluids several studies have demonstrated the dispersal of ligand stabilised nanoparticles. Johnston and Korgel *et. al.* [60] demonstrated the dispersal of fluorocarbon-coated silver nanoparticles in supercritical CO_2. They synthesized novel, fluorocarbon ligand functionalized nanoparticles and observed their dispersal in supercritical CO_2 in a temperature controlled, stainless steel, variable-

volume view cell fitted with sapphire windows. The point at which the particles dispersed in the fluid was identified when the fluid turned yellow. The dissolved nanoparticles were characterized by in-situ UV-visible absorption spectroscopy through the sapphire windows of the cell. Due to the nature of these results and the TEM images of the dispersed particles, it was suggested that dispersal of these particles had no effect on the average core diameter of the nanoparticles. The potential use of supercritical fluids to size separate polydisperse metal nanoparticles was not reported either.

The first study into the solubility of alkanethiol stabilized gold nanoparticles in supercritical fluids was published by Johnson *et. al.* [19]. In this study a bimodal mixture of alkanethiol gold nanoparticles of two distinct core sizes was placed into a glass vial contained inside a temperature controlled pressure vessel which was filled with supercritical ethane. Following compression of liquid ethane (to a pressure above P_C) in a pump cooled to the desired temperature, the ethane was transferred into the heated pipework (which was maintained at a temperature above T_C) which allowed the ethane to move from its liquid to supercritical phase.

The pressure vessel was isolated at that pressure and temperature for 12 hours followed by the rapid depressurization of the vessel. The dissolved nanoparticles were collected by bubbling the gaseous ethane through a layer of acetone. Nanoparticles which precipitated out of solution before leaving the vessel and the pipework were recovered by washing out the apparatus with ethane and combining the recovered particles with those collected filtered from the acetone layer. The UV-visible absorption spectrum of the dissolved particles was recorded and compared with the spectra of the undissolved particles which remained in the glass vial and the original bimodal mixture.

A comparison of the UV-visible absorption spectra (Figure 6) showed that the original bimodal mixture and the undissolved sample had very similar plasmon band absorptions at around 520 nm. The presence of these peaks in these samples indicated that nanoparticles with an average

core diameter of above around 2 nm were present as this plasmon band is absent in the spectra of smaller particles. The plasmon band is absent from the spectrum of the particles which were dissolved in the supercritical ethane which suggests the absence of nanoparticles with a core diameter of more than around 2 nm. Although this is a useful result it does not indicate the extent to which the smaller nanoparticles had been removed from the undissolved sample as the spectrum would still exhibit the plasmon band absorption if it contained the smaller particles or not. TEM images of these samples may have provided a more conclusive result which demonstrated the effectiveness of this technique at completely separating the two components of the mixture. Although it is entirely possible that only a small amount of the nanoparticles of average core size less than 4 nm was removed, it is impossible to ascertain this from the results provided. This study is significant as it established that it was possible to extract one size of nanoparticles from a bimodal mixture to some extent, it therefore opened up the possibility of further study. The effect of varying the pressure of the supercritical fluid on the separation of such samples being one of the major areas left for investigation.

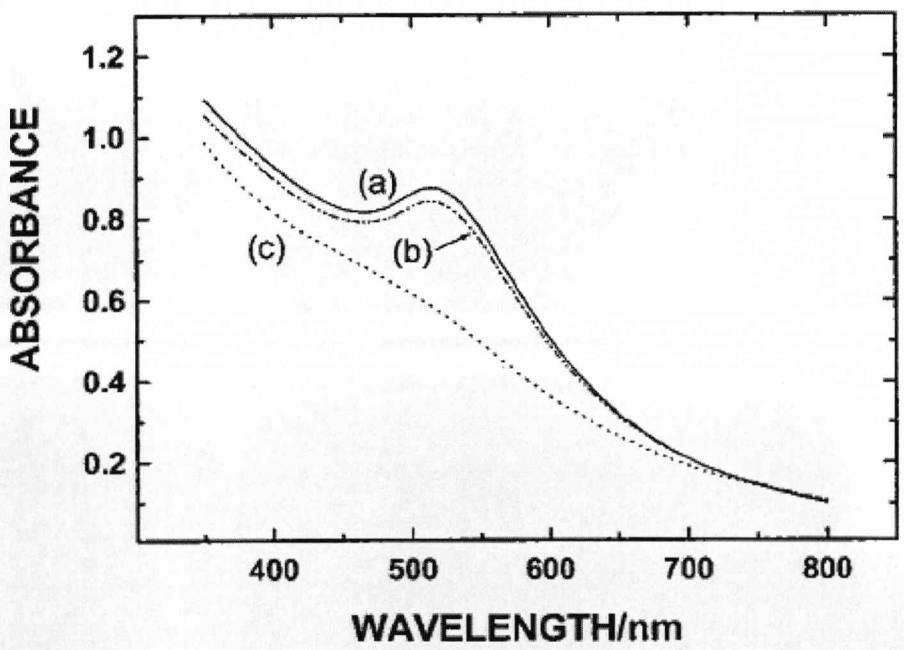

Figure 6 (previous page). UV-Visible absorption spectra for: (a) the original sample, (b) the residual fraction, and (c) the fraction dissolved in the supercritical fluid from the Johnson *et. al.* study [19].

The solubility of metal nanoparticles in supercritical fluids is dependent on the Gibbs free energy of solubilisation; this is a function of the radius of the particle. In dilute solutions the particle-particle interactions can be considered to be negligible (with regard to Gibb's free energy determination) and as a consequence, the Gibb's free energy is the balance between particle-particle interactions in the solid, particle-solvent interactions in the solution and solvent-solvent interactions. The solvent contributions have a high dependence on the pressure of the solution. The decreased solubility with increasing particle radius is due to interactions in the solid phase.

Johnston and Korgel *et. al.* [49] followed up their original study by adopting an approach to the subject similar to that of Johnson *et. al.* [19]. In this study the size-selective solubility of polydisperse samples of both gold and silver nanoparticles stabilized by dodecanethiol ligands were investigated as a function of pressure of the fluid.

The solubility of a bimodal mixture of gold nanoparticles (average core diameters of 1.8 and 4.2 nm) was studied at a range of pressures from 138 to 414 bar. By analysing the dissolved nanoparticles using in-situ UV-visible absorption spectroscopy it was seen that the spectra of the fractions dissolved in the lowest pressure experiments show little or no plasmon band character; this is typical of absorption spectra observed for nanoparticles with an average core diameter of below 2 nm (which would be expected of the 1.8 nm nanoparticles). As the pressure of the fluid was increased, the supercritical fluid density increased accordingly. The spectra obtained at higher pressures exhibited a plasmon band resonance at a wavelength of around 510-520 nm. This is typical of nanoparticles larger than around 2 nm (due to the continuous band electronic structure of

nanoparticles in this size range). Even at the highest pressure it was difficult to observe a very prominent plasmon band absorption at 510-520 nm in the spectrum, this suggests that the largest particles remained insoluble, even at the highest pressure the experiment was carried out at.

The proposed explanation for this pressure dependent solubility was the fact that at lower pressures the steric repulsion weakens as a consequence of decreased ligand solvation. This leads to a stronger Van der Waals attraction between larger particles and allows them to precipitate easier than smaller nanoparticles due to the smaller Van der Waals forces between these particles.

During this study Korgel and Johnston [49] performed the same experiment on dodecanethiol stabilized silver nanoparticles. The same type of size dependent solubility was observed for silver nanoparticles. In order to verify this, TEM images of the undissolved samples were recorded, it was confirmed from the analysis of these images that the average core size of nanoparticles dissolved at lower pressures was significantly lower than those dissolved in the supercritical ethane at higher pressures.

From these studies it has been established that supercritical ethane is a rather poor solvent for alkanethiol stabilized nanoparticles. In order to achieve reasonable results high solvent densities are required, the easiest way to achieve this is to increase the pressure of the fluid.

2.1.5 Scaled Particle Theory

The scaled particle theory of fluids has been used to determine the reversible work function required to introduce a spherical particle into a fluid consisting of spherical particles [61]. The theory introduces the concept that work is required to exclude the centres of solvent molecules (diameter σ_1) from any specified area of space (a sphere of diameter r in Figure 7) in order to dissolve a solute molecule (diameter σ_2). For a fluid consisting of N spherically symmetrical molecules possessing a hard core

of diameter σ_1 and exerting the attractive force consistent with the volume V of the fluid, to exclude the centres of all N molecules from a spherical region of space of radius r in the volume V, the region of space is assumed to be a cavity in the fluid. The probability of such a cavity existing is denoted by $\rho_0(r, \rho)$, where ρ is the number density of the fluid (N/V) (Equation 2).

$$\rho_0(r, \rho) = e^{-W(r, \rho)/kt} \qquad \textbf{(2)}$$

$W(r,\rho)$ represents the reversible work needed to produce a cavity of radius r in the fluid (Figure 7).

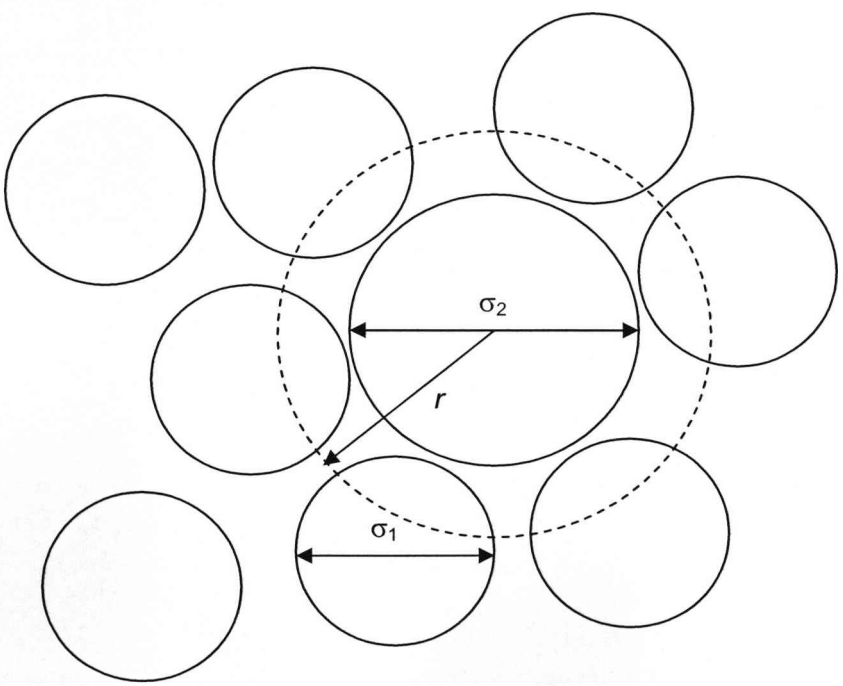

Figure 7. A spherical cavity of radius r created by the presence of a hard-sphere solute with diameter σ_2 in a hard sphere fluid of molecules with diameter σ_1

This theory has been used to predict the solubilities of hard sphere solutes in gas solvents from the determination of Henry Law constants. For dilute systems the Henry Law constant includes contributions from the

Gibbs free energy of cavity formation (as discussed above) and the Gibbs free energy of interaction between solvent and solute. Scaled particle theory is used to determine an expression for the Gibbs free energy of cavity formation.

Applying scaled particle theory to the system of solid nanoparticles dissolved in supercritical fluids is likely to be more complicated due to the increased interactions between fluid molecules compared to gas molecules. In order to adapt Scaled Particle Theory for metal nanoparticles in supercritical fluids it seems likely that an additional term needs to be added to the Henry Law Constant determination which represents the Gibbs free energy of extracting a particle from the solid to vapour phase. The applicability of this theory will be discussed in Chapter 6.

2.2. Ligand Stabilized Gold Nanoparticles

2.2.1 Instability of Gold Nanoparticles

The inherent instability of metal nanoparticles has been the largest obstacle for researchers to overcome in the quest to study their physical properties and potential applications. In order to perform solubility tests a literature search was conducted to find a range of possible techniques for the preparation of stable metal nanoparticles, the results of this search form the basis of the preliminary solubility testing covered in the following chapters. It was found that over time nanoparticles, both dry and in solution, had a tendency to adhere together [37, 40]. This was found to lead to the irreversible formation of an aggregate of nanoparticles. In order to inhibit these processes the repulsive forces between metal nanoparticles have to be sufficient to prevent particles adhering together in aggregates. It was found that repulsive forces between metal nanoparticles could be introduced by one of two mechanisms, steric repulsion and electrostatic (charge) repulsion.

The mechanism of steric repulsion of nanoparticles involves the adsorption of a ligand (e.g. polymer or alkanethiol) to the surface of the nanoparticle core. The steric bulk of the ligand physically blocks the approach of other nanoparticles and prevents flocculation. The advantages of this mechanism include the fact that many types of nanoparticles can be modified in this way relatively simply and the repulsive effect is often found to be effective. Some of the disadvantages include the expense and difficulty of obtaining a suitable ligand for this purpose and the difficulty to subsequently flocculate the system if desired. The other primary mechanism, electrostatic (or charge) stabilization occurs as a consequence of repulsion between particles due to the distribution of charges around the metallic core. One of the measures of stability of a system of electrostatically stabilized colloidal particles is the zeta potential; this measures the magnitude of the electronic interaction between particles in a system [37, 40, 62-64].

It has been shown that many nanoparticles in an aqueous colloidal solution can carry an electronic charge. The charge on the particle may occur as a result of the nature of the particles and the surrounding solvent. Particles bearing surface groups may be ionised which result in an overall charge on the particle, in this situation the strength of the charge will be dependent on the acidic or basic strengths of the surface groups and the pH of the solution. Some crystal lattices will dissociate in solution. If the acidic ion dissociates more preferentially than the basic ion (or vice-versa) this will result in an overall charge on the particle. The nanoparticle may also be modified by the adsorption of a charged species onto its surface [62, 64].

As a consequence of the charge present on the surface of a particle, the distribution of ions surrounding the particle will be affected. As an example consider a negatively charged particle, the ions in the surrounding medium will become arranged in such a way that a layer of positive ions will surround the particle. In the liquid outside of this inner region (known

as the Stern layer, see Figure 8) another, less well defined layer will develop. This layer is known as the diffuse region, in this region there will be a greater mixture of ions than in the Stern layer. In the diffuse layer there is a point, known as the slipping plane. On the interior of the slipping plane the particle and the surrounding layers are considered as a single entity. The potential at the slipping plane is referred to as the zeta potential [62].

The zeta potential is defined as the charge that a particle will have in a specific medium. The magnitude of this potential is used as a measure of the stability of a system of nanoparticles in solution. If the potential of all particles in a system is large (either negative or positive) then the particles will repel each other but as the potential tends towards zero the repulsion between particles diminishes and the particles will be more likely to aggregate. In general if the zeta potential of a system is more negative than -30 mV or more positive than +30 mV the system can be considered to be stable.

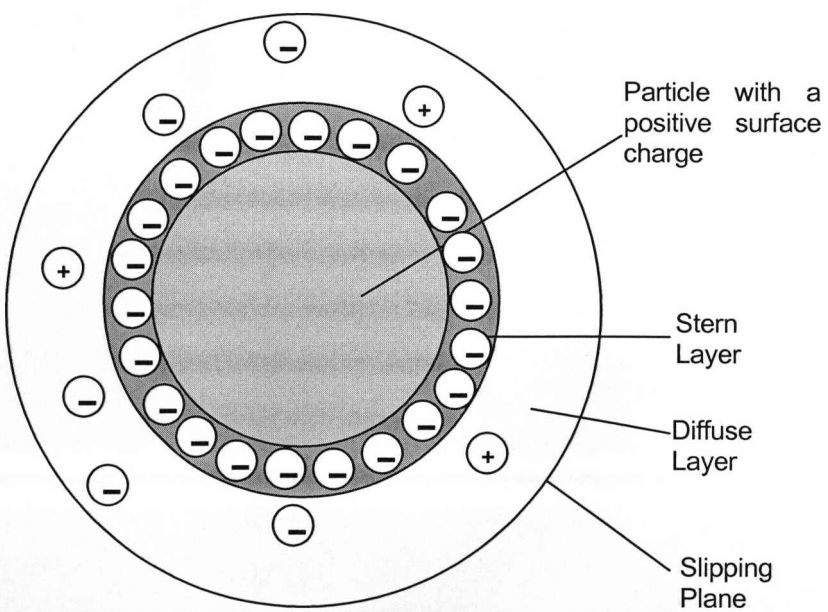

Figure 8. Electrical double layer of charged nanoparticles.

The pH of a system may directly influence the stability of the nanoparticles. The pH of a system is the most important factor upon which zeta potential is dependent; therefore, a pH will always be quoted with a zeta potential value. In order to understand this we can consider a system of positively charged nanoparticles, if the surrounding medium is made more acidic then the particles will gain more positive charges, however, if the medium is made more alkaline then the build up of negative charge in the surrounding medium will eventually result in the positive charge on the particles being neutralized resulting in a zeta potential of zero (this is known as the isolectric point). At the isoelectric point the stability of the system will be lowest. If the medium were to be made even more alkaline then a build up of negative charge will occur and the zeta potential will become negative and move away from zero resulting in increased stability of the system [62, 64].

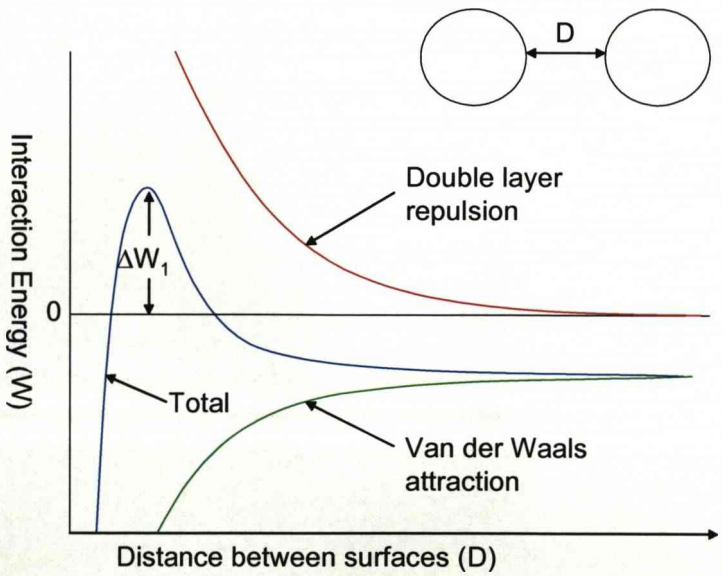

Figure 9. Illustration of the energetic interactions between two particles as they approach each other.

DLVO (Derjaguin, Landau, Verwey and Overbeek Theory) theory [65-70] is used to describe the energetic interactions between nanoparticles in solution. DLVO theory states (Equation 3) that the stability of a particle in solution is dependent upon its total potential energy function (V_T). The theory proposes that V_T is determined by calculating the net effect of competing contributions:

$$V_T = V_A + V_R + V_S \qquad \textbf{(3)}$$

where Vs, V_A and V_R represent the potential energy contributions due to the solvent, due to attraction between solid particles and due to repulsion between solid particles respectively. The contribution of V_S may only make a small contribution to the total potential energy over the last few nanometres of separation, the balance between V_A and V_R is more significant. The effects of these contributions are much larger than that of the solvent potential energy, these effects also cover much greater distances. The attractive potential energy may be defined in terms of the Hamaker constant (A) and the particle separation (D):

$$V_A = -A/(12.\Pi.D^2) \qquad \textbf{(4)}$$

The repulsive potential is a more complex function:

$$V_R = 2.\Pi.\varepsilon.a.\xi^2 \exp(-\kappa D) \qquad \textbf{(5)}$$

where a is the particle radius, ε is the dielectric constant, κ is a function of the ionic composition, ξ is the zeta potential and Π is the solvent permeability.

The theory defines the stability of a colloidal system as the sum of the attractive potential (due to van der Waals attraction between particles) and the repulsive potential (due to electric double layer repulsion) that

occur between particles in a colloidal system as they pass each other due to continuous Brownian motion.

DLVO theory proposes that an energetic barrier, created by the double layer repulsion between particles, prevents two or more particles approaching and aggregating. If the particles were to collide with sufficient energy to overcome this barrier then the van der Waals attractive forces will be sufficient to bring them into contact and cause them to adhere to each other.

In order for a particle to approach another it must overcome energy barrier ΔW_1 (Figure 9) which is the resultant energy determined by adding the attractive effects of the Van der Waals forces between particles and the double layer repulsion between particles.

Aggregation will be avoided in systems where the repulsion between particles is sufficiently high as to energetically prohibit two or more particles aggregating. If no such repulsion exists in a system aggregation will occur over time. When, for example, the zeta potential of a system is reduced (by variation of the pH of a system for example) a secondary minimum in the potential of the system can be created which allows the reversible formation of flocs of aggregated particles. These aggregates are robust enough not to be broken up by Brownian motion but can be dispersed under agitation.

Metal nanoparticles can be stabilized by either or both of these techniques. Alkanethiol stabilized metal nanoparticles are primarily stabilized by steric repulsion [4, 63].

2.2.2 Synthesis of Simple Ligand Stabilized Metal Nanoparticles

In order to avoid aggregation of metal nanoparticles it is necessary to stabilize individual particles. Particles may be stabilized sterically or electrostatically.

One of the most commonly cited techniques for the synthesis of stable metal (primarily gold and silver) nanoparticles in the size range 1-10 nm is that proposed by Brust and Schiffrin *et. al.* [4]. In their publication they demonstrated a simple, two-phase technique for the preparation of alkanethiol stabilized gold nanoparticles.

The synthetic approach is based on the simple two-phase reduction of a Au(III) complex, hydrogen tetrachloroaurate. The gold complex is transferred from an aqueous solution to an organic phase by the phase transfer agent tetraoctylammonium bromide. In the organic phase the complex was reduced by addition of sodium borohydride in the presence of an alkanethiol. The alkanethiol becomes bound to the surface of the particles (Figure 10) during the nucleation and growth stages and controls the growth of the particles and provides steric stabilization.

Figure 10. An illustration of a metal core stabilized by surface bound alkanethiol ligands [37].

The synthesized particles were very stable both in organic solvents as well as in solid form. It has been shown that nanoparticles become less reactive in ligand exchange reactions within a few hours of synthesis, this is believed to be due to reorganization of binding sites on the surface of the nanoparticles [71]. The particles could be analysed by IR spectroscopy, UV-visible absorption spectroscopy and TEM. The lack of a plasmon band

in the UV-visible absorption spectrum of the particles (which form brown coloured solutions) suggested that these particles had an average core diameter of less than 2 nm. TEM images supported this as they showed a sample of nanoparticles with a size range of 1-3 nm and an average diameter of between 2.0 and 2.5 nm at which point little or no plasmon band absorption is expected.

One of the inconvenient features of nanoparticles prepared in this way is the fact that the phase transfer agent, tetraoctylammonium bromide, remains tenaciously bound to the final product [72]. This has the effect of stabilizing the solid state of the particles and, therefore affects solubility. It was demonstrated that other filtration and purification techniques that had been used to size-separate metal nanoparticles were ineffective at removing this impurity.

Schiffrin and Johnson *et. al.* [72] demonstrated a simple technique for the removal of this impurity by Soxhlet extraction. It was shown that a series of extractions in acetone over a time period of 12 hours was effective at removing much of the impurity. The amount of TOABr extracted over time was measured by Liquid Chromatography and Time of Flight Mass Spectroscopy. It was shown that most of the impurity that could be removed had been extracted after 12 hours. This was supported by comparing XPS measurements of the original and purified samples of particles. An immediate increase in the solubility of the purified particles in acetone-toluene mixtures was detected; the nanoparticles could be reprecipitated from these mixtures by the addition of TOABr to the solution.

It has been proposed that the stabilization of the solid state occurs as a consequence of the strong specific adsorption to gold ions of Br^- ions which provides electrostatic adsorption sites for the quaternary ammonium ions in the nanoparticle shell [72]. The effect of interdigitation by the alkyl chain of the stabilizing ligand and those of the TOABr may also contribute

to the increase in the lattice energy with a corresponding decrease in the solubility.

In a follow up to their original publication, Brust and Schiffrin *et. al.*[25] demonstrated the versatility of their synthetic approach by reporting the ability to create stable functionalized gold nanoparticles by simple modification of their original technique to prepare alkanethiol stabilized nanoparticles. The key aim of this procedure was to functionalize gold nanoparticles with a bifunctional organic molecule which allowed the molecule to act as a ligand by bonding to the metal core like an alkanethiol ligand but with the second functional group remaining unbound to the core and, therefore, affecting the chemical properties of the particles.

p-mercaptophenol functionalized nanoparticles were prepared in a single phase system. An ethanolic solution of hydrogen tetracholoroaurate was prepared; to this aqueous sodium borohydride was added in the presence of *p*-mercaptophenol. The resulting nanoparticles formed brown solutions (indicating core diameters equal to or below approximately 2 nm) in alcohols, ethyl acetate and alkaline aqueous solutions. The particles sizes varied between 2.4 nm and 7.6 nm. Infrared spectra of the samples showed that the ligand was bound to the gold surface through the thiol functionality and that the phenolic hydroxyl groups could be esterified.

Ligand-place exchanges are amongst the most reliable and versatile strategies available for the functionalization of metal nanoparticles. Murray *et. al.* [27, 34, 35, 73-75] proposed a mechanism by which place-exchange reactions of ligand stabilized metal particles may occur [28]. In this publication it was shown that a new thiolate ligand may be incorporated into an alkanethiolate stabilized metal nanoparticle by mixing the new thiol (R'SH) with the alkanethiolate (RS) stabilized gold particles (see Scheme 1).

$$X(R'SH) + (RS)_mMPC \longrightarrow x(RSH) + (RS)_{m-x}(R'S)_xMPC$$

Scheme 1 (previous page). General reaction scheme for a place-exchange reaction of an alkanethiolate stabilized monolayer protected cluster nanoparticle (MPC) by a different alkanethiolate (R'SH) [28].

This study revealed many of the mechanistic details of this important class of reaction. It was found that the stoichiometry of the place-exchange reaction was 1:1. The displaced thiolate appears in solution in the form of a thiol (RSH), the entering ligand is removed from solution as it becomes bound to the metal core, this process (and the 1:1 stoichiometry) can be followed by ^{1}H NMR. It was additionally proposed that the stoichiometry was due to the possibility that the rate-determining step involved the protonation of an existing thiolate ligand by an R'SH molecule. The rate was also shown to decrease with increasing size of the new ligand and increasing chain length of original protecting monolayer. Additionally, a variation in the ease with which different sites on the surface of a cluster could be ligand exchanged was observed. It was found that vertex sites of the cluster exchanged relatively easily whereas other sites (such as interior terrace sites) appeared to be almost completely noninterchangeable which supported the argument for an associative rate determining step. Experimental evidence also suggests the exchange of thiolate ligands between these easy to exchange sites [28]. Another study into this reaction showed that when a less than stoichiometric quantity of the incoming ligand is used, the functionalized products had polydisperse compositions of the organic ligand shells [76].

2.2.3 Metal Nanoparticles and Polymers

The earliest observation of polymer stabilized metal particles occurred in the 18th century when Helcher [77] recorded that starch was able to stabilize water soluble gold particles. Since the 18th century there have been considerable advances in both nanoparticle and polymer

sciences, these advances have led to a wide range of polymers being used to stabilize metal nanoparticles and the advanced study of the properties of particles synthesized in this way. The most common approach to the preparation of polymer modified gold nanoparticles is the in-situ reduction of metal salts in a solution of the polymer matrix [78, 79]. An alternative technique, gaining popularity, involves the polymerization of a matrix around the pre-formed metal nanoparticles. Metal salts can often be reduced either by dissolved reducing agents (such as $NaBH_4$) or by the solvent (such as alcohol present in the reflux of gold salt in methanol/water in the presence of Polyvinylpyrrolidone, PVP). Other reduction techniques commonly employed in the synthesis of metal nanoparticles with polymers include photolysis and electrochemistry of metal salts in the presence of a polymer matrix.

Lennox et. al. [80] described the first successful blending of premade Au nanoparticles into premade polymer matrices with a thorough dispersal of nanoparticles throughout the matrix. The main advantage of this technique over other techniques used to embed particles within a polymer matrix is the degree of control when synthesising both the nanoparticles and the polymer. The simple technique also allows scope for versatility by modification as the primary requirement for the polymer is the presence of a thiol functional group which can be incorporated into a variety of polymers with ease.

It has been found that nanoparticles functionalized by some polymers can show a high degree of chemical stability. It has also been shown that only a small amount of a polymer which acts as a good stabilizer is needed to prevent aggregation of a sample of metal nanoparticles. Linear polymers with thiol functionality will stabilize gold nanoparticles in a similar way to alkanethiol stabilization of metal nanoparticles discussed before [58]. These particles can be prepared by a simple reduction of the metal salt (typically $HAuCl_4.4H_2O$ in the case of gold) by $NaBH_4$ or another suitable reducing agent.

Hollow spheres of polymers have been obtained by preparing polymer stabilized metal nanoparticles followed by the removal of the metal particle at the core of the polymer layer. These spheres have found use as conductive capsules and can be produced by the calcinations and dissolution of gold-seeded ceramic hollow spheres [81-84].

In chapter 2.1.3 the synthesis of gold nanoparticles reduced by $NaBH_4$ in the presence of PMAA (poly(methacrylic acid)) [33, 57] was discussed. This technique leads to the creation of highly monodisperse gold nanoparticles with pre-defined average core diameters which can be controlled by variation of the starting gold:polymer ratio.

2.3 Ligand Stabilized Silver Nanoparticles

2.3.1 Introduction

In Chapter 1 the Lycurgus Chalice was introduced, it is one of the oldest objects containing nanoparticles known to science [24]. The British Museum analysed the cup and found that the particles present had an average core diameter of around 70 nm and were actually an alloy of gold and silver. The early history of silver nanoparticles parallels that of their gold analogues with primary applications being addition to glass to give a coloured effect. Whereas stained glass made from gold nanoparticles were ruby red, those made with silver nanoparticles were yellow.

In the 20^{th} century a simple technique to prepare stabilized silver nanoparticles was demonstrated. The technique was based on the Turkevich method [1] for the synthesis of gold nanoparticles; aqueous solutions of $AgNO_3$ were reduced by mixing in an aqueous solution of sodium citrate under reflux. As in the Turkevich method the reduction is observed rapidly, the solution turns yellow indicating the presence of silver nanoparticles. Later, the Creighton method used $NaBH_4$ as a reducing agent and led to the formation of nanoparticles with an average core size of

around 10 nm [85], this has become one of the most commonly employed techniques for the synthesis of silver nanoparticles [86].

The plasmon absorption of silver nanoparticles is very significant [86]. The interaction of visible light with silver nanoparticles is more efficient than the interaction of light with any other organic or inorganic particle of the same dimensions. Additionally the plasmon resonance can be tuned to any particular wavelength in the visible spectrum as demonstrated in the Lycergus cup where an alloy of silver and gold particles transmits red light.

The synthesis of silver nanoparticles has been studied at length and the effect of varying the metal salt, stabilizing ligand and the reducing agent has been reported [40, 87-89]. The oxidation of unfunctionalized silver particles is inhibited by their large positive reduction potential which makes the oxidation thermodynamically unfavourable. A number of techniques have been attempted to prevent aggregation of the nanoparticles including the use of electrical double layers that form around nanoparticles in low-ionic-strength suspensions. In high-ionic-strength or organic suspensions the nanoparticles may be protected by adding ligands to the surface of the metal core such as monlolayers of organic molecules, surfactants, polymers and dendrimers. A variation in the nature of functionalized nanoparticles can often be observed due to differences in the way that the ligands interact with the metal particles.

There are several limitations of the techniques used to synthesize silver nanoparticles which are similar to the problems encountered during the synthesis of gold nanoparticles. A range of particle sizes is often produced due to the limitations of these techniques, as mentioned earlier it is vital to modern nanoscience to limit polydispersity in any nanoparticle synthesis technique. It can also be difficult to prepare silver nanoparticles of any desired size. Most of the existing synthetic techniques allow some flexibility in reaction conditions which result in the ability to prepare

different size particles, however, there are limits to these customizations and many sizes remain difficult to prepare [40].

2.3.2 Polymer Stabilized Silver Nanoparticles

The use of polymer ligands in the functionalization of silver nanoparticles has been reported and is currently an active area of study. One technique described by Mallick *et. al.* [90] employs the use of an ultra-violet irradiation technique to functionalize colloidal silver with Methoxypolyethylene glycol (MPEG). The attached MPEG groups act as stabilising groups for the nanoparticles. The reducing agent is produced by CH_2CH_2-OH present in MPEG which acts as a scavenger of $H^{\cdot}$ and $OH^{\cdot}$ radicals produced by the direct photolysis of water by a UV source and becomes $CH_2CH^{\cdot}$-OH. Metal atoms are then reduced by the produced reducing agent and have a tendency to cluster together due to the fact that the binding energy between two transition metal atoms is higher than the atom-solvent bond energy. The growth of these particles is inhibited by the presence of the MPEG functionality which stabilizes the nanoparticles at a set size or range of sizes.

An alternative strategy was described by Gao *et. al.* [91] in which stabilized silver nanoparticles are prepared using two-armed polymers with a crown ether core. A custom designed two-armed polymer with a crown ether core was added in solution to Ag^+. Because of complexing of the crown ether present within the polymer and the Ag^+, aggregates of Ag^+ and polymer were formed. The bound Ag^+ could be subsequently reduced photochemically, leaving Ag nanoparticles surrounded by the polymer which acted as a stabilising shell. One of the most intriguing observations from this synthesis was the fact that the photoluminescence of the silver nanoparticles stabilized by this polymer was increased upon photoexcitation at 343 nm due to the complexing effect between the crown ether and the silver nanoparticles, compared to the standard

photoexcitation wavelength of silver nanoparticles, 408 nm. A degree of size control over the produced nanoparticles was incorporated into the synthesis by changing the initial concentration of polymer and by variation of the molecular weight of the polymer used. The average core diameter of the synthesized particles decreased with the increasing molecular weight of the polymer used, and the polymer and the Ag^+ concentration, respectively.

Churmanov *et. al.* [92, 93] demonstrated the encapsulation of silver nanoparticles into a polymer shell by encapsulation polymerization, resulting in a chemically stable system. Silver particles were coated by polymerization of styrene and/or methacrylic acid in emulsions of oleic acid. The silver nanoparticles become coated with a well-defined, uniform layer of polymer. The thickness of this layer may be modified by changing the starting concentration of the polymer. The polymer coating could be viwed in TEM images by the use of negative staining by phosphotungstic acid. The particles were only formed in the presence of oleic acid due to the fact that it is readily adsorbed on the particles (carboxylic acids have high affinity for the oxide layer present on the surface of silver). It was shown that the encapsulating layer resulted in chemical stabilization of the particles and the retention of their optical properties. Additionally covalent attachment of proteins to the polymer has been demonstrated which may result in more widespread use of this technique.

2.4 Applications of Metal Nanoparticles

One of the most interesting applications of ligand stabilized metal nanoparticles is their use in biosensors. Changes in the colours of samples of metal nanoparticles occur as a consequence of aggregation. Mirkin *et. al.* [94-105] have studied the development of colorimetric biosensors based upon nanoparticle-DNA conjugates. A simple technique using a gold nanoparticle functionalized by non-complimentary DNA oligonucleotides capped with thiol groups has been demonstrated. When DNA which is

complimentary to the two grafted sequences, was added to the solution a colour change is observed (from red to purple) as a consequence of the formation of a polymer network which resulted in the aggregation of the gold nanoparticles. This technique can be modified to detect specific DNA sequences.

It is hoped that metal nanoparticle based electronic devices will become a major application of this research in the near future. Single electron transfer behaviour has been observed in metal nanoparticle systems. In these systems a nanoparticle is placed in the gap between two contacts, the particle represents a Coulomb blockade and exhibits single electron charging behaviour due to its small capacitance [18]. A recent example of an application in this area is that of Leong *et. al.* [106]. A system based on gold nanoparticles and pentacene (an organic semiconducting compound) for use as a memory device. In this device citrate stabilized gold nanoparticles are deployed in an ordered arrangement on a layer of pentacene; these particles act as the charge-storage component of the system. Under negative voltage holes (charge carriers) were injected into the semiconducting (pentacene) layer, when a positive voltage was applied the holes were removed. It is hoped that this technology can be developed and used to replace silicon based memory devices as they have the potential to be cheaper and more versatile.

Other applications of stabilized metal nanoparticles include use in catalysis [107], use in novel gas sensors [108] and the exploitation of optical properties in the production of screens and filters [109].

2.5 Closing Remarks

This review of relevant literature has shown that the study of metal nanoparticles, specifically the preparation of monodispserse fractions of these particles, is an active area of research. There are a number of synthetic and separation based routes available to achieve this goal.

The following chapters will provide details of the experiments conducted to separate polydisperse samples of metal nanoparticles and to obtain more detailed solubility information for some of the monodisperse samples.

Chapter Three

Synthesis, Characterization and Solubility Testing of Alkanethiol Stabilized Au Nanoparticles

Chapter 3 Synthesis, Characterization and Solubility Testing of Alkanethiol Stabilized Au Nanoparticles.

3.1 Alkanethiol Stabilized Au Nanoparticles

3.1.1 Introduction

This chapter reviews several synthetic techniques used to prepare ligand stabilized gold nanoparticles to be used later in solubility measurement and separation experiments. Included in this chapter is a review of the problems related with these synthetic techniques and the reasons why improvements are needed.

A discussion of a simple purification technique which resulted in a significant improvement in the solubility and characterizability of nanoparticles is also presented. The chapter is concluded by a summary of the preliminary solubility testing and a discussion of the suitability of nanoparticles prepared by the two-phase technique for use in later experiments.

3.1.2 Synthesis of Dodecanethiol Stabilized Gold Nanoparticles

In order to obtain solubility data for various types of metallic nanoparticles it was desirable to use a synthetic technique that would produce highly monodisperse samples of nanoparticles which were stable under standard laboratory conditions over a period of up to six months. The two-phase synthesis of gold nanoparticles [4] discussed in the introductory chapter was one of the techniques studied. It is known from previous work that stable gold nanoparticles in the size range 1-10 nm can be produced. The versatility of this technique also made it an appropriate choice for this project, the chemical and physical properties of the product could be varied to an extent by changing the nature of the stabilizing ligand (e.g. using ligands with different terminating groups [25]). It has also been established

in earlier studies that variation of the gold:thiol ratio leads to a controllable variation in the average core diameter of the nanoparticles obtained.

The first sample of gold nanoparticles prepared by the two phase technique was stabilized by dodecanethiol. Previous studies had shown that dodecanethiol stabilized nanoparticles were particularly stable and much of the early research on alkanethiol stabilized gold nanoparticles used this ligand. Later comparisons were made with analogous preparations of gold nanoparticles stabilized by propanethiol, pentanethiol and octanethiol.

3.1.3 Experimental

Alkanethiol stabilized gold nanoparticles were prepared by reduction of a gold compound in the presence of the relevant alkanethiol. A gold:thiol ratio of 3:1 was selected for this synthesis. An aqueous solution of hydrogen tetrachloroaurate was prepared (0.35g, 30 mM) and mixed thoroughly for 3 hours (without heating) with a solution of tetraoctyl ammonium bromide (2.18 g, 50 mM) in toluene. The organic layer was then extracted (the aqueous layer was now clear and contained none of the gold starting material). To this solution 0.51 g of dodecanethiol was added to form an opaque, cloudy suspension. An aqueous solution of sodium borohydride (25 mL, 0.01 mol) was added under continued agitation, there was a sudden colour change from cloudy white to a very dark brown colour solution. The solution was allowed to react for a further three hours followed by extraction of the organic layer. In order to remove excess thiol the organic layer was reduced to 10 mL by rotary evaporation and was added to 400 mL of ethanol, the mixture was then kept at a temperature of around -20 °C until a dark brown precipitate was observed. The precipitate was removed by filtration and washed further with ethanol; the particles were then dissolved in toluene and were ready for analysis and application.

3.1.4 Analysis

UV- Visible Absorption Spectra and Gold Nanoparticles

UV-Visible absorption spectroscopy is one of the most commonly used techniques to characterize metal nanoparticles. The absorption of visible light by metal nanoparticles has been one of their most distinguishing properties since their discovery [22, 23, 110, 111]. The intense red colour that is commonly observed in gold nanoparticles is absent in both the bulk form of gold and individual atoms (and indeed very small clusters).

These plasmon electronic transitions are excited by UV-Visible electromagnetic radiation which is useful for characterization. The position and shape of the maximum absorbance can be used to estimate an average core diameter of gold nanoparticles. As is customary with absorption spectroscopy, the extinction coefficient can be determined by obtaining the absorption spectrum of a highly monodisperse sample of known concentration and using the Beer-Lambert law.

It should be pointed out at this stage that many of the UV-Visible Absorption spectra recorded for this thesis were performed on an apparently malfunctioning instrument. The general shapes of the spectra are correct so the conclusions drawn from these spectra are unaffected but some spectra have high levels of noise and some small features are not representative of the samples analyzed.

The nanoparticles formed a brown solution in toluene indicating that the average core diameter of the sample was below approximately 2 nm as larger nanoparticles have distinct plasmon band resonances which result in strongly coloured solutions (deep red for nanoparticles in the 2-10 nm size range). Smaller nanoparticles do not produce the characteristic coloured solutions due to the absence of the plasmon band which occurs as a consequence of the electronic structure of small nanoparticles. The UV-Visible absorption spectrum (Figure 12) shows no absorbance maximum at

around 520 nm which agrees with the initial observation that the nanoparticles were smaller than 2 nm.

This process is an example of the 'two-phase' synthesis technique discussed in earlier chapters. This technique has been chosen as it is effective in the synthesis of stable metal nanoparticles under 10 nm, it also permits an easy comparison with the results of other groups performing similar experiments (most of the literature on similar investigations have made use of alkanethiol stabilized gold nanoparticles in the 1-10 nm size range) and due to the expected compatibility (with regards to solubility) with the desired supercritical fluid, ethane. The two-phase synthesis works via the transfer of tetrachloroaurate ions from the aqueous to organic layer, tetraoctyl ammonium bromide acts as the phase transfer agent. Once in the organic phase the Au (III) ions are reduced by sodium borohydride in the presence of dodecanethiol.

This type of reaction is highly versatile and a short investigation into the effect of changing the length of the alkyl chain of the stabilizing ligand on solubility of the product will be conducted throughout this chapter. The same synthesis was repeated with octanethiol added as the stabilising ligand. Again a brown coloured solution was formed; the absorption spectrum (Figure 11) shows only a very weak peak at around 520 nm meaning the average core diameter was below or around 2 nm.

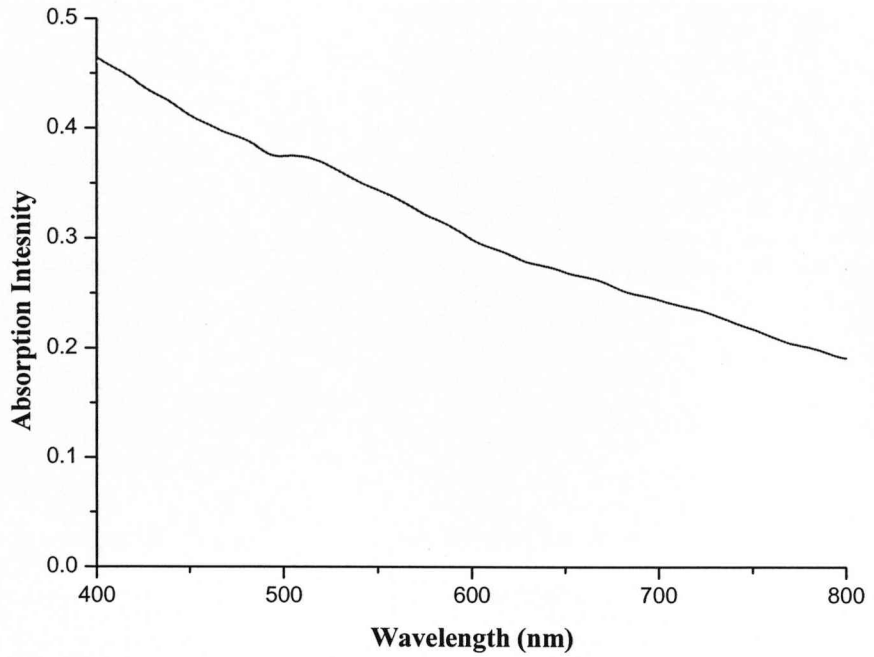

Figure 11. Typical UV-visible absorption spectrum of dodecanethiol stabilized gold nanoparticles prepared by the two-phase synthesis with a 3:1 gold:thiol ratio.

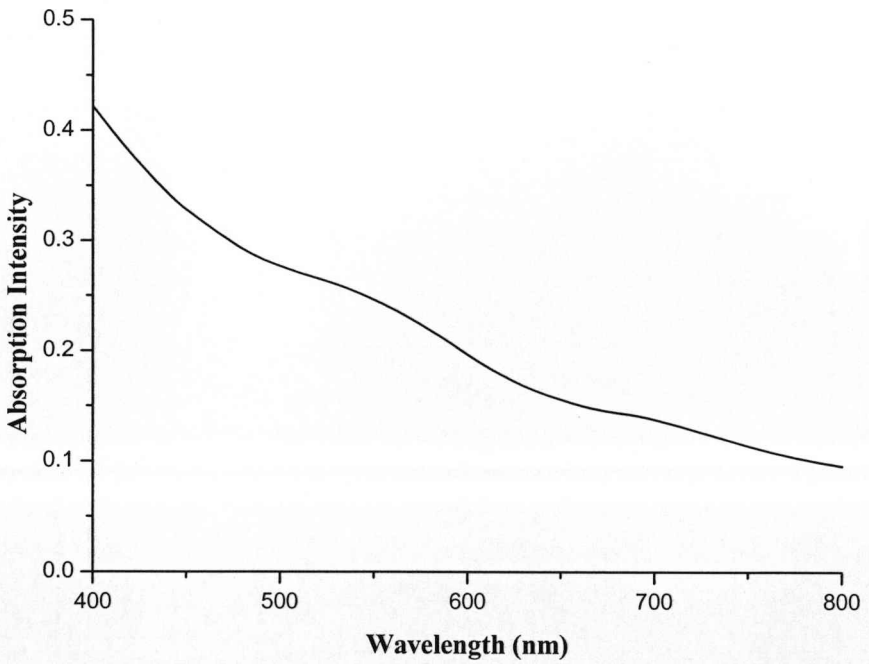

Figure 12. Typical UV-visible absorption spectrum of octanethiol stabilized gold nanoparticles prepared with a 3:1 gold:thiol ratio.

3.1.5 Solubility Testing

Preliminary Experiments

Preliminary solubility testing was conducted by taking a fixed volume (2 mL) of the stock solution of as prepared dodecanethiol stabilized gold nanoparticles and placing it into a small glass vial (open at one end, diameter of 2 mm), the solvent was evaporated slowly (at room temperature) leaving solid particles dried on the interior of the vial. Dry samples of nanoparticles were used as the presence of liquid toluene inside the high pressure vessel would make the analysis more difficult. As the critical point of toluene would not be reached in the pressure vessel it seems likely that the nanoparticles would remain dissolved in toluene as they are expected to be much more soluble in toluene than supercritical ethane.

The vial was sealed in a high pressure vessel and exposed to supercritical ethane at a fixed pressure for a period of time between 12 and 72 hours. When UV-Visible absorption spectra of the samples of starting and undissolved samples were compared there was no difference in the intensity of the absorptions indicating there was no change in concentration of undissolved nanoparticles between the start and the end of the experiment. No material was recovered from the high pressure vessel for analysis by absorption spectroscopy. When the amount of starting material was doubled there was little variation in the solubility of the particles. It was obvious at an early stage that none of the product was dissolved at pressures in the range 0-200 bar. Experiments at higher pressures showed slight weight changes between the original and undissolved sample but this was not supported by UV-Visible absorption spectroscopy as no dissolved nanoparticles were recovered from the vessel. It was decided that further modifications would need to be made to the synthesis of these nanoparticles in order to disperse them in supercritical ethane.

The absorption spectrum of the dissolved sample from the 200 bar experiment with octanethiol stabilized gold nanoparticles is shown in Figure 13. The spectrum of the recovered sample shows a minimal absorption which is only a minute fraction of the intensity of the absorption of the sample originally added to the high-pressure vessel (represented by the absorption spectrum of the standard volume of stock solution). The absorption spectrum of the sample dissolved in supercritical ethane is free of a plasmon band peak at around 520 nm. In the original sample a slight plasmon band absorption was observed which suggests that some of the nanoparticles present in the sample had an average core diameter over 2 nm, none of these larger nanoparticles appeared to have dissolved in the supercritical ethane.

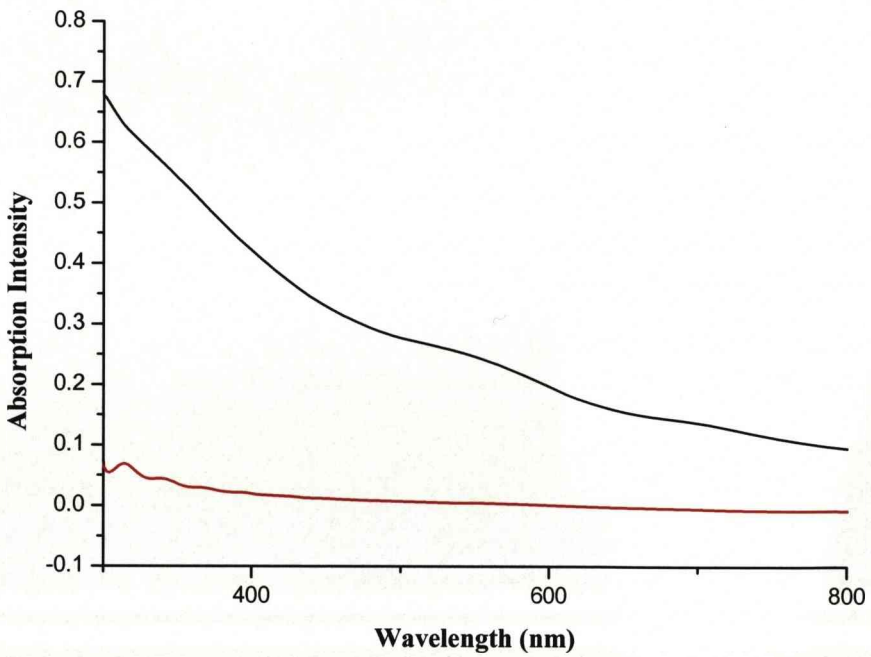

Figure 13. UV-visible absorption spectrum of octanethiol stabilized gold nanoparticles as prepared (black) and those which were recovered as the dissolved fraction from the 200 bar high pressure experiment (red).

A range of alkanethiol stabilised nanoparticles (C4-C12) were tested in the high pressure vessel. A wide range of pressures (50 – 300 bar) were used in order to test the solubility behaviour of these nanoparticles with the variation of supercritical fluid density, the duration of the experiments was also varied to see if allowing the fluid more time to disperse had an effect. As well as alkanethiol stabilised nanoparticles, a simple ligand exchange was used to produce mercaptophenol stabilized nanoparticles (mixing alkanethiol stabilised nanoparticles with a toluene solution of p-mercaptophenol at room temperature for an hour) [25], none of these samples showed significant solubility.

In another attempt to modify the experimental set-up the above experiments were repeated with agitation (provided from a magnetic flee placed inside the vessel) and by the substitution of the glass vial with a modified design with both ends open (allowing the supercritical fluid to circulate more freely). Neither of these modifications improved the outcome of the experiments but the modified glass vial was used for all future experiments due to the potential advantages this design could provide.

It was decided that the best course of action would be to investigate a way of modifying the nanoparticle synthesis process to yield more soluble nanoparticles. The following section describes the application of a novel purification technique developed by another group at the University of Liverpool.

3.2 Soxhlet Extraction for the Purification of Gold Nanoparticles

3.2.1 Introduction

Soxhlet extraction was originally developed for the extraction of lipids from solid materials [112, 113]; the process has been applied to a number of other purifications since [114-117]. The extraction works by

making use of a solvent in which the desired compound is insoluble but the impurity is highly soluble. The technique works by placing the solid compound onto a thimble (typically a disposable cellulose based tube with one closed end), usually by allowing a solution of the compound to dry onto the thimble. The thimble is placed into the main chamber of the extractor (Figure 14). In a flask below the chamber the solvent is continuously heated and allowed to evaporate. The solvent vapour passes into a condenser above the main chamber, once it condenses, the liquid passes into the chamber, eventually submerging the thimble. When the chamber is almost full of solvent it is emptied by a siphon arm built into the side of the chamber. The siphoned solvent is returned to the heated flask for further reflux.

In the case of gold nanoparticles produced by the two-phase synthetic technique it was found that the phase transfer agent used in the first stage of the synthesis (tetraoctylammonium bromide) becomes tenaciously retained in the product [72, 118]. Repeated precipitation of alkanethiol stabilized gold nanoparticles has been shown to be ineffective at removing this impurity. The retention of this quaternary ammonium salt has been shown to affect the solubility of the metal nanoparticles by stabilising the solid form of the product.

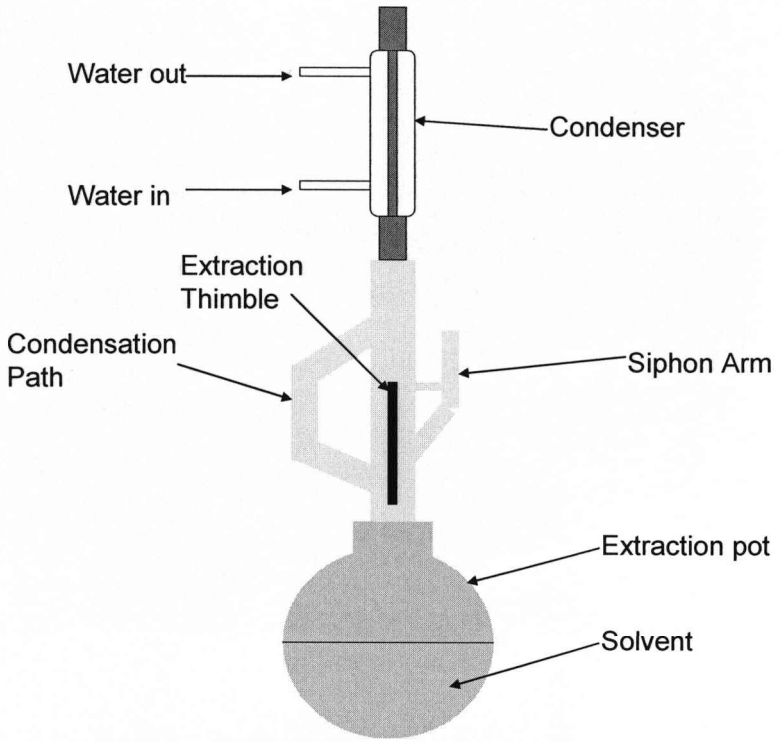

Figure 14. Schematic diagram of soxhlet extraction apparatus.

It was predicted that the impurity becomes bound to the nanoparticle by the incorporation of the quaternary ammonium and bromide ions into the ligand shell which stabilizes the gold core. Bromide ions show strong specific adsorption to gold surfaces which may provide electrostatic adsorption sites for quaternary ammonium (TOA^+) ions in the ligand shell [119]. It is also considered by some [120] that interdigitiation occurs between the alkyl chains of the stabilizing ligands of the nanoparticles and those of the tetraoctylammonium ions which results in stabilization of the solid form of the product due to an increase in lattice energy. The effect of this impurity on the solubility of metal nanoparticles prepared by this technique is a major consideration when analysing their physical properties.

The use of soxhlet extraction to remove the phase transfer agent from the product was first demonstrated by C. A. Waters *et. al.* in 2003

[72]. This paper demonstrated the purification of a sample of gold nanoparticles prepared by the two-phase synthesis with a gold:thiol ratio of 4:1. The gold nanoparticles were placed onto an extraction thimble and purified by continuous extraction in acetone over a 12 hour period. Acetone makes an ideal candidate for extraction solvent as alkanethiol stabilized gold nanoparticles are completely insoluble in this solvent, the impurity, however, is soluble in acetone. A number of simple analytical tests were performed on the purified sample in order to demonstrate the extraction of the impurity. The Matrix-Assisted Laser Desorption-Ionisation Time-of-Flight (MALDI-TOF) mass spectrum of the sample before and after purification was recorded. A comparison of the spectra shows that the mass peaks in both are identical, thus confirming the fact that the metallic cores of the nanoparticles are not changed by the extraction process. A major peak is observed in the MALDI-TOF mass spectrum of both samples at a mass to charge ratio of 466.5 Da, this peak corresponds to the TOABr impurity and proves that it exists in the final product in sufficient quantities to be detected by this technique.

The mass of impurity removed was measured by recording the intensity of the TOA^+ peak in the Micromass Liquid Chromatography Time of Flight Mass Spectrum of the fraction obtained from each 3 hour cycle. It was demonstrated that after 12 hours of extraction as little as 5×10^{-3} % of the impurity was present in the sample of nanoparticles. The solubility of the purified nanoparticles in an acetone-toluene mixture was compared to that of the unpurified nanoparticles. It was shown that the purified nanoparticles remain soluble at an acetone composition of 10%, whereas the unpurified material was completely insoluble at this solvent composition. In order to demonstrate the sensitivity of the nanoparticles to the presence of a small amount of TOABr, very small quantities of TOABr ($1.3 - 5.1 \times 10^{-4}$ M) were added to the solution. Upon addition of TOABr, the purified nanoparticles immediately became insoluble.

It was decided at this stage that in order to maximise the potential for size-separation studies and to improve the accuracy of solubility measurements, all samples of gold nanoparticles prepared by the two-phase synthetic technique would be purified by soxhlet extraction. The following subchapters present some of the findings made with regard to the effect of soxhlet extraction on the solubility of gold nanoparticles and on the mass spectroscopy analysis of the purified and unpurified particles.

3.2.2 Experimental

Dodecanethiol stabilized gold nanoparticles were synthesized as before by the two-phase technique using a 3:1 ratio of gold to thiol (further synthetic details are given in chapter 3.1.2). These nanoparticles were analyzed by UV-visible absorption spectroscopy, MALDI-TOF mass spectroscopy and Transmission Electron Microscopy (TEM). A 100 ml sample of the gold nanoparticles in toluene was then placed onto a cellulose soxhlet thimble of 25×100 mm and allowed to dry under standard laboratory conditions overnight. The thimble was then placed into the main chamber of the extractor; the acetone was refluxed by heating the flask and running cold water continuously through the exterior chamber of the condenser. The removal of the impurity was seen by a colour change in the acetone from colourless to a slight brown colour and then, eventually, to a darker brown colour. The extraction was run over four cycles, each of three hour duration, at the conclusion of each the solvent was replaced.

The analysis of the nanoparticles by UV-visible absorption spectroscopy (Figure 15) shows that there is no change in the characteristics (i.e. peak shape and position) of their spectra following soxhlet extraction. The same peak is observed in both spectra, the difference in absorbance intensity occurs as a consequence of the different concentrations of the samples of nanoparticles.

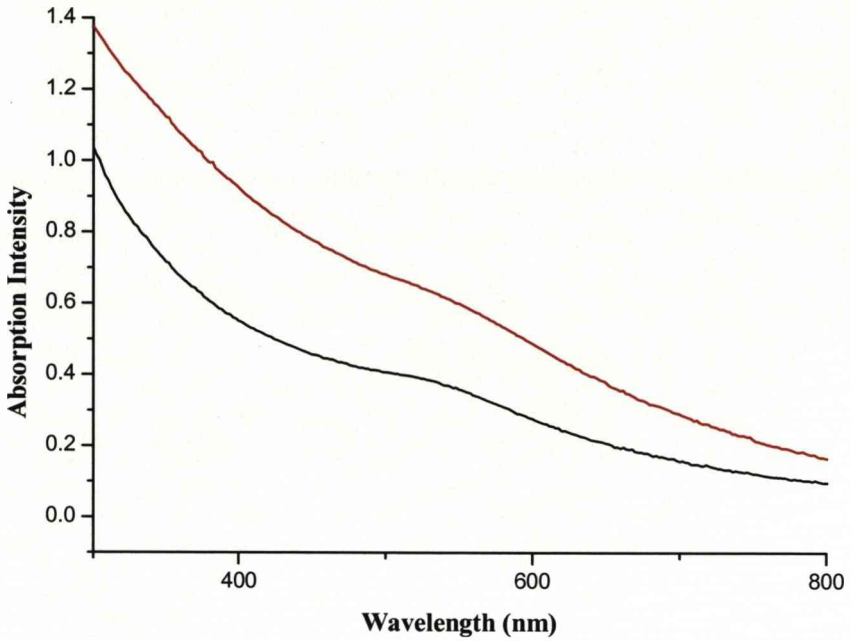

Figure 15. UV-visible absorption spectra of the purified (black) and as prepared (red) samples.

MALDI-TOF Mass Spectroscopy

By comparing the MALDI-TOF mass spectra of the two samples a clear difference in the two samples can be seen. MALDI-TOF mass spectroscopy is a very useful analytical tool in the characterization of alkanethiol stabilized gold nanoparticles. Mass spectra of metal nanoparticles have been used to identify which stable metal clusters are present within a sample. However, there are limitations with regard to using the technique to determine the relative proportions of each cluster within a sample, as the relative intensities of the peaks can vary significantly between several measurements of the same sample. In spite of this limitation, the technique remains a useful qualitative tool for identifying which clusters are present in a sample.

There have been several published examples [121-124] of the use of MALDI-TOF mass spectroscopy in the analysis of alkanethiol (and

similar ligand) stabilized gold nanoparticles, notably from the Royce W. Murray group [27, 53, 125]. The mass spectra of gold nanoparticles prepared by the two-phase synthetic technique are dominated by the presence of a peak corresponding to the phase transfer agent. It is often very difficult to obtain anything but this peak which is one of the reasons why this technique has not been fully exploited for the analysis of these particles.

Matrix Assisted Laser Desorption Ionisation – Time of Flight Mass Spectrometry is a technique commonly employed to characterize polymers and proteins due to a decreased amount of energy reaching the molecule (and, therefore, resulting in a decreased chance of fragmentation) compared to other mass spectroscopy (MS) techniques. Recently MALDI-TOF is increasingly being used in the characterization of metal nanoparticles [125]. Different 'magic number' size clusters correspond to particular molecular weights so the peaks of a mass spectrum correspond to the various stable magic number clusters which make up the sample.

MALDI-TOF MS utilises an ultraviolet absorbing matrix material which is mixed in excess with the sample to be analysed in a suitable solvent. The mixture is placed onto a sample probe tip. When the sample is exposed to vacuum conditions the solvent is removed which results in co-crystallized sample molecules homogeneously dispersed throughout the matrix. When the tip is irradiated by the laser pulse, the energy of the laser is transferred to the matrix which becomes partially vaporized. As a consequence of this the sample is carried into the vapour phase and charge is imparted to the sample molecules from the matrix. This is referred to as a 'soft' ionisation technique as the energy of the laser pulse is transferred to the matrix first which then imparts some of that energy to the sample which results in ionisation. This technique is used when samples frequently

fragment during ionisation with other MS techniques. The accuracy of the process is improved by repeating the process by repeated laser shots.

Detection of the ionized particles occurs as the particles move through the Time of Flight (TOF) analyser. Each molecule is subjected to the same potential energy difference but smaller particles will arrive at the detector in a shorter time than larger particles. The impact of the particles with the detector is recorded by a signal generated by the detector. The mass spectrum is essentially a recoding of the detector signal as a function of time. This spectrum is usually converted into a conventional mass spectrum due to the fact that a molecule of mass m and charge z is known to travel the distance to the detector in a time proportional to $(m/z)^{1/2}$.

In order to demonstrate the effect of purification, the MALDI-TOF mass spectra of two samples of dodecanethiol stabilized gold nanoparticles are presented (Figure 16). Both samples correspond to the same gold nanoparticles, however, the first spectrum (Figure 16A) was obtained for nanoparticles as prepared, the second spectrum (Figure 16B) corresponds to the same nanoparticles after four 3 hour long cycles of purification by soxhlet extraction, as described above. In spectrum A there are no obvious peaks which correspond to the clusters present in the sample; the only identifiable peak in this spectrum is that of the phase-transfer agent. This is a familiar result when analysing gold nanoparticles by this technique, the peaks corresponding to the metal clusters are often too weak to be detected. Spectrum B shows the measurement of the purified sample of gold nanoparticles, the separate peaks corresponding to the different clusters present in the sample can be easily identified. These peaks correspond to those identified in previous studies on metal clusters by mass spectroscopy and for a full analysis please refer to the characterization of dodecanethiol stabilized metal nanoparticles later in this chapter. The strong peak at around 460 Da corresponding to the phase transfer agent remains present but in a very much lower concentration compared to as prepared nanoparticles. This peak is caused by the impurity retained in the final

product. The presence of the TOA^+ ion is known to cause very strong peaks in MALDI-TOF mass spectra, even in low concentrations [71].

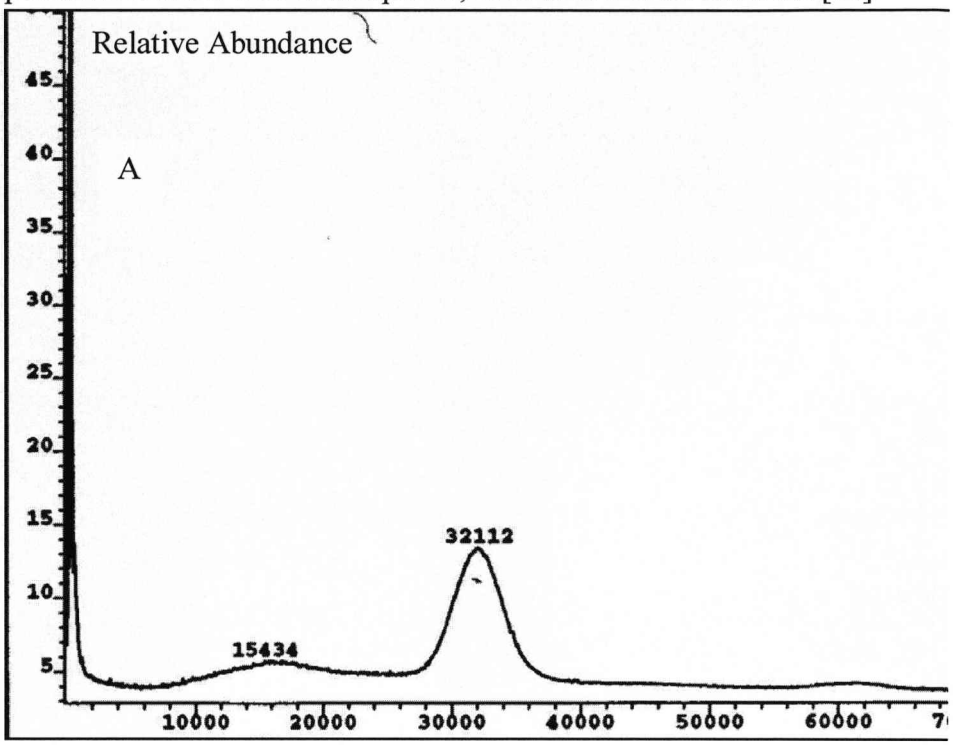

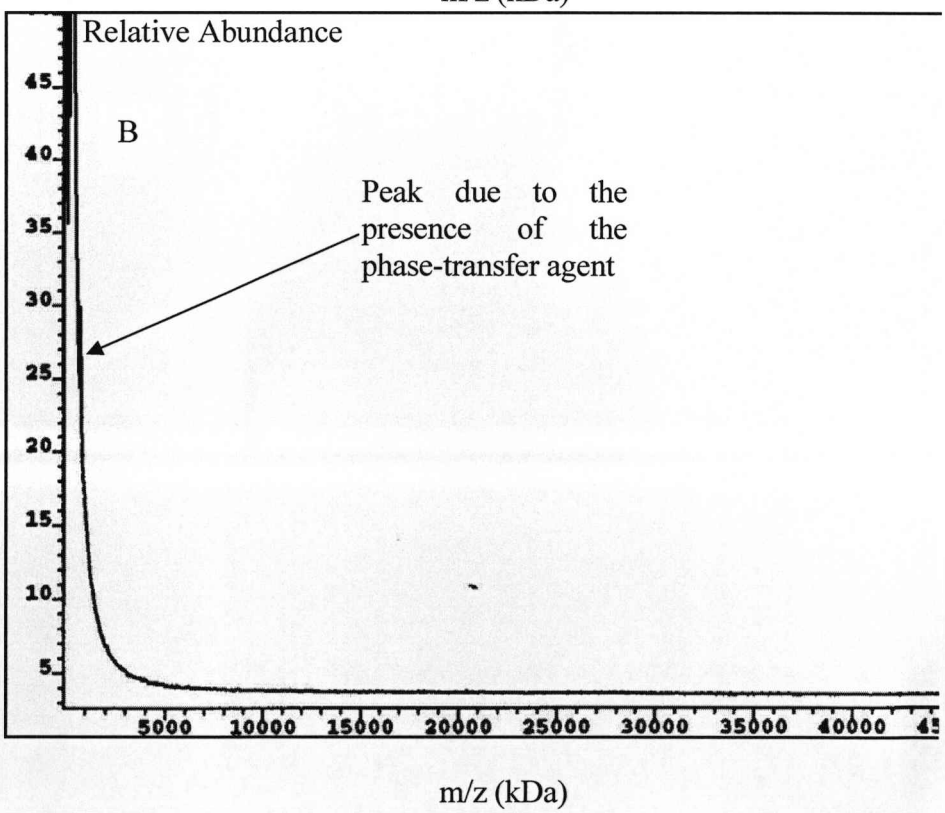

Figure 16 (previous page). The MALDI-TOF mass spectra obtained for the as prepared sample of soxhlet purified dodecanethiol stabilized gold nanoparticles (A) and the unpurified sample of the same nanoparticles (B).

The peaks corresponding to the metal nanoparticles seen in spectrum B compare well with those seen in publications [71] using this technique. It seems likely that the purification by soxhlet extraction allows analysis by MALDI-TOF mass spectroscopy due to an increase in the relative concentration of metal nanoparticles in the sample relative to the concentration of phase transfer agent. This purification technique is, therefore, particularly useful if MALDI-TOF analysis of the nanoparticles is required.

Transmission Electron Microscopy

Transmission electron microscopy (TEM) images of metal nanoparticles allow the determination of the average core size of nanoparticles captured in the image as well as the distribution of size (commonly referred to as the polydispersity) of the nanoparticles in the sample. In order to get reliable information about the average core size and polydispersity it is necessary to measure a representative portion of the sample by electron microscopy. This can be done by analyzing a large area of a TEM image with image processing application such as ImageJ [126].

TEM images of the nanoparticles were recorded at the Liverpool Electron Microscopy Centre using an FEI 120 kV Tecnai G 2 Spirit BioTWIN spectrometer. The basic principle of TEM is to use a beam of electrons, produced by heating a filament (Tungsten or LaB6 in this case) at voltages between 60 and 120 kV (100 kV was used for all Gold nanoparticle measurements), to resolve structures below 200 nm. The beam of electrons is fired through a vacuum tube towards the sample. Magnification and focus can be adjusted by a series of electromagnetic

lenses. The images are then resolved on a phosphor fluorescent screen and can then be recorded on camera (see Figure 17) [127].

It is necessary for the sample to be thin enough to allow electrons to pass through. Monolayers of gold nanoparticles in the size range 1-100 nm work suitably with TEM and can be placed onto TEM grids by evaporating a droplet of a solution of nanoparticles onto the grid.

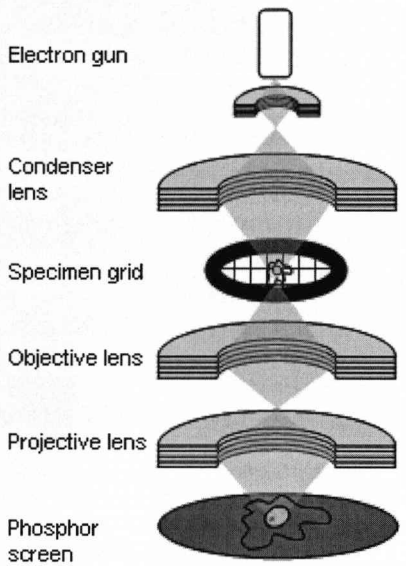

Figure 17. Schematic view of a Transmission Electron Microscope highlighting the key stages of the process [128].

Analysis of a sample of dodecanethiol stabilized gold nanoparticles dried onto a carbon coated copper grid by TEM shows that there is a wide range of nanoparticle diameters present in the sample in the range 1-10 nm (Figure 18). The average core diameter of these nanoparticles has been determined (from analysis of the TEM images) as being 2.4 nm. The polydispersity of nanoparticles produced by conventional synthetic techniques is one of the key concerns of this chapter. As mentioned in the introduction, in order to maximize the potential electronic applications of

noble metal nanoparticles, much higher degrees of monodispersity are necessary. Another problem raised by the polydispersity of these nanoparticles is the difficulties that arise in obtaining solubility data as a consequence. Solubility measurements must be made on highly monodisperse samples, otherwise the data obtained will only be valid for a sample with exactly the same distribution of sizes as that measured.

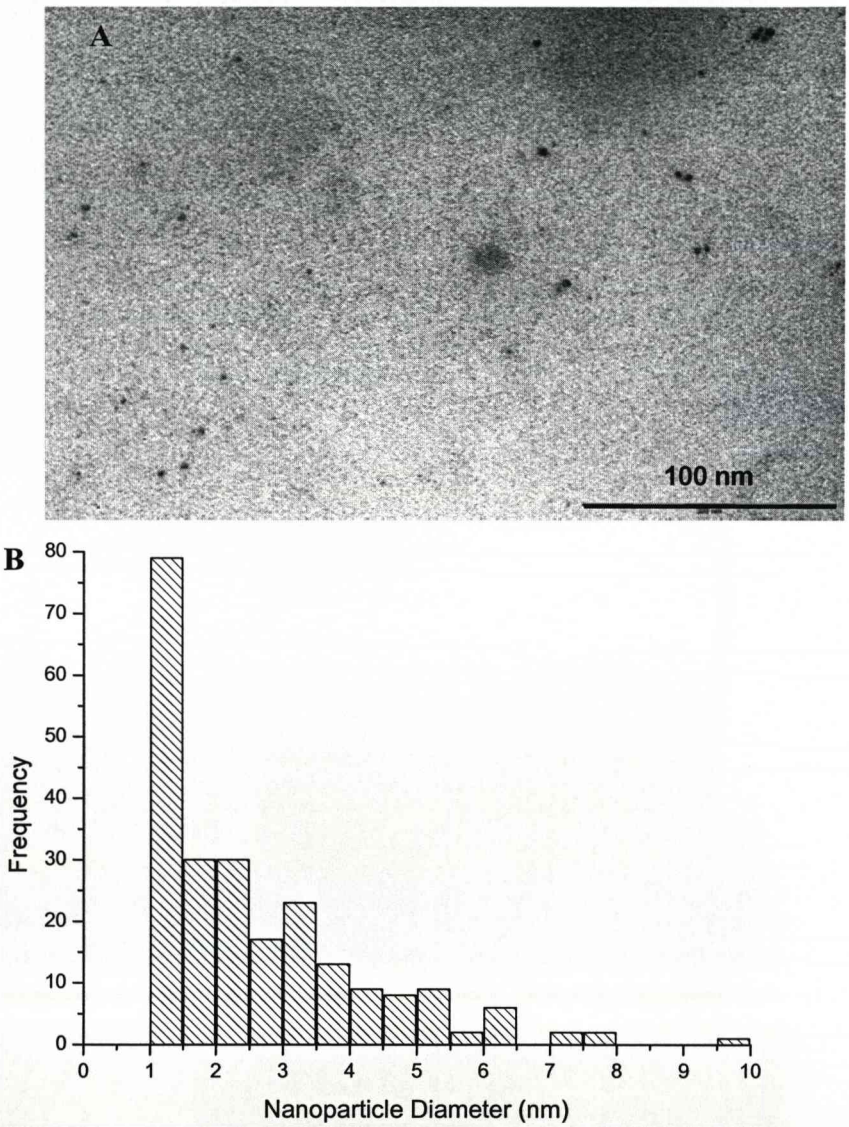

Figure 18. TEM image of dodecanethiol stabilized gold nanoparticles prepared with a 3:1 gold:thiol ratio (A) (scale bar equals 100 nm) and the distribution of sizes present from an analysis of the images of this sample (B).

3.2.3 Solubility Measurements

As well as improving the ease with which nanoparticles can be characterized by MALDI-TOF mass spectroscopy there is another major advantage to using soxhlet purification. As mentioned above, the solubility of purified nanoparticles in acetone-toluene mixtures was shown to be greater than that of unpurified samples. In order to determine the improved solubility of the nanoparticles following purification, a repeat of this simple experiment was performed as well as another simple study of the variation in solubility in supercritical ethane.

A series of acetone-toluene mixtures were prepared starting with 100 % acetone and ending with 100 % toluene, the proportion of toluene was increased in 10 % increments (i.e. the second solution was 90 % acetone and 10 % toluene). A small amount of the "as prepared" and the purified samples of gold nanoparticles were separately tested in each of these mixtures. The undissolved nanoparticles were collected by filtration and weighed. A significant observation was recorded from these measurements; a proportion of the purified sample dissolved, even when the volume of toluene in the solvent mixture was at the 10 % level. By way of contrast the unpurified nanoparticles became insoluble at a solvent mixture composition of 50 % toluene. The purified sample became completely insoluble in the 10 % toluene mixture upon addition of minute quantities ($1 - 5 \times 10^{-4}$ M) of TOABr to the mixture. These results correspond with the published findings [72] but these tests were based closely on those conducted in the paper so this is to be expected. The next test will be more relevant to this project as it assesses the effect of the purification on the solubility of gold nanoparticles in supercritical ethane.

Solubility measurements were recorded by drying a standard volume (2 ml) of a stock solution of the alkanethiol stabilized gold nanoparticles onto the inside of an open ended glass vial. The solvent was

allowed to evaporate overnight and the vial was then carefully (carried in a sample jar and moved with tweezers) weighed and placed in a pressure vessel. The pressure vessel was filled with supercritical ethane to the desired pressure (see Chapter 4 for more details about this process) and then isolated for 18 hours. The fluid was then released through a layer of acetone (or deionised water), some dissolved material was expected to precipitate in this layer and some was expected to precipitate inside the vessel before depressurization so the inner walls were washed with toluene and the washings were combined with any nanoparticles recovered from the acetone layer. The sample vial containing the undissolved nanoparticles was then carefully reweighed and the dissolved and undissolved residues were then analysed by a number of techniques.

The solubility measurements in supercritical ethane were recorded by two independent techniques. As well as recording the weight change of the sample (as described above), the results were verified by comparison of the UV-visible absorption spectrum of the nanoparticles before placement into the high pressure vessel (in 5 mL of toluene) with that of the recovered, undissolved nanoparticles (performed by washing the nanoparticles from the inside of the vial into 5 mL of toluene). The interior of the high pressure vessel was also washed out with toluene, the solvent was then evaporated and any recovered material combined with nanoparticles which precipitated in the deionized water layer and dissolved in 5 mL of toluene for analysis.

The solubility measurements of the unpurified dodecanethiol stabilized gold nanoparticles showed that there was an insignificant weight change over the full range of pressures (50 – 300 bar) tested. The absorption spectra supported this as there was minimal change between the spectra of the original sample and that of the undissolved sample after periods of time varying between 12 hours and 3 days in the high pressure vessel. The same procedure was repeated with unpurified octanethiol stabilized gold nanoparticles. A similar outcome was achieved, the mass

and the absorption spectra of the undissolved nanoparticles changed minimally at all pressures and over all time periods.

The same procedure was repeated for a sample of Soxhlet-purified gold nanoparticles. For the first time in the project alkanethiol stabilized gold nanoparticles were observed to dissolve in supercritical ethane. Dissolved nanoparticles were observed at all pressures, by both weight change measurement and by comparison with the absorption spectra of the nanoparticles added to the vial and those recovered from the high pressure vessel at the end of the experimental run. Coloured solutions of precipitated nanoparticles were recovered from the vessel across the range of pressures investigated. When samples from these experiments were analysed (in a standard volume of toluene) the absorption spectra obtained for the dissolved samples were typical of those expected for alkanethiol stabilized gold nanoparticles in the size range 2-5 nm due to the presence of a plasmon band absorption at around 520 nm (Figure 19). This was a very significant observation as the spectra of the nanoparticles originally placed into the vessel had only a very weak plasmon band absorption (Figure 15, black line) which indicated the average core diameter of the original nanoparticles was somewhat smaller than that of the sample of nanoparticles which dissolved in the supercritical ethane.

Such was the improvement in solubility between the two sets of (essentially identical) nanoparticles, it was decided that Soxhlet extraction would be incorporated into the preparation of all samples of gold nanoparticles prepared by the two-phase synthetic technique.

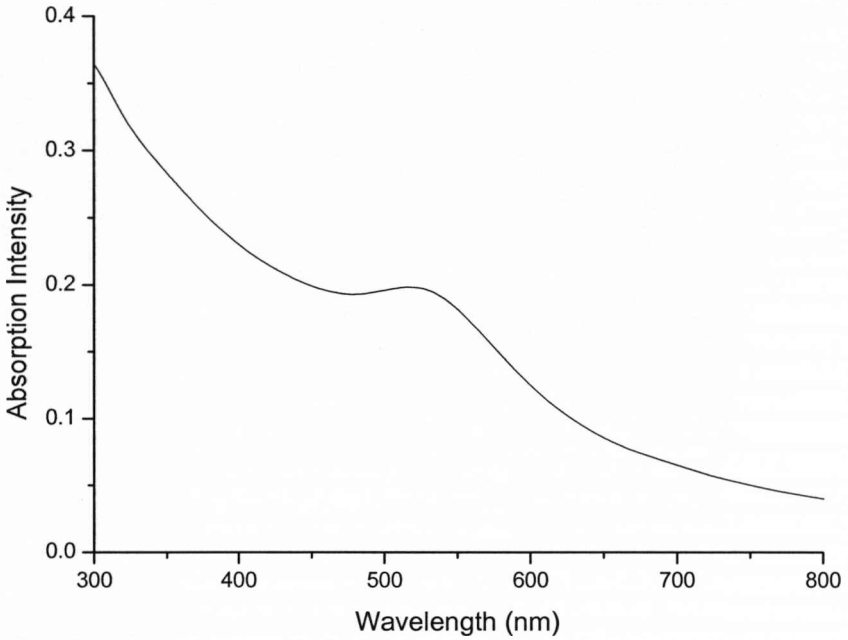

Figure 19. UV-Visible Absorption Spectrum alkanethiol stabilized gold nanoparticles which dissolved in supercritical ethane at a pressure of 150 bar over a time period of 12 hours.

3.3 Variation of the Alkanethiol Stabilizing group

3.3.1 Synthesis of Pentanethiol Stabilized Metal Nanoparticles

The versatility of the two-phase synthesis of gold nanoparticles was established in the introduction [4, 37]. In order to show some of the possible variations on the basic technique the alkanethiol functional group was varied and the effect on the stability and solubility of the products as well as the average core diameter (and size distribution) of the nanoparticles were measured. It is known [129, 130] that, in general, the stability of alkanethiol stabilized gold nanoparticles decreases with length of the alkyl chain beyond C12 of the ligand. This occurs due to less effective steric stabilization of the metal core by the adsorbed ligand

monolayer and the fact that longer chain alkanethiols are more strongly bound to the gold core.

The basic preparation technique does not vary from that used to prepare nanoparticles with dodecanethiol functional groups. Each basic synthesis was followed by Soxhlet extraction in order to maximise the solubility of the nanoparticles produced [72].

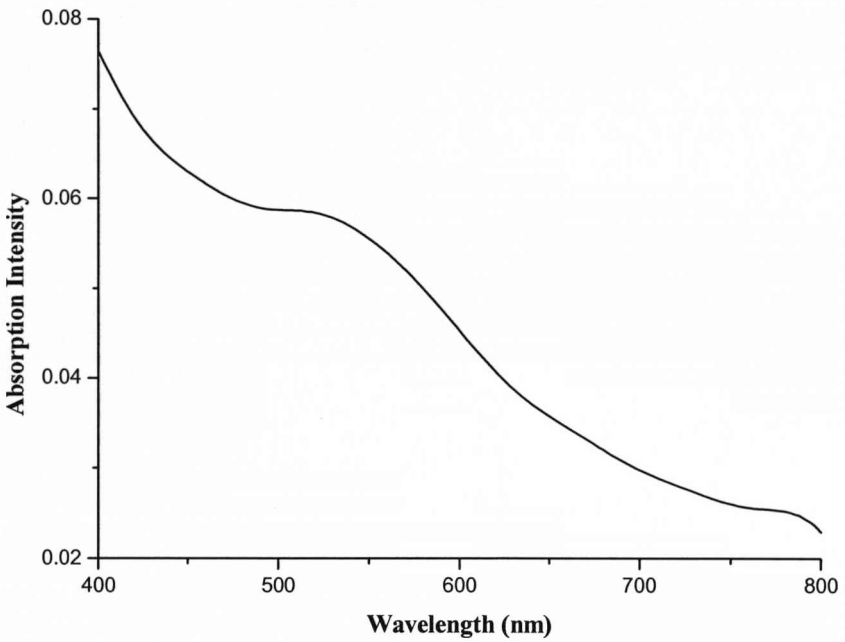

Figure 20. The UV-visible absorption spectrum for a sample of pentanethiol stabilized gold nanoparticles prepared via the two-phase reduction technique.

Figure 20 shows the UV-visible spectrum for a sample of pentanethiol stabilized nanoparticles (again produced with a 3:1 gold:thiol ratio) after Soxhlet extraction. There is no qualitative difference between this spectrum and that of a sample of gold nanoparticles of the same size stabilized with a different alkanethiol. The spectrum is defined by the electronic behaviour of the metal core of the nanoparticles. The presence of the plasmon band absorption at around 520 nm shows that the average core

diameter of nanoparticles was in the 2-5 nm range. In order to obtain further information about the core diameters it was necessary to analyse this sample with TEM.

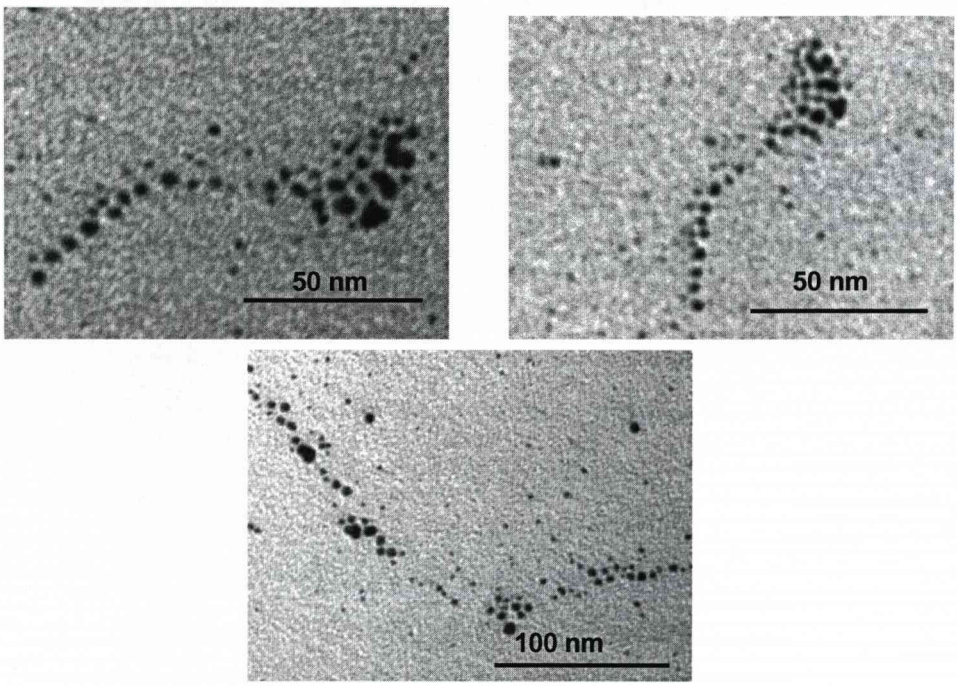

Figure 21. A selection of TEM images of the sample of pentanethiol stabilized gold nanoparticles prepared via the two-phase reduction technique. The scale bars read 100 nm.

Figure 21 shows some of the TEM images obtained for this sample of pentanethiol stabilized gold nanoparticles. From a simple inspection of these images it seems that there is a range of particle sizes present within the sample, this is verified by ImageJ [131] analysis of the images (Figure 22). Another interesting characteristic is the tendency for some of the nanoparticles to come together in 'bands', it is possible that the nanoparticles have formed a network due to extensive interdigitation between alkanethiol chains. As a consequence of the short length of the alkyl chain of the stabilizing ligand it is likely that the metal cores will come into close contact and the resulting Van der Waals attraction may result in aggregation of the sample over a short period of time.

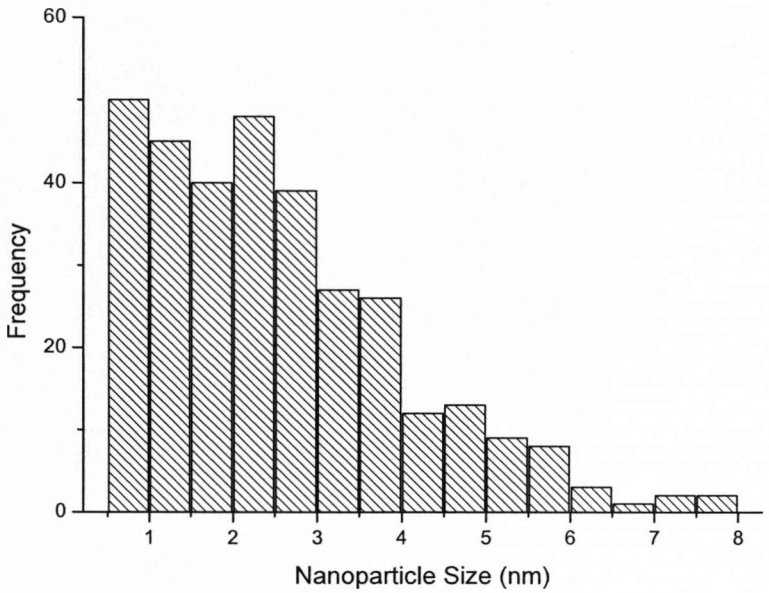

Figure 22. The analysis of one of the TEM images, using ImageJ [126] software, of the sample of pentanethiol stabilized gold nanoparticles prepared via the two-phase reduction technique showing the size distribution of nanoparticles.

The size distribution histogram shows that there is a large degree of polydispersity in the sample. The UV-visible absorption spectrum shows evidence of plasmon band absorption which is accounted for by the presence of gold nanoparticles larger than 2 nm in the TEM images. The plasmon band absorption is weak which may be explained by the fact that many of the nanoparticles producing the band are near the lower limit of 'free electron' behaviour in gold nanoparticles [10, 37]. It is also likely that the plasmon absorption is smoothed due to the fact that there are a number of nanoparticles below 2 nm contributing to the absorption spectrum. The average core diameter determined from analysis of the TEM images is 2.3 ± 3.4 nm.

A sample of these nanoparticles was placed into the open ended glass vial, weighed and then placed and isolated in the pressure vessel.

After subjecting the sample to a range of pressures of supercritical ethane it was clear that these nanoparticles are quite unstable under these conditions. When the glass vial was removed at the end of the experiment the nanoparticles remained dried to the interior of the vial but now had a metallic lustre. The nanoparticles were no longer soluble in toluene and it was assumed that aggregation had occurred as a consequence of the conditions the nanoparticles were subjected to in the high pressure vessel. This aggregation can occur due to the increased temperature and pressure and the poor stabilization afforded by pentanethiol ligands which allows the attractive forces between the cores to result in aggregation.

3.3.2 Synthesis of Propanethiol Stabilized Metal Nanoparticles

Propanethiol stabilized gold nanoparticles were also prepared. Most research based on alkanethiol stabilized gold nanoparticles has used nanoparticles stabilized by larger alkanethiols due to the additional steric stabilization afforded to the nanoparticles. A sample of propanethiol stabilized gold nanoparticles was prepared, characterized and then placed in supercritical ethane for a set time in order to compare the solubilities of these nanoparticles with those of the more commonly studied, longer alkanethiol chain (C8-C12) stabilised gold nanoparticles.

The nanoparticles were, as with other alkanethiols, prepared by the two-phase synthesis technique using a 3:1 gold:thiol ratio [4]. The nanoparticles were then washed in an excess of ethanol (in order to remove excess thiol) and dissolved in toluene. The excess TOABr salt was removed by Soxhlet extraction [72]. The nanoparticles were characterised by UV-Visible absorption spectroscopy (Figure 20) and TEM.

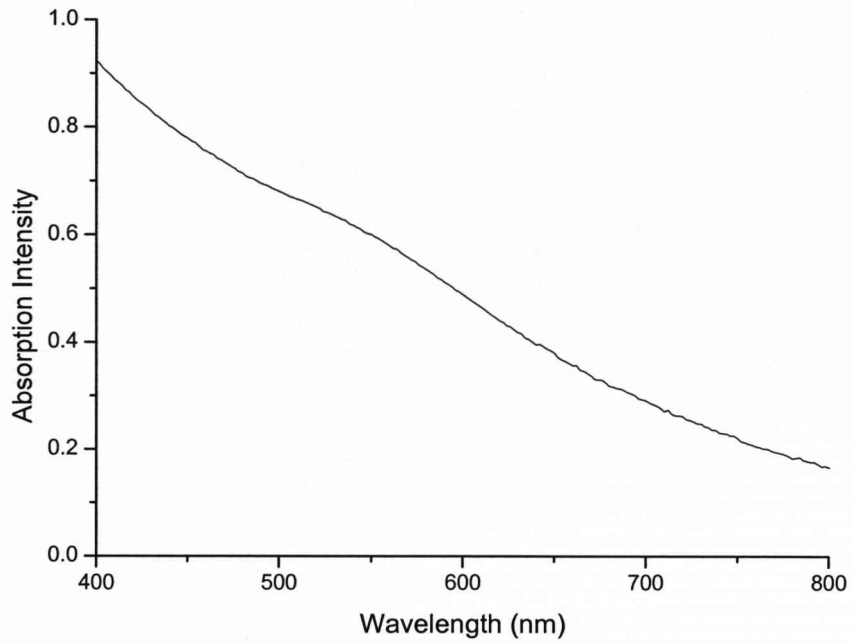

Figure 23. UV-visible absorption spectrum of propanethiol stabilised gold nanoparticles dissolved in toluene.

The UV-visible absorption spectrum (Figure 23) shows a very weak plasmon band absorption which indicates a sample of nanoparticles with a small average core diameter (below around 2 nm as above this size the plasmon band absorption would be much more intense). In order to determine the precise average core diameter and the distribution of sizes present in the sample TEM images were analysed (Figure 24).

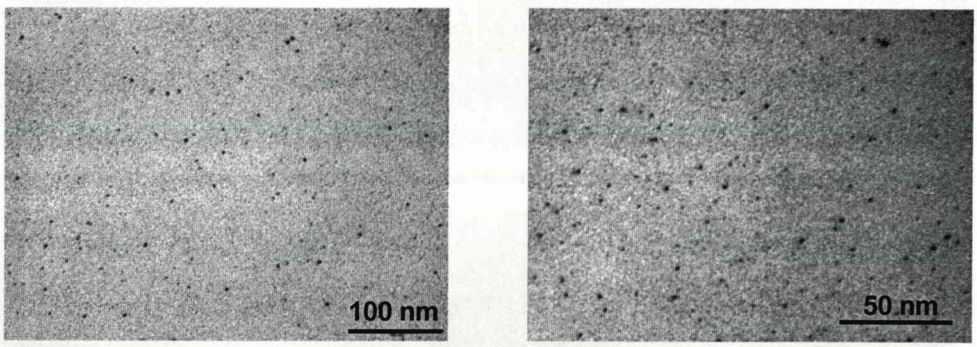

Figure 24. A selection of TEM images of the sample of propanethiol stabilized gold nanoparticles prepared via the two-phase reduction technique.

The TEM images show what appears to be an approximately monodisperse sample of nanoparticles. Figure 25 shows the distribution of core diameters determined from the TEM images using the ImageJ software [126]. One of the considerations of using the two-phase synthesis is the difficulty with which a monodisperse sample can be prepared. Higher degrees of monodispersity are desirable for use in potential electronic applications. One of the key issues is the difficulty in reproducing monodisperse syntheses of alkanethiol stabilized gold nanoparticles as the polydispersity is so sensitive to reaction conditions.

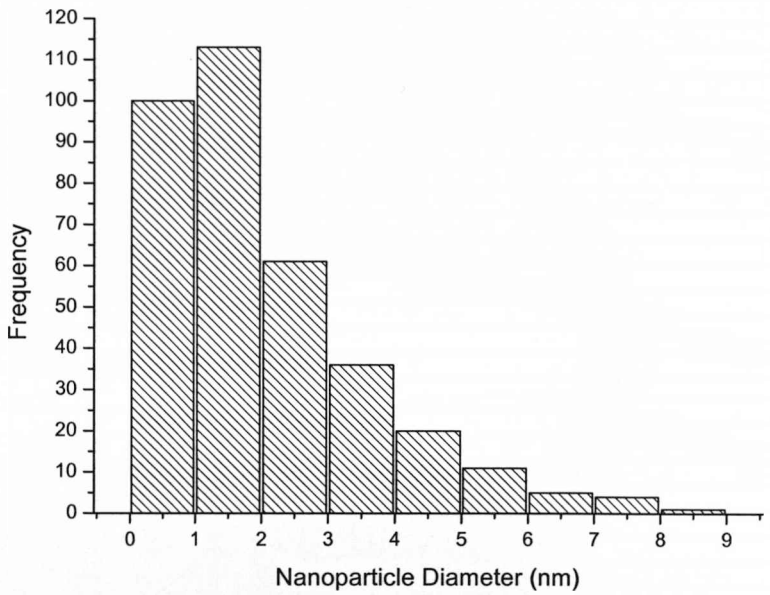

Figure 25. An analysis using ImageJ software [126] of the core diameter sizes present within the TEM image captured for a sample of propanethiol stabilized gold nanoparticles.

There are difficulties with using nanoparticles stabilized by small chain alkanethiols due to the decreased stability of the nanoparticles. The primary mechanism of stabilization by alkanethiol ligands is steric so the shorter the alkyl chain length, the less efficient the stabilization effect. This effect was observed for both pentanethiol and propanethiol stabilized gold

nanoparticles. When left under standard laboratory conditions aggregates were observed to form within several months of synthesis. When placed in the high pressure rig for testing with supercritical ethane both samples of nanoparticles (i.e. those stabilized by propane- and pentane- thiol) aggregated to an extent. This made determining solubilities very difficult and raised other practical issues, the cleaning of the vial at the end of the process being one. It was decided that as a consequence of the practical difficulties and the inability to effectively characterize the undissolved sample, the main study would use octanethiol and dodecanthiol stabilized gold nanoparticles.

3.4. Other Synthetic Techniques

3.4.1 Synthesis of Gold Nanoparticles via the Citrate Reduction Technique.

Another technique [1, 2] commonly used for preparing stable noble metal nanoparticles is the reduction of a metal salt in an aqueous solution of sodium citrate. As in the two-phase technique, hydrogen tetrachloroaurate is commonly used as the metal salt. The nanoparticles produced by this technique have been shown to be very stable (due to the electrostatic stability provided by the adsorbed ligands), more monodisperse (however, silver nanoparticles produced by this technique are likely to be more polydisperse than their gold analogues [132]) compared to particles prepared by many alternative approaches and with a degree of size control. The citrate reduction is commonly employed in the preparation of gold nanoparticles but has been shown to be effective in the synthesis of stable samples of nanoparticles of various metals, including silver [132].

The citrate reduction technique has a number of advantages including the monodispersity of the product, the ability to customize the

average core size of the product by modifying the ratio of gold salt to reducing agent and the ability to synthesize stable nanoparticles in the 10-100 nm size range. There are also several disadvantages to this technique including: a significant increase in the polydispersity and loss of defined shape occur in the synthesis of nanoparticles with a core diameter above around 30 nm, the inability to produce stable gold nanoparticles in the size range 1-10 nm (i.e. the sizes that much of the current interest in the field is focused on) and the fact that the product is not soluble in nonpolar, organic solvents, such as hexane and ethane [1, 2, 132]. Citrate stabilized gold nanoparticles were prepared by bringing 20 mL of an aqueous, 1.0 mM solution $HAuCl_4$ to the boil and then adding 4 mL of a 2 % of tri-sodium citrate dihydrate. The solution rapidly turned a dark brown colour which soon became a very deep red, corresponding to the strong plasmon band resonance typical of gold nanoparticles above around 5 nm (2-4 nm gold nanoparticles exhibit weaker plasmon band absorptions).

The nanoparticles were characterized by Transmission Electron Microscopy (Figures 26 and 27) and UV-visible absorption spectroscopy (Figure 25). An analysis, using ImageJ software [126], of the high magnification TEM image produces an average core diameter of 28.71 nm. A similar analysis of a lower magnification image gives an average core diameter of 24.11 nm.

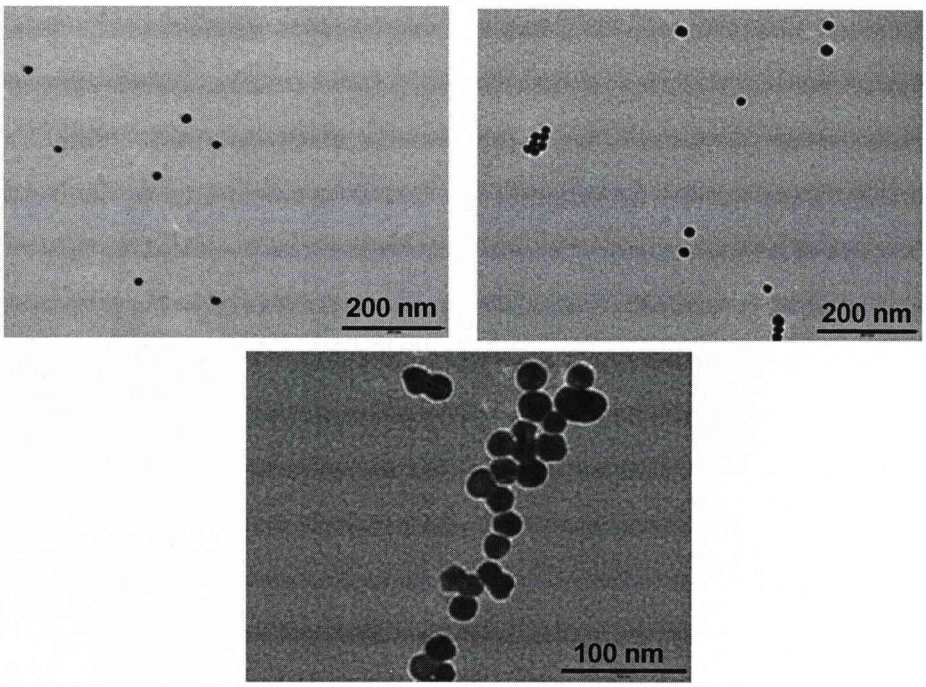

Figure 26. A selection of TEM images captured for a sample of gold nanoparticles prepared by citrate reduction. The scale bar reads 200 nm in the top images and 100 nm in the bottom image.

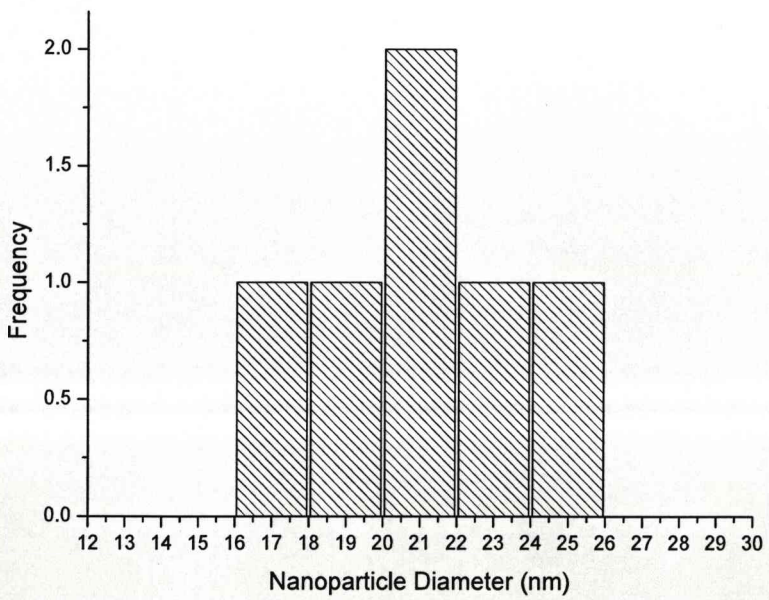

Figure 27. Analysis, using ImageJ software, of a TEM images captured for a sample of gold nanoparticles prepared by citrate reduction.

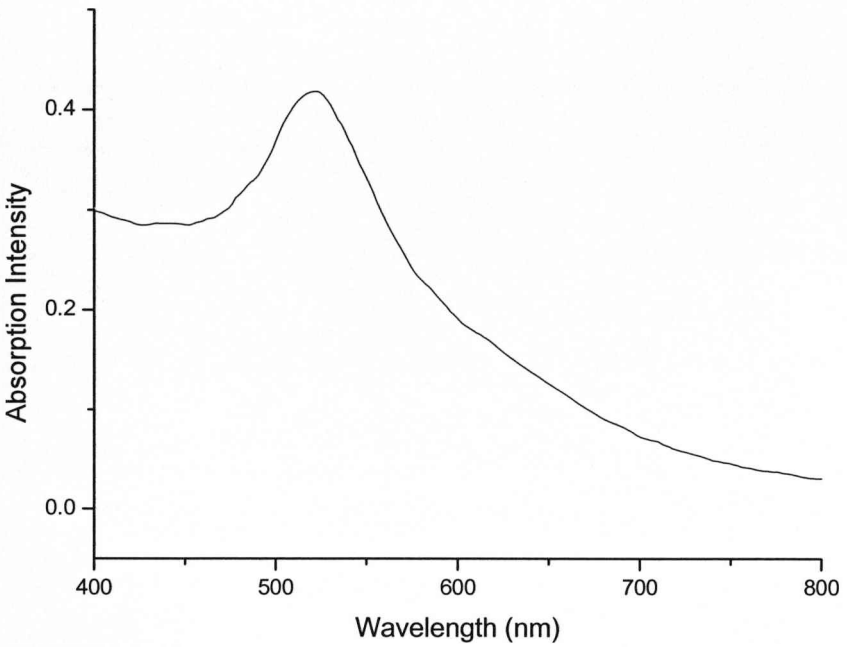

Figure 28. UV-visible absorption spectrum of a sample of gold nanoparticles prepared by citrate reduction.

The UV-visible absorption spectrum (Figure 28) shows a well defined maximum absorption at a wavelength of 522 nm, the plasmon band absorption. The average core diameter of the nanoparticles prepared by this technique appears to be approximately 24 nm but it is difficult to obtain accurate values of core diameter and polydispersity from an analysis of the TEM images which scan such small quantities of the total synthesised sample. Complementary analysis was conducted by Dynamic Light Scattering (DLS).

Dynamic Light Scattering

Dynamic light scattering makes use of fluctuations of light scattered by particles in a medium due to Brownian motion. The fluctuations are random and are related to the translational diffusion coefficient D and, therefore, to the diameter of the particles [133]. The

use of DLS as a tool in size determination of nanoparticles has become popular in the past decade. The technique offers several advantages over microscopy based analysis, including the fact that DLS is able to analyze a large sample of material in solution, whereas most microscopic techniques require considerable time and effort to obtain representative images, there is also the possibility of less accurate results from microscopy unless a large number of particles are captured in TEM images.

The radius of the particles is calculated by determination of the diffusion coefficient, D. D is determined during the analysis of the behaviour of fluctuations in the scattered intensity analyzed by the 'autocorrelation function' From the diffusion coefficient the radius of the particles can be calculated from the Stokes-Einstein equation (equation 6):

$$D = (k_b T/(6\Pi\eta R))C_S \qquad \textbf{(6)} \qquad [133]$$

where k_B is the Boltzmann constant, T is the temperature, η the solvent viscosity and C_S is the Cunningham correction factor [133]. This correction factor takes into account the increased mobility of the particle in a gas due to non-continuum effects.

The process makes use of measurements based on the physical behaviour of all particles used in the sample unlike techniques which use a small section of the entire sample (such as the image captured by an electron microscope). DLS also provides data based on the condition of the nanoparticles in solution rather than the dry form of the nanoparticles which may be subject to additional aggregation or degradation. Electron microscopy, in general, requires a dry sample of material placed onto a metallic grid. There are limitations in the use of DLS. One of the biggest considerations when interpreting a size determined by DLS is that the size obtained is the product of a mathematical function operated on the light scattered by the sample rather than a direct physical measurement. It

is possible that the mathematical model used to predict the light scattering behaviour of the nanoparticles analyzed isn't suitable in all cases.

DLS was performed on a Viscotek 802 DLS particle sizer (830 nm light used) with the measurement cavity set to a temperature of 298.15 K and the laser intensity set to produce a baseline count of 300 k/s. Each sample was placed in a clean and dry 10 μL 90° quartz glass cuvette which was placed into the instrument. The sample was left for 5 minutes to equilibrate and once the temperature reading and photon intensity base line had stabilized ten repeat measurements of five second intervals were taken and analyzed using OmniSIZE^{TM} software.

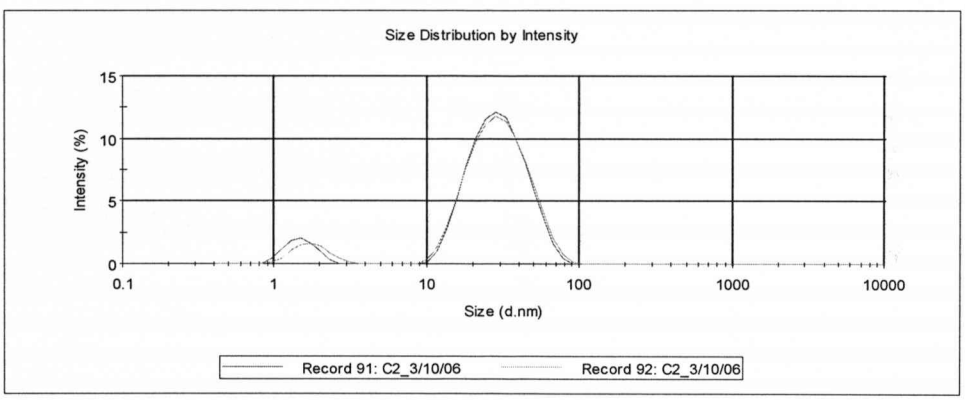

Figure 29 DLS analysis of the sample of gold nanoparticles prepared by citrate reduction.

The DLS intensity distribution (Figure 29) suggests an average core diameter of 31.7 nm and that the sample is relatively polydisperse. The intensity distribution of DLS data is likely to show a more polydisperse result than anticipated as the intensity of light scattered in DLS is related to the radius of spherical particles and for larger particles light is scattered much more intensely.

The average core diameter of the nanoparticles produced by the citrate reduction can be varied by modifying the ratio of gold to reducing agent (allowing a similar method of control over product size to the two-phase reduction technique). The concentration of aqueous citrate solution added to the solution of hydrogen tetrachloroaurate was halved and the average core diameter and UV-visible absorption spectrum (Figure 30) of the products measured.

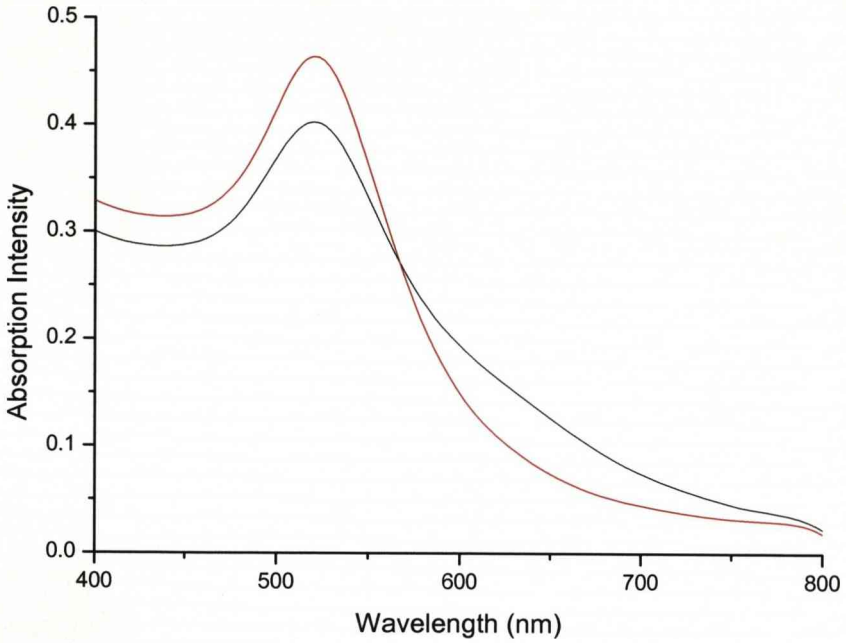

Figure 30. A comparison of the UV-visible absorption spectra of the sample of gold nanoparticles prepared by reduction with 1 (red) and 2 (black) % citrate solutions.

The UV-visible absorption spectra of both samples are shown in Figure 30, it can be seen that that the nanoparticles produced by the more dilute citrate solution produce a higher absorbance maximum (which may suggest a larger average core diameter than the particles prepared with a more concentrated citrate solution). Additional information is gained from DLS analysis of these nanoparticles.

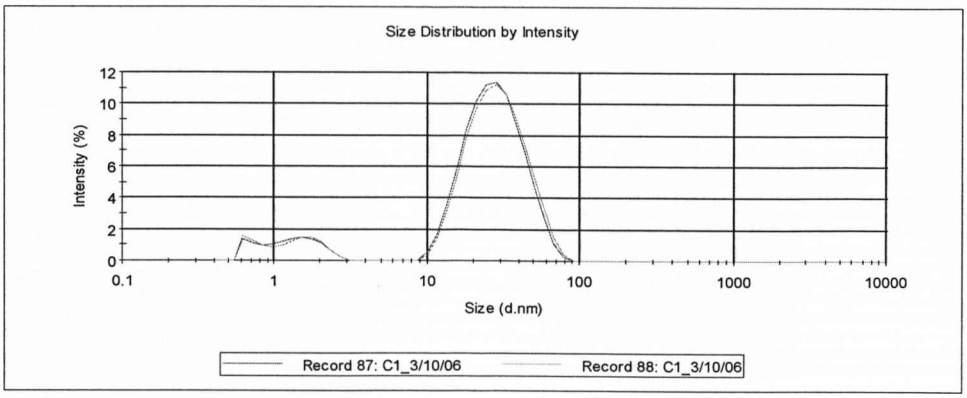

Figure 31. DLS analysis of the sample of gold nanoparticles prepared by reduction in a 1% Citrate solution.

Analysis of a solution of nanoparticles by DLS (Figure 31) suggests that the average core diameter of this sample was approximately 30.7 nm. The core diameter is essentially unaffected by the change in gold:reducing agent ratio according to this result which is inconsistent with expectations. The variation in the absorption maximum in the UV-visible spectrum suggests that there is a difference in the average core diameter of the two samples of nanoparticles.

In summary, the citrate technique is an effective method for producing stable gold nanoparticles in the size range of 10-100 nm. It is possible to modify the size of the core diameter by variation of the gold:thiol ratio. As citrate stabilized nanoparticles are insoluble in alkanes such as ethane an alternative supercritical fluid would have to be used such as supercritical carbon dioxide.

3.5 Summary

This chapter has summarized the synthetic approaches used to prepare samples of gold nanoparticles for solubility testing. The two-phase reduction of a gold salt by sodium borohydride in the presence of an

alkanethiol leads to the formation of sterically stabilised gold nanoparticles. The size of the product could be varied by changing the gold:thiol ratio during synthesis. The products had a reasonable degree of monodispersity which compares very well with many of the alternative synthetic techniques for producing nanoparticles. Smaller chain alkanethiols appear to be less effective at stabilising gold nanoparticles, these nanoparticles tend to aggregate over shorter periods of time (less than six months under standard laboratory conditions) compared to alkanethiols with a chain length of C8 and above. This finding is supported by studies in relevant literature [129, 130] Nanoparticles stabilised by shorter chain alkanethiols also tend to aggregate when subjected to supercritical ethane. It is likely this occurs at the elevated temperatures in the pressure vessel this process occurs at an accelerated rate as the increased kinetic energy of the nanoparticles is greater than the energetic barrier created by the stabilising ligands. The Au-S bond can also be cleaved at elevated temperature which leaves the nanoparticles unprotected from aggregation As expected this effect is most pronounced for shorter chain alkanethiol ligands as the strength of the Au-S bond decreases with decreasing alkane chain length. Literature studies suggest that C12 is the chain length for an alkanethiol ligand stabilizing a gold nanoparticle as the effect of increasing Au-S bond strength is offset by the fact that weakly bound multilayers of ligands form when larger chain alkanethiols are used which hinders the development of 3-D superlattices [4, 129, 130].

It was discovered at an early stage that the solubility of gold nanoparticles in supercritical ethane is significantly improved by incorporating a soxhlet extraction step into the synthesis. By removing some of the tenaciously bound tetraoctlyammoniumbromide impurity the solid nanoparticles becomes much more soluble in a toluene-acetone mixtures due to the loss of the stabilization of the solid form which occurred as a consequence of both electrostatic interactions between the impurity and the metal particles and the interdigitation of the alkyl chains

of the stabilizing ligands and those of the impurity which results in steric stabilization of the solid form of the nanoparticles.

Basic solubility testing on a range of metal nanoparticles shows that the only nanoparticles with a significant degree of solubility are those which have been purified by Soxhlet extraction. The extra stabilization of the solid form by the tertiary butyl ion impurity raises the Gibbs energy of solubilisation which results in a greatly decreased solubility in supercritical fluids, especially for larger nanoparticles as the increase in energy is related to the core diameter. Purified nanoparticles stabilized by dodecanethiol and octanethiol ligands showed the best solubility in supercritical ethane. It is likely that the additional steric stability of longer chain nanoparticles prevents aggregation of the nanoparticles in supercritical conditions.

Gold nanoparticles larger than 10 nm have been prepared by the citrate reduction technique. These nanoparticles are stabilized by electrostatic effects, and as no phase transfer agent is used in the synthesis there is no need for a soxhlet extraction step. A simple test to demonstrate the effect of varying the gold:reducing agent ratio was performed. The particles were not tested in the high pressure vessel as they are insoluble in ethane due to the nature of the stabilizing ligand. It is possible that the particles may be analysed in the same way using CO_2 as the supercritical fluid but that was beyond the scope of this study.

Chapter Four
The Separation of a Sample of Alkanethiol Stabilized Gold Nanoparticles

4.1 A New Approach to Separation

4.1.1 Introduction

There are a number of synthetic procedures used to prepare stable metal nanoparticles [1, 2, 4, 37], several of these techniques were discussed in earlier chapters (Chapters 1-3). One of the issues surrounding the use of these techniques is the difficulty to produce highly monodisperse samples of metal nanoparticles. The preparation of metal nanoparticles using established synthetic techniques such as the 'two-phase' reduction of Au(III) in the presence of an alkanethiol [4] or the citrate reduction of Au(III) [1] can lead to products with a range of polydispersities. A number of factors during synthesis influence the core diameters and the range of sizes produced. As well as the ratio of starting materials (specifically the gold to thiol ratio), the rate of agitation, reaction temperature and the time taken to add the reducing agent can have an influence on the average core diameter and polydispersity of the products [4, 26, 31, 37].

The unique electronic properties of stable metal nanoparticles play a major role in potential future applications [8, 14, 16, 134]. In order for this potential to be realised it is necessary to have precise control of the average core size and the degree of monodispersity during synthesis of nanoparticles. Although the previously described techniques have relatively good degrees of control over core diameter and polydispersity it is still necessary for this to be improved. As the electronic properties of metal nanoparticles are size dependent the presence of nanoparticles with a core diameter slightly different to the average core diameter can lead to a number of distinct, different responses to electromagnetic stimuli from this single sample [8, 26, 37]. This behaviour is undesirable as they make it impossible to maximise the rich potential of these materials in usable applications. Highly monodisperse samples of stable metal nanoparticles are needed since these samples have defined, predictable electronic properties.

In order to produce nanoparticles suitable for applications which make use of these electronic properties new techniques are being developed which lead to greater control over the core diameter and higher degrees of monodispersity in products. One of the approaches used to achieve this goal is to synthesize metal nanoparticles and then 'fractionate' them into monodisperse samples by a number of techniques [48, 51] (a more complete discussion of the techniques used to fractionate polydisperse samples was presented in Chapter 2.1.2). The use of supercritical fluids in the separation of mixtures of nanoparticles has been previously demonstrated [19, 60, 135, 136] but their use in separating a single sample of polydisperse nanoparticles into individual size fractions is yet to be demonstrated. This chapter demonstrates the potential of using supercritical fluid to extract individual size fractions from a single polydisperse sample of metal nanoparticles.

4.1.2 Experimental

An aqueous solution of hydrogen tetrachloroaurate (0.32 g, 0.03 M) was mixed with a solution of tetraoctyl ammonium bromide in toluene (2.21 g, 0.05 M), dodecanethiol was then added (the molar ratio of gold to thiol was 3:1). An aqueous solution of sodium borohydride (25 mL, 0.01 mol) was rapidly added to reduce the $AuCl_4^-$ ions. Following agitation the organic phase was extracted and reduced to 10 ml by evaporation. The crude product was washed with 400 ml of ethanol to remove excess thiol. The particles were precipitated by leaving the mixture for several hours at a temperature below -10 °C. The precipitated particles were filtered off, dissolved in the minimum amount of toluene and washed again in ethanol following the above procedure.

In order to minimize the amount of the quaternary ammonium ion impurity in the product further purification was necessary [72]. This was achieved by drying the solution of alkanethiol stabilized gold nanoparticles

onto a 25×100 mm Soxhlet thimble. The thimble was then placed into a soxhlet extractor. AnalaR grade acetone was used as the cleansing solvent. The extraction was run in four consecutive cycles, each of three hour duration.

From a stock solution of purified dodecanethiol stabilized gold nanoparticles 2 mL was withdrawn and placed into a glass vial (open at both ends). The solvent was evaporated leaving solid nanoparticles; the vial was then reweighed and placed, carefully, into the stainless steel high pressure vessel. This vessel was then attached to a high pressure rig (Figure 32) which allowed the transfer of supercritical ethane into the vessel. Ethane was transferred from the gas cylinder E into the high pressure pipework with valves V1 and open and all others closed. The pump, P, was then isolated by closing valve V2 and the ethane compressed to the desired pressure above the critical pressure of ethane. The pump was cooled with dry ice to keep the ethane in its liquid state during compression. When the desired pressure had been reached the ethane was transferred to the high pressure pipework by opening valve V3 and then closing it off when the pressure gauge showed that it had entered the pipework. The pipework between valve V3 and the reaction vessel was heated to 318 K, above the critical temperature of ethane. As the ethane flowed through the pipework it passed into the supercritical state. Valve V4 was then opened to allow the supercritical fluid to pass into the reaction vessel, the pressure was monitored by pressure gauge P3. Valve V4 was then closed and the pressure vessel isolated for 18 hours. The vessel was insulated and temperature controlled (T2) at 318 K using heating tape wrapped around the vessel.

At the end of the experiment valve V5 was opened and the vessel was depressurised. The vapour was passed through a layer of deionized water where any particles that had passed through the pipework without precipitating were collected. Further particles precipitated within the pipework and the vessel as a consequence of the reduction in pressure. In

order to recover these particles the apparatus was disassembled and washed throughout with toluene. The solvent used to recover these particles was evaporated and the dry particles were combined with those collected in the water and redissolved in a standard volume (5 mL) of solvent for analysis. The undissolved particles were collected from the open ended glass vial in a standard volume of toluene (5 mL). The masses of both the dissolved and the undissolved nanoparticles were recorded for each experimental run after evaporation of the solvent. The experiment was repeated at approximately 50 bar intervals between 50 and 300 bar. Initial experiments were performed over periods of 18 hours; some additional experiments subjected the nanoparticles to supercritical ethane for 12 hours and 3 days periods.

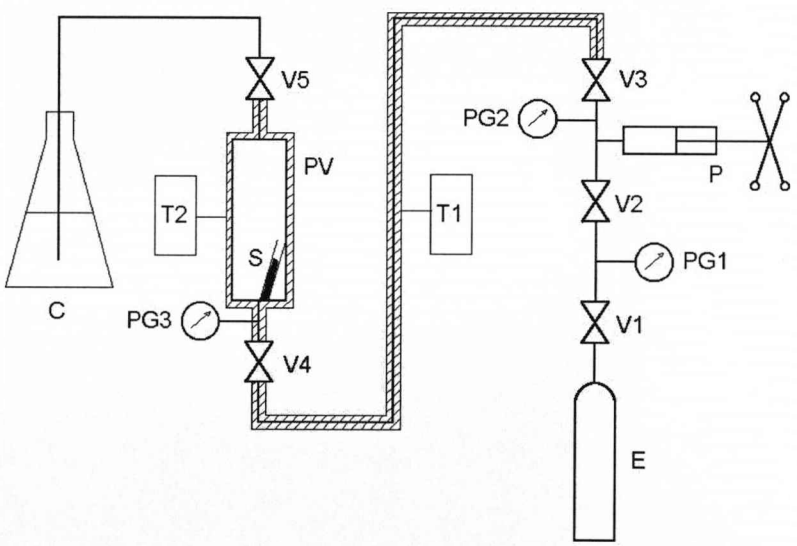

E – Pressurised Ethane Cylinder
V 1-5 – Valves
PG 1-3 – Pressure Gauges
P – Pump
T – Temperature control devices
S – Sample of nanoparticles
PV – Pressure Vessel

Figure 32. Schematic diagram of the high-pressure apparatus used for all solubility and separation experiments [19].

4.1.3 Results and Discussion

The recovered particles were analyzed using a number of techniques. Due to the strong dependence of the optical properties of these particles on their core diameters [14, 37, 137], UV-visible absorption spectroscopy is one of the most useful techniques used to analyze the samples. Complementary techniques used in this study include MALDI-TOF Mass Spectroscopy, Transmission Electron Microscopy (TEM) and Dynamic Light Scattering (DLS).

The UV-Visible absorption spectrum results of one of the earliest experiments are shown below (Figure 33). The spectrum of the undissolved nanoparticles at a pressure of 276 bar show a distinct absorption maximum at around 520 nm. This kind of absorption is typical of the spectra of gold nanoparticles with a core diameter above around 2 nm due to the electronic properties associated with gold nanoparticles of this size [111, 138].

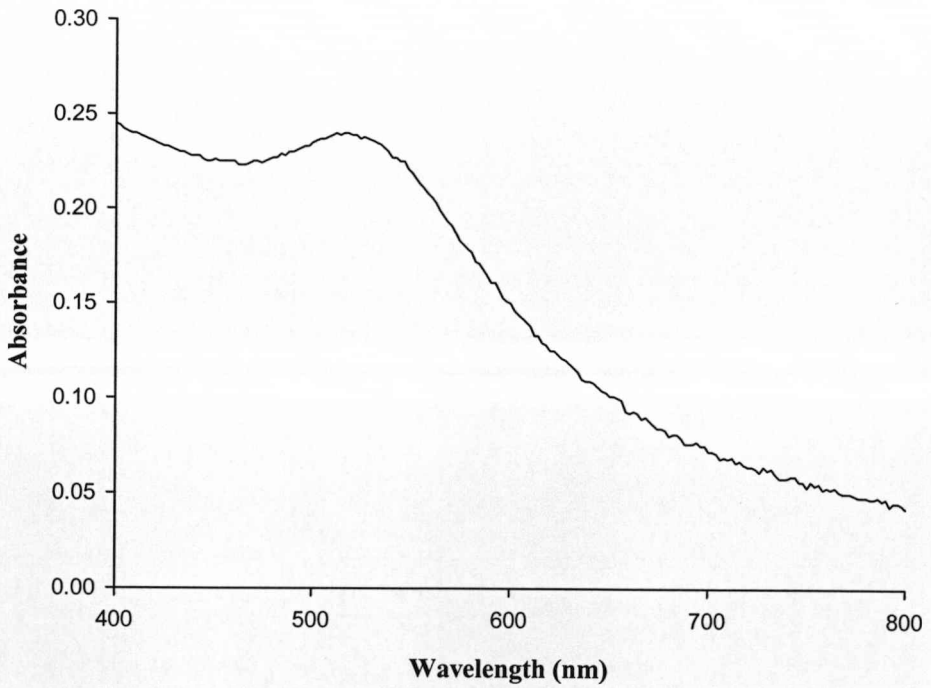

Figure 33 (previous page). UV-Visible absorption spectrum of dodecanethiol stabilised gold nanoparticles that remained undissolved in 276 bar supercritical ethane.

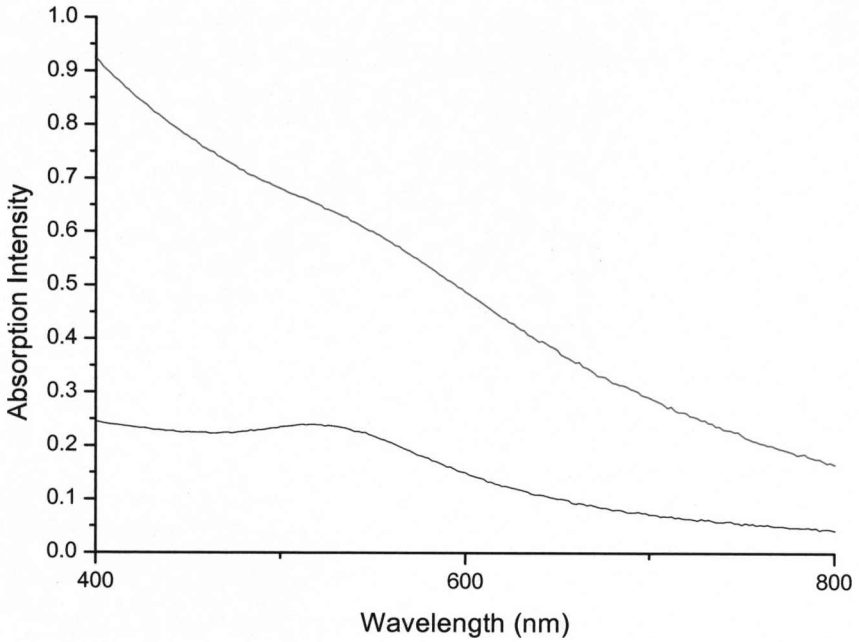

Figure 34. Comparison of the UV-Visible absorption spectra of undissolved (black) and dissolved (green) samples of dodecanethiol stabilised gold nanoparticles in 276 bar supercritical ethane.

When the spectra of the dissolved and undissolved nanoparticles are compared (Figure 34) distinct differences can be seen. The spectrum of the dissolved nanoparticles displays almost no plasmon band absorbance which indicates that the nanoparticles in this sample had an average core diameter below approximately 2 nm. The colours of these two solutions reflect the differences seen in their absorption spectra; the undissolved sample was pink due to the presence of the plasmon band resonance, whereas the dissolved sample was brown. At this point it seemed clear that the two samples consisted of different size nanoparticles, the undissolved sample consisting of larger nanoparticles and the dissolved sample of smaller nanoparticles. This was a significant finding as both of these different sizes of nanoparticles originated from the same sample of

nanoparticles. This illustrated the ease with which distinct size fractions can be separated using supercritical fluids.

In this discussion the terms 'small' and 'large' are commonly used to describe nanoparticles. In this context these labels refer to the assumptions made about the core diameters of nanoparticles from analysis of the UV-Visible absorption spectra. A small particle exhibits little or no plasmon band absorption in its UV-Visible absorption spectrum due to the quantized electronic states of gold nanoparticles below around 2 nm. A large particle is one with a core diameter above about 2 nm, the electronic properties of these nanoparticles can be described by the free electron model and they are characterized by strong plasmon band absorptions in their UV-Visible absorption spectra.

A simple experiment was performed to determine whether the system had reached saturation solubility. A repeat experiment was conducted using double the amount of the standard volume of stock solution of gold nanoparticles dissolved in toluene (i.e. 10 mL), all other conditions were the same as the previous run. A comparison of the UV-Visible Absorption spectra (Figure 35) of the undissolved and dissolved samples extracted from the high pressure vessel shows that the absorbance of the dissolved particles has changed very little compared to the original experiment whereas the absorbance of the undissolved sample increased almost threefold. This would seem to suggest (assuming there are no changes in the extinction coefficient of the particles between the two experiments) that the system was either at or above saturation during the second experiment. The plasmon band absorptions of the two samples are similar in nature to those obtained for the two samples in the original experiment which demonstrates that in spite of the fact that the total amount of nanoparticles dissolved increases when a larger initial quantity of nanoparticles is placed in the high pressure vessel, the size selectivity at a given pressure is preserved.

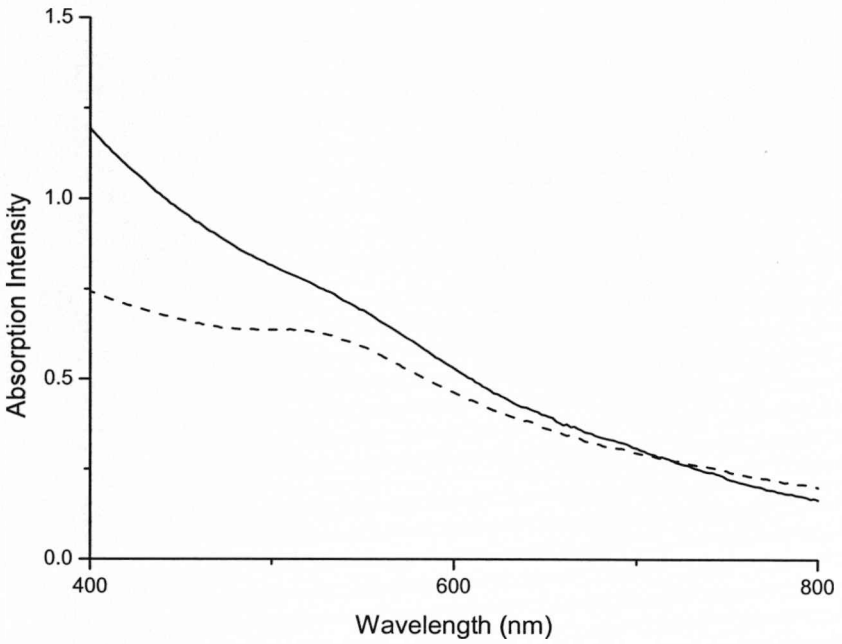

Figure 35. Comparison of the UV-Visible absorption spectra of undissolved (dashed) and dissolved (solid black) samples of dodecanethiol stabilised gold nanoparticles in 276 bar supercritical ethane, starting with double the amount of gold nanoparticles in the glass vial.

The original experiment was then repeated (using the original volume of stock solution) over a pressure range of 50-200 bar. The standard volume of nanoparticles was transferred to the glass vial by the procedure described above. Once the dried nanoparticles were contained in the vial it was then weighed and transferred into the high pressure vessel which was then filled with supercritical ethane at the desired pressure (using the previously described technique, Chapter 3.2.3) and isolated for 18 hours. At the end of the experiment the sample was extracted from the vessel using the previously described technique (Chapter 3.2.2) and the glass vial was carefully reweighed. The measurements were made at approximately 50 bar intervals between 50 bar to 300 bar (at a constant temperature of 318 K).

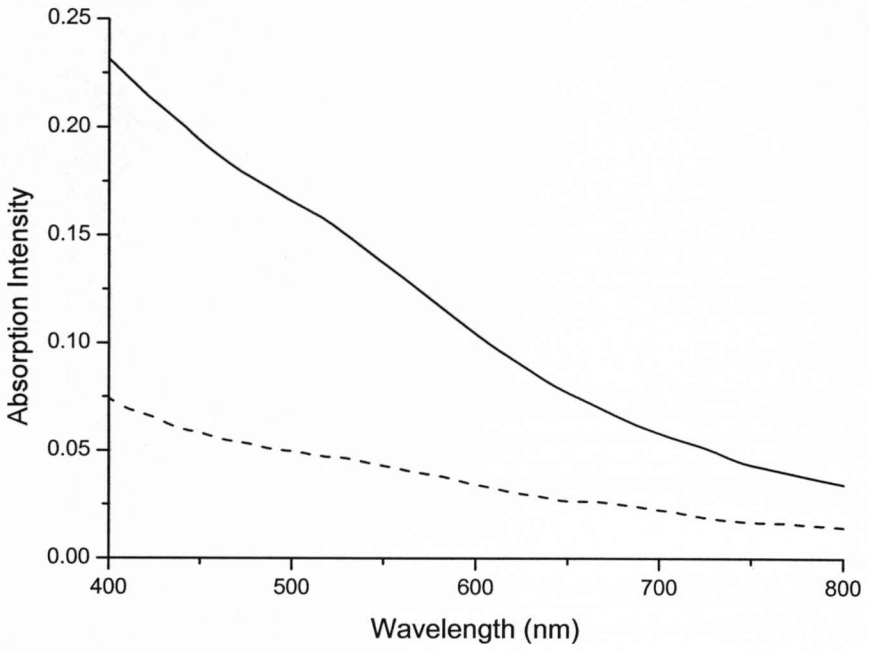

Figure 36. Comparison of the UV-Visible absorption spectra of undissolved (solid black) and dissolved (dashed black) samples of dodecanethiol stabilised gold nanoparticles in 150 bar supercritical ethane.

A comparison of the absorption spectra at 150 bar (Figure 36) shows only a small amount of gold nanoparticles dissolved in the supercritical fluid. At this pressure the absence of pronounced absorption maximum at a wavelength of 520 nm indicates that the quantity of smaller nanoparticles in both samples was very high at this pressure. It seems likely that a small quantity of the smaller nanoparticles were removed from the sample which resulted in the low absorbance of the dissolved nanoparticles and the spectrum of the undissolved sample being dominated by spectral characteristics of smaller gold nanoparticles.

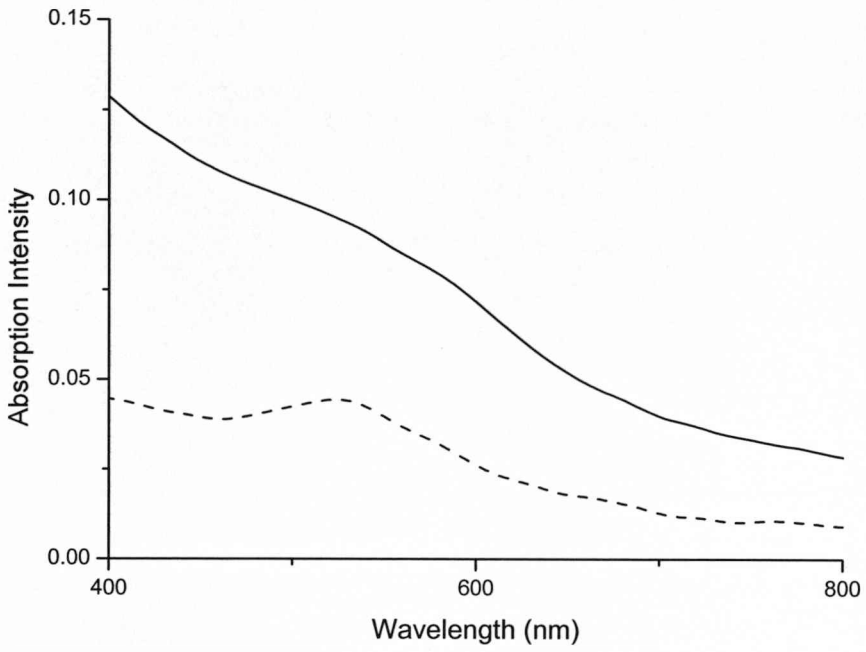

Figure 37. Comparison of the UV-Visible absorption spectra of undissolved (dashed black) and dissolved (solid black) samples of dodecanethiol stabilised gold nanoparticles in 249.6 bar supercritical ethane.

A comparison of the UV-visible absorption spectra obtained for the dissolved and undissolved samples of nanoparticles recovered after exposure to 249.6 bar supercritical ethane (Figure 37) shows a similar result to that observed in the 276 bar experiment. The spectrum of the undissolved sample has a pronounced plasmon band absorption, whereas for the dissolved sample it is absent at the same absorption, implying a similar separation of sizes has occurred. The amount of material which dissolved at this pressure is less than that dissolved at 276 bar as predicted by the behaviour of supercritical fluids.

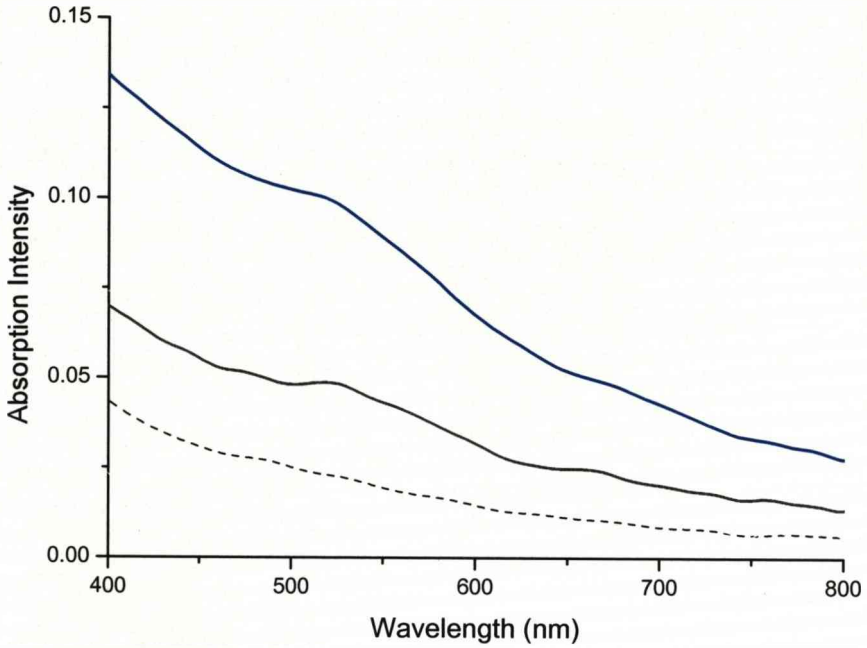

Figure 38. UV-visible absorption spectra for the dissolved samples of alkanethiol stabilized gold nanoparticles in supercritical ethane at the pressures (Blue 250 bar, black 200 bar, black dashed 100 bar) shown.

By comparing the UV-visible absorption spectra (each measured in 5 mL of toluene) of the dissolved nanoparticles (Figure 38) recovered from each experimental run (i.e. those that precipitated in water following depressurization of the vessel, combined with those that were washed from the inside of the apparatus by toluene) there are a number of conclusions that can be drawn. It can be seen that there is a proportional relationship between the amount of material that dissolves and the pressure of the supercritical fluid, this is to be expected due to the rapid increase in density of supercritical fluids with increasing pressure. It is also observed that the presence and intensity of the plasmon band absorption seen in the absorption spectra of dissolved samples varies with pressure. A distinct maximum in the absorption spectrum of larger nanoparticles (2 nm and above) appears at around 520 nm. At higher pressures (at or above 200 bar)

a greater number of larger nanoparticles dissolve, resulting in the appearance a weak plasmon band. At lower pressures this plasmon band absorption is absent as the larger nanoparticles are expected to be completely insoluble at these pressures. This finding is consistent with literature findings of comparable studies on the separation bimodal mixtures of nanoparticles in supercritical fluids [19, 136].

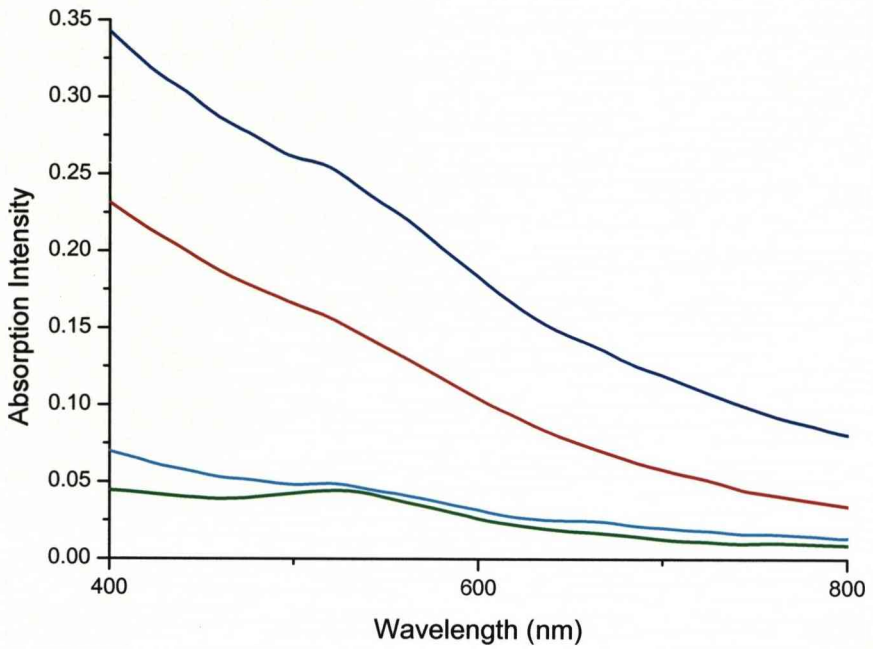

Figure 39. UV-visible absorption spectra for the undissolved samples of alkanethiol stabilized gold nanoparticles in supercritical ethane at the pressures (Blue 50 bar, red 100 bar, sky blue 200 bar, green 250 bar) shown.

The variation in absorbance with pressure in the spectra of the undissolved nanoparticles (Figure 39) is consistent with that seen for the dissolved nanoparticles. A decrease in the intensity of the absorption (corresponding to a decrease in the total amount of undissolved nanoparticles present) is seen as the pressure of the experiment increases. This occurs as a consequence of a greater amount of nanoparticles

dissolving due to the increasing density of the supercritical fluid at higher pressures. The intensity of the plasmon band absorption also varies with pressure. As the pressure of the supercritical fluid was increased the intensity of the plasmon band absorption of the spectra of the undissolved samples increased. At lower pressures only smaller nanoparticles were soluble leaving mostly larger nanoparticles (with their characteristic plasmon band absorption) which means that the strength of the plasmon band absorption of these samples increases as the pressure increases until the point is reached at which the larger nanoparticles also become very soluble (which is higher than any pressure used in this experiment).

TEM images of the samples from the 276 bar experiment were recorded at a number of resolutions (Figure 37) which was useful for the determination of the average nanoparticle diameter and distribution of sizes present in each sample.

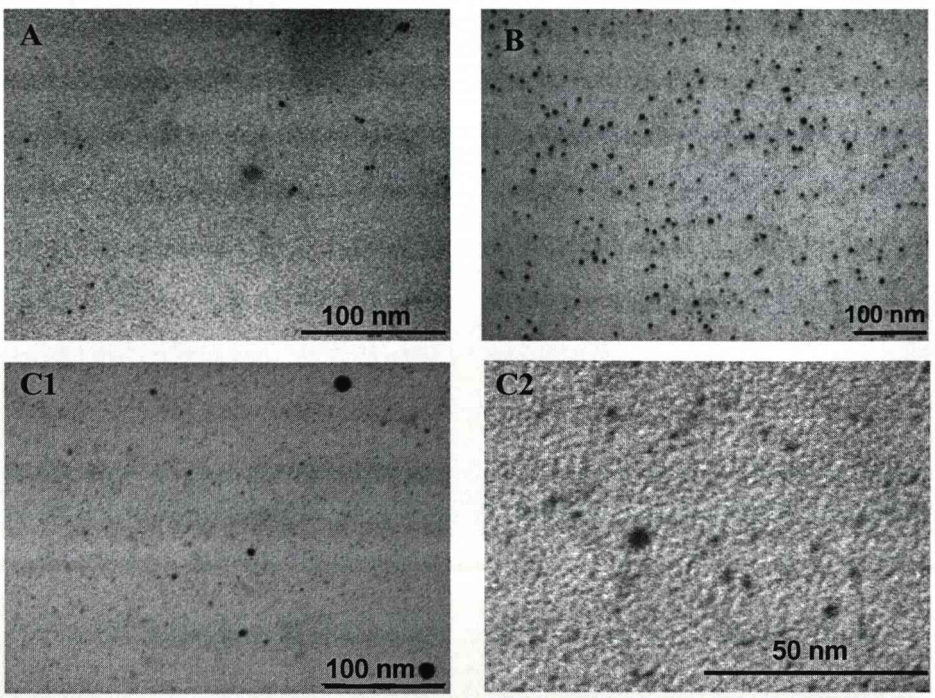

Figure 40 (previous page). Transmission Electron Micrographs of the Nanoparticles before the experiments (A), the undissolved particles (B) and the dissolved particles (C1 and C2) recovered from supercritical ethane at 276 bar and 318 K. The scale bars are equal to 100 nm.

The analysis of the TEM images (Figure 40) of the samples recovered from the pressure vessel after the experiment at 276 bar supports the conclusions reached from the analysis of the UV-vis spectra. A clear difference between the average core diameters of the two samples can be seen. The undissolved particles (B) have a larger average core diameter and more uniform size distribution than the particles seen in the images of the dissolved particles (C). By using ImageJ [126] image processing software the average core diameters have been determined as 2.3 nm for the dissolved nanoparticles and 4.4 nm for the undissolved nanoparticles (Figure 41). It is also worth noting that at this pressure some of the larger nanoparticles have dissolved in the supercritical fluid at this pressure.

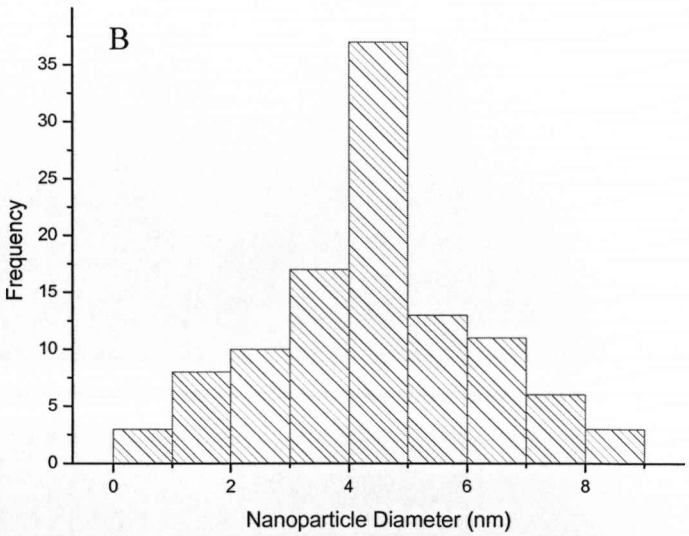

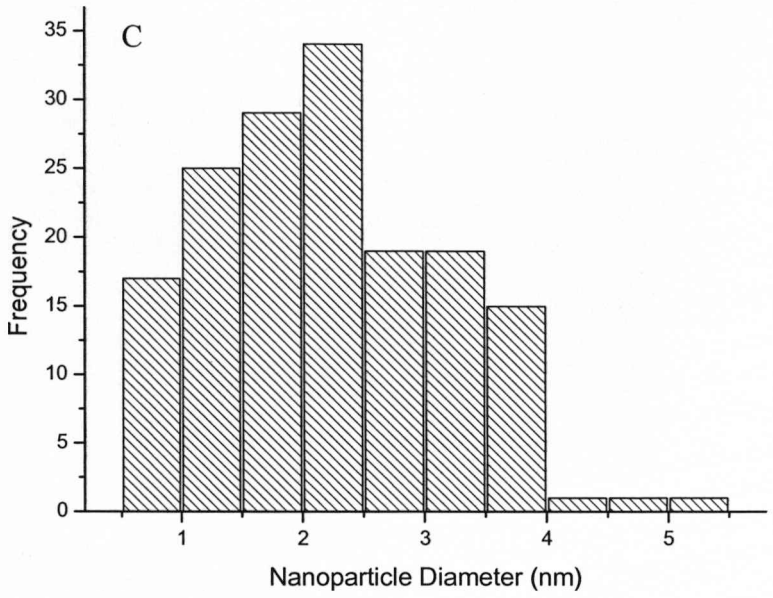

Figure 41. Core diameter distribution histograms from ImageJ [126] analysis of the TEM images of the undissolved particles (B) and the dissolved particles (C) recovered from supercritical ethane at 276 bar and 318 K. The scale bar equals 100 nm.

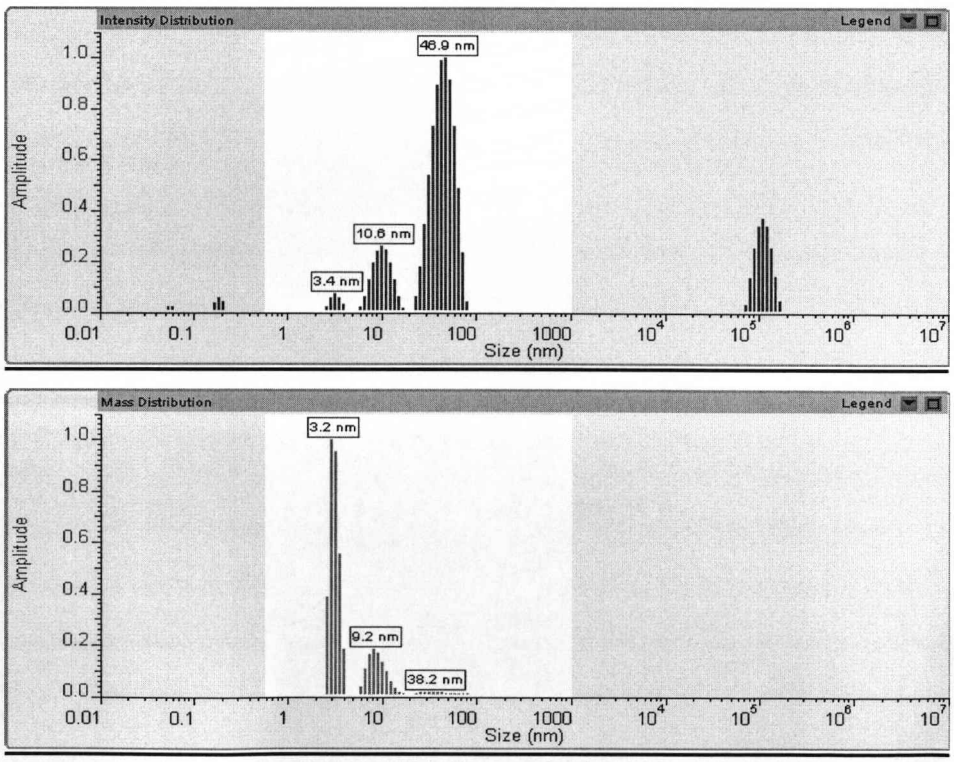

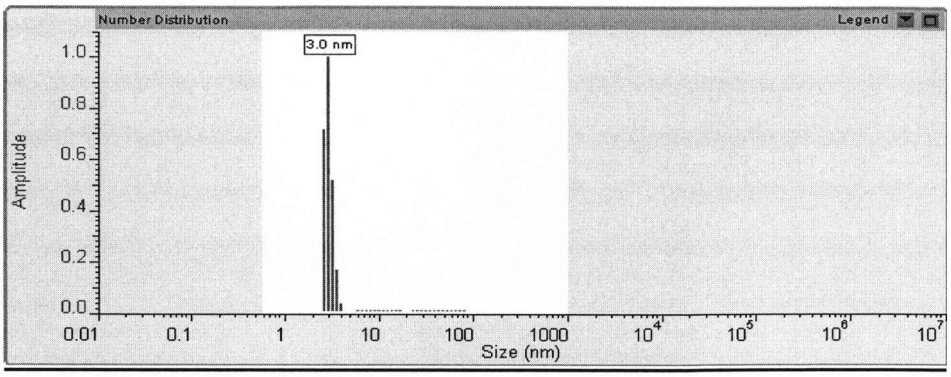

Figure 42. DLS nanoparticle core radius distribution histograms of the undissolved particles recovered from the high pressure vessel following the 276 bar experiment.

Figure 42 shows the results of the DLS analysis of the undissolved sample of gold nanoparticles recovered from the pressure vessel after the 276 bar experiment. The peaks in the DLS images correspond to the hydrodynamic radii of the metal nanoparticles. The intensity and the mass distribution results confirm that there are a number of different size nanoparticles present in the analysed sample. It is likely that any peaks above 10 nm correspond to aggregated nanoparticles and unfiltered dust particles. The intensity of the peaks associated with larger nanoparticles appear greater (particularly in the intensity distribution) due to the fact that larger particles scatter light much more effectively than smaller particles. The number distribution of the sample suggests an average core radius of 3.03 ± 0.30 nm. From the DLS number intensity results, therefore, an average core diameter of 6.06 ± 0.30 nm is obtained. This value is somewhat higher than that determined from analysis of the TEM image. Differences can occur between the results obtained by these two techniques, DLS can have advantages over TEM as its analysis is based on a far greater proportion of the total sample compared to that used by the TEM analysis.

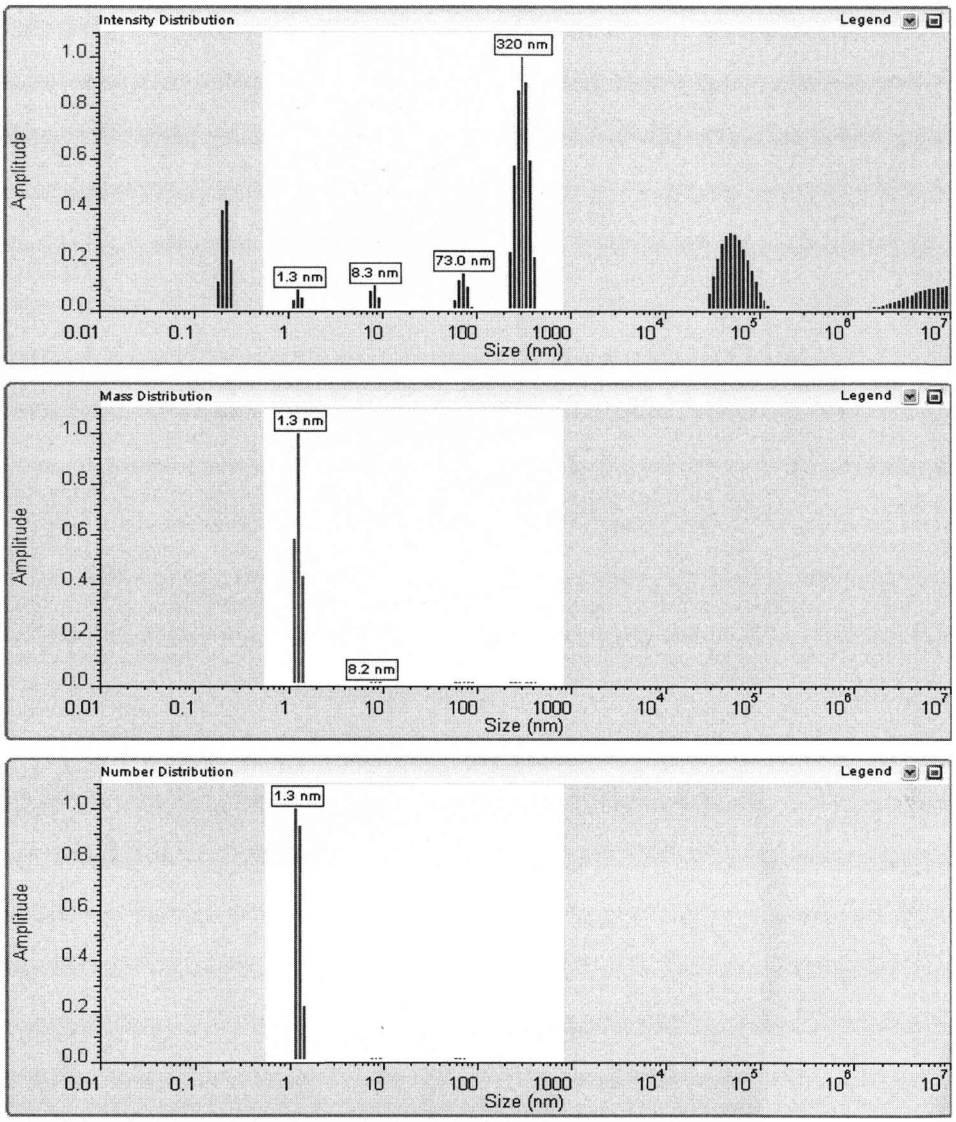

Figure 43. Nanoparticle core radius distribution histograms determined from DLS analysis of the dissolved particles recovered from the high pressure vessel following the 276 bar experiment.

Figure 43 shows the DLS data for the dissolved gold nanoparticles recovered from the vessel after the 276 bar experiment. Apart from the presence of some large particles in the sample (which may occur because of aggregation of the metal particles or the presence of artifact molecules in the cuvette) the data seems to correspond well with the results of other analysis (UV-Visible absorption spectra and TEM images) of the particles. The main peak in the number and mass distributions appears to

be centered on 1.3 nm. The 1.3 nm peak is also one of two significant peaks in the intensity distribution along with 8.3 nm. From this number the average core radius is determined as being 1.3 ± 0.09 nm. An average core diameter of 2.6 ± 0.18nm compares well with the value of 2.4 nm obtained from TEM analysis of the same sample.

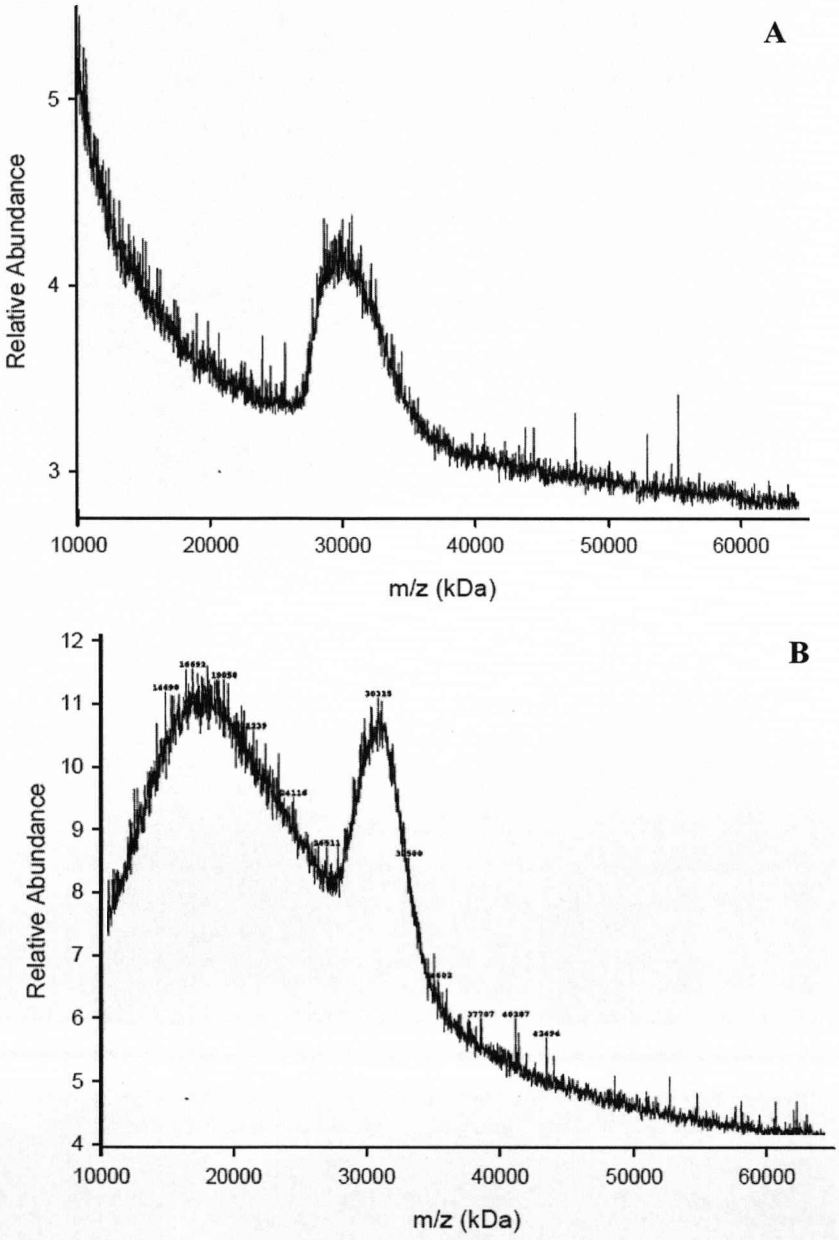

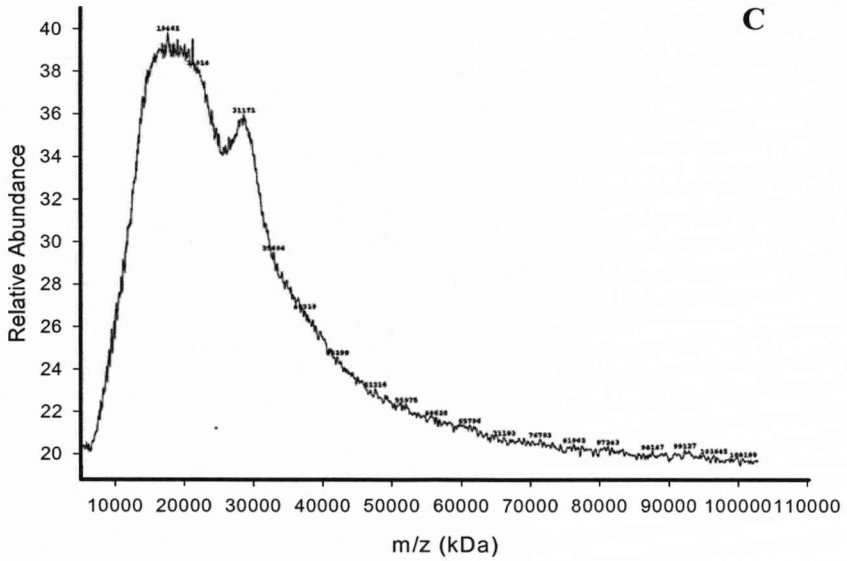

Figure 44. MADI-TOF Mass Spectra of the undissolved nanoparticles (A) and the dissolved nanoparticles (B) recovered from the 276 bar experiment and the dissolved nanoparticles recovered from the 100 bar experiment (C).

MALDI-TOF analysis of the nanoparticles is useful as it can assist in the identification of which "magic number" clusters are present in a sample. As described in the introduction the metallic atoms forming the nanoparticles gather together in discrete clusters. The numbers of atoms in these clusters is often referred to as a "magic number" of atoms [125]. Clusters containing a "magic" number of metal atoms will benefit from additional stability compared to clusters with a non-magic number of metal atoms. In many systems some variation of the precise magic numbers is often observed which exists as a consequence of slight geometric rearrangements based on the magic number conformation (i.e. missing or additional vertex atoms).

Figure 44A shows the MALDI-TOF MS of the undissolved nanoparticles, this shows a single peak centred at 30 kDa. Previous research [125] has shown that this peak can be attributed to the Au_{147}

cluster. The same 30 kDa peak is seen in the spectrum of the dissolved particles, together with a second peak centred on 16 kDa. The 16 kDa peak has been assigned to the Au_{79} cluster; this peak appears quite broad which suggests that the number of similar stable clusters exist around this magic number structure (i.e. other metal clusters with the same basic structure as Au_{79} but with extra or missing vertex atoms). It appears likely that the Au_{147} clusters are responsible for the plasmon band absorption seen in the UV-Visible Absorption of these particles. The complete absence of this peak in the spectrum of the dissolved (Figure 44B) particles supports the argument from the UV-Visible absorption spectra and TEM images that only the smaller clusters are dissolved at a pressure of 276 bar (and, as a matter of fact, all lower pressures measured as well). The MALDI-TOF spectrum of the undissolved particles shows that some of the smaller nanoparticles are present together with the larger clusters (those responsible for the plasmon band absorption).

Figure 44C shows the MALDI-TOF Mass Spectrum for the sample of nanoparticles dissolved after exposure to 100 bar supercritical ethane for 12 hours at a temperature of 318 K. The principle of tunable solubility in supercritical fluids would suggest that there would be a pressure at which only the smaller sized particles (those with a MALDI-TOF MS peak centred on 16 kDa) would be dissolved. In practice it was very difficult to find the precise pressure at which this happens, however, the mass spectrum of the nanoparticles dissolved in the supercritical ethane at 100 bar is unique. The peak which corresponds to the larger gold clusters (i.e. the 30 kDa peak) appears to be dwarfed by the peak corresponding to the smaller nanoparticles. Although the intensity of MALDI-TOF mass spectra cannot be used to accurately quantify the ratio of metal clusters present in the sample for these types of samples, this spectrum qualitatively shows that a much smaller concentration of larger metal cluster particles were present compared to results at all higher pressures. The complete fractionation of a sample of polydisperse

nanoparticles may be hindered if the point at which larger fractions of nanoparticles become soluble occurs before all of the smaller nanoparticles have been removed.

In order to explain these observations the factors which dictate the solubility of particles in supercritical fluids must be considered. The solubility of any particles in such a medium depends on the Gibbs free energy of solubilization of that particle in a supercritical fluid [19]. This energy is dependent on the radius of the particles, in dilute solutions particle-particles interactions are negligible and the Gibbs energy is determined by the balance between particle-particle interactions in the solid, particle-solvent interactions in the solution and solvent-solvent interactions, the latter two being strongly pressure dependent [19]. It has been proposed that the decrease in solubility with increasing particle size occurs as a result of interactions within the solid.

For a spherical nanoparticle with a radius R its polarizability (α_S) is given by equation 7:

$$\alpha_S = R^3 \qquad (7)$$

The total polarizabiliy of the nanoparticles includes a contribution from the alkane chains of the stabilizing ligands. This contribution increases with ligand chain length at a factor of R^2. The interaction energy of the solid due to the metal cores increases with α^2 (R^6) if the cores are perfectly spherical. From this it seems that the main contribution to the total interaction energy originates from the cores.

For smaller particles the significance of the contribution of the alkyl groups to the polarizability of the molecule increases. The breakdown of the free electron model for small metal particles is also significant. At sizes below around 2 nm discrete energy levels are present so polarizability can be expected to decrease more rapidly with R compared to the predictions of the free electron model. Additionally, for small metal nanoparticles the particle-particle interactions are dominated by the interactions between alkyl chains so solubility is expected to increase for

decreasing radius. Further theoretical study is necessary to determine the precise explanation for the increasing solubility of smaller radius nanoparticles.

4.2 Approximate Concentration from UV-Visible Spectra

4.2.1 Introduction

In order to determine approximate values for the solubility of these nanoparticles it is necessary to use both the UV-visible absorption spectra and TEM images of the nanoparticles. Liu *et. al.* [139] described a simple technique which may be used to determine the molar extinction coefficient for a metal nanoparticle of a given size independent of stabizing ligand or solvent. By using the calculated extinction coefficient together with the Beer-Lambert law it is possible to estimate the concentration of nanoparticles in the sample which has been analyzed from the absorbance maximum.

In order to determine a relatively reliable way of calculating the extinction coefficient of metal nanoparticles of given core diameters, Liu *et. al.* performed a simple study which involved determining the concentration of a solution from high resolution TEM data and then substituting that value into the Beer-Lambert Law using the UV-Visible absorption spectrum of the same sample.

The extinction coefficient was found by calculating the concentration of the nanoparticles present in the sample by assuming that the nanoparticles adopt an fcc structure (with a density ρ=19.3 g/cm^3). The average number of gold atoms present in each nanoparticle (N) was expressed as:

$$N = 30.89602D^3 \qquad \textbf{(8)}$$

where D is the average core diameter of the nanoparticles as determined from TEM images of the particles. The molar concentration of solutions of nanoparticles could be determined (Equation 9) by dividing the total

number of gold atoms (N_{total}, which is equal to the amount of gold salt added to the reaction solution) over the total number of gold atoms per nanoparticle (N). The volume of reaction solution is expressed as V and N_A represents Avagadro's Number:

$$C = N_{Total} / (NVN_A) \qquad \textbf{(9)}$$

4.2.2 Extinction Coefficient Calculation

The extinction coefficients at 506 nm were determined for a number of differently functionalized gold nanoparticles by measuring the maximum UV-visible absorption spectroscopy and using the maximum absorption of the plasmon band to calculate the concentration of nanoparticles from the Beer-Lambert Law. It was found that a linear relationship of the double logarithm of extinction coefficient versus nanoparticle diameter was applicable to all gold nanoparticles studied, independent of the capping ligands used to protect the nanoparticles [48], the published mathematical relationship was used to produce Figure 45. In spite of the expected variations in extinction coefficient due to varying dielectric constants of the solvents used or the various stabilization effects that occur as a consequence of the variety of ligands used to stabilize the nanoparticles, it was concluded from this study that the size of the nanoparticles dictates the plasmon band resonance.

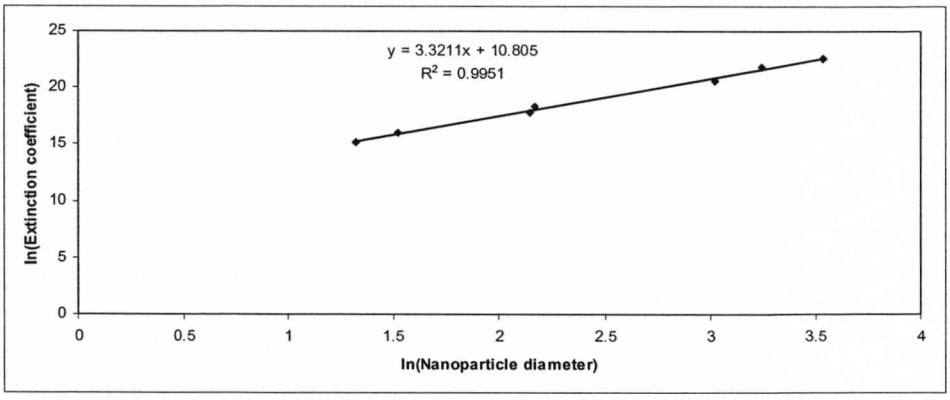

Figure 45. Double logarithm plot of extinction coefficient versus nanoparticle diameter.

Due to the polydisperse nature of many of the samples produced and isolated it was difficult to determine an accurate value for the extinction coefficient of these nanoparticles. In order to obtain an estimate of the amount of nanoparticles dissolved for the most monodisperse sample (i.e. those dissolved at the highest pressure) the calculation was performed on the dissolved nanoparticles from the 276 bar run assuming the vessel had a volume of 20.44 cm3 and the density of ethane at that pressure was 0.334 g/m^3. The calculation gave the result in the form of a concentration of moles of nanoparticles dissolved per gram of ethane. The result was determined as being 3.9×10^{-9} molg^{-1}.

4.3 Separation of a mixture of two samples

In order to demonstrate the versatility of this technique in the separation of size fractions from polydisperse samples of nanoparticles it was decided a simple investigation would be conducted into the isolation of the two components of a bimodal mixture of nanoparticles from a 1:1 mixture of gold nanoparticles with different average core diameters. The investigation is similar in nature to those conducted in a number of earlier

publications [19, 49] but is included here in order to highlight similarities with the separation of a single sample of polydisperse gold nanoparticles.

A 50:50 mixture of 2 and 5 nm dodecanethiol stabilized gold nanoparticles (both prepared via the two-phase reduction technique [4]) was prepared in toluene. Before the two components were mixed a clear difference in the optical behaviour of the two components could be seen from the colours of the solutions. The 2 nm nanoparticles created a brown coloured solution whereas the larger (4 nm) nanoparticles resulted in the formation of a pale red colour solution (Figure 46).

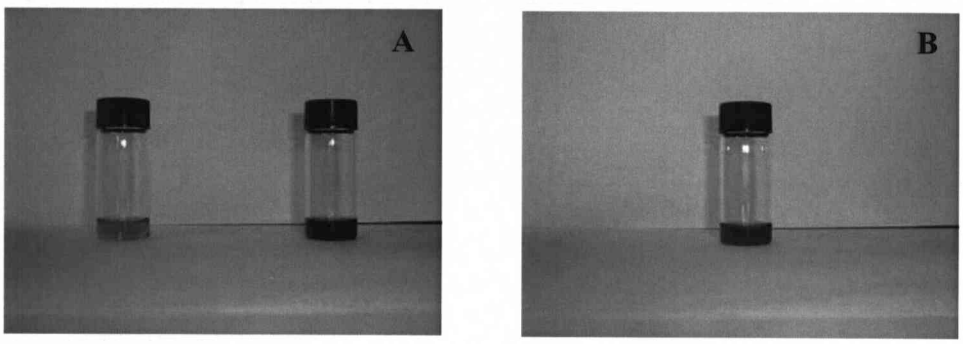

Figure 46. Photographs of the original solutions used to make the bimodal mixture (A) and of the bimodal mixture produced (B).

The separation experiments were conducted over the same time period as earlier investigations and a range of pressures between 100 and 300 bar were used. Due to the low concentrations of dissolved material recovered it was decided that the analysis would be conducted by focusing on the absorption spectra of the undissolved material. A standard volume of the mixture was dried onto an open ended vial and then confined in the vessel with supercritical ethane over a period of 18 hours in the same way as the earlier experiments. As the gold nanoparticles used in this study were functionalized by the same stabilizing ligands as those studied in the separation experiment, the recovery procedure was identical (i.e. the dissolved fraction consisted of nanoparticles washed off the high pressure

apparatus using toluene combined with additional particles recovered by bubbling the fluid through deionized water during depressurization).

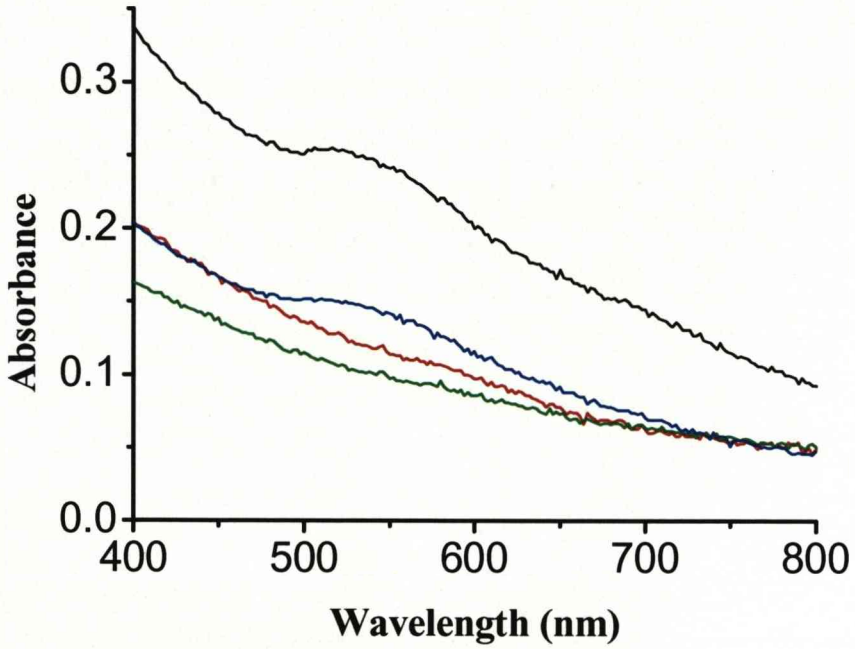

Figure 47. UV-Visible absorption spectra of the undissolved samples of nanoparticles recovered from the high-pressure rig and that of the original mixture. (Black – original sample, blue – 100 bar, red – 150 bar, green – 200 bar)

Figure 47 shows a comparison of the UV-Visible absorption spectra for the undissolved portions from all three samples and that of the original mixture of nanoparticles. From this comparison it can be seen that the plasmon band absorption is absent in the spectra of the samples recovered from the rig at higher pressures. Following on from earlier work it seems likely that the elimination of this peak from the spectra at 150 and 200 bar occurs as a consequence of the selective removal of the larger nanoparticles from the samples at higher pressure. A stronger plasmon band absorption can be seen in the spectra recorded for the sample recovered after the experiment at 100 bar and in the spectrum of the

original mixture. This simple process has demonstrated the versatility of the technique in isolating size fractions of metal nanoparticles from mixtures as well as individual samples of polydisperse nanoparticles.

4.5 Closing Remarks

This chapter has reviewed the investigation into the behaviour of polydisperse samples of gold nanoparticles prepared by the two-phase reduction technique in supercritical ethane. It was seen that as a consequence of the solubility of nanoparticles depending on the average core diameter, specific size ranges of the polydisperse sample can be dissolved in supercritical ethane and therefore extracted from the original sample. The exact size range which is removed from the sample can, in principle, be varied by modification of the pressure of the supercritical fluid. The results of this investigation showed that the size range of the nanoparticles that dissolved (and therefore, those which did not dissolve) did indeed vary with pressure.

In order to make use of this technique in the post-synthesis fractionation of polydisperse samples of nanoparticles several issues must be addressed including the lack of current information on the precise pressures of the supercritical fluid required to dissolve nanoparticles of specific sizes. Another issue is the iterative nature of this technique, in order to completely fractionate a sample a number of experimental runs are required, starting at the lowest pressure at which nanoparticles dissolve and increasing with each successive experiment (ideally removing one size fraction each time the pressure is increased). This is a time consuming process and other experimental set-ups such as the corkscrew apparatus [48] mentioned in chapter 2.1.2 used to isolate monodisperse fractions of nanoparticles when exposed to a CO_2 anti-solvent at a range of pressures would need to be developed to make this process viable. It is also worth highlighting the fact that this is a small-scale laboratory process. In order to

perform this process on a large-scale it would be necessary to find less cumbersome ways of recovering dissolved and undissolved samples of nanoparticles at the end of each experimental run.

Chapter Five

The Application of DDT-PMAA in the Synthesis of Metal Nanoparticles.

5.1 Introduction

A literature search was carried out to find a simple, versatile and effective technique to produce highly monodisperse metal nanoparticles. It would be desirable for the technique to lead to the rapid production of highly monodisperse samples of stable gold nanoparticles with a defined core diameter and a minimum size distribution in sufficient quantities for an ongoing study of their solubility properties. It was also advantageous to find a technique which was versatile enough to allow the synthesis of a series of metal nanoparticles with a range of sizes (nanoparticles in the size range 1-10 nm being of particular interest for this study). The ability to vary the adsorbed ligand was also desirable as this would allow a comparison of the effect of the stabilising ligand on the solubility of nanoparticle.

An effective and versatile technique was described in a publication by Brust and Cooper [57]. A more detailed review of this article appears in the earlier chapters (Chapter 2.1.3, Page 14). This technique was shown to be simple, fast, versatile to modification and effective. This synthetic technique was based on the use of a thioether terminated polymer (Structure 1) which was added to the solution of metal salt prior to reduction of the gold salt, following addition of the reducing agent a deep red aqueous solution of metal nanoparticles stabilised by the polymer was produced, TEM images and DLS analysis showed that these particles exhibited extraordinary monodispersity. In order to produce gold nanoparticles soluble in organic solvents (such as hexane and toluene) a simple ligand transformation was performed which resulted in alkanethiol ligands replacing the polymer ligands attached to the gold core. It was shown that the core diameter of the products could be varied by changing the concentration of the water soluble polymer relative to that of the gold starting material during the initial stage of the synthesis.

The use of this polymer stabilising unit is a relatively new concept which means a substantial amount of further work needs to be carried out before the full extent of its usefulness is known. The polymer chain can be terminated by a different alkanethioether group which allows the easy formation of differently functionalized metal nanoparticles. There is also some scope for using different metals and varying the reducing agent used to prepare the particles [5, 57]. This chapter summarizes the attempts to develop a novel application for DDT-PMMA in the synthesis of metal nanoparticles. In Chapter Six the focus will switch to the synthesis of monodisperse gold nanoparticles using this polymer and a study of the solubility of some of these nanoparticles.

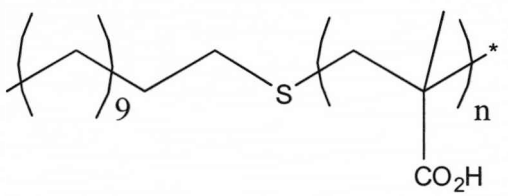

Structure 1. Dodecanethioether terminated poly(methacrylic acid).

5.2 A New Approach

5.2.1 DDT-PMAA with the Citrate Reduction

The first set of experiments attempted to create highly monodisperse gold nanoparticles with a larger core diameter than those produced by the modified two-phase synthetic approach used in the literature [33, 57]. This experimental approach made use of the same polymer (DDT-PMAA), again added in a range of concentrations relative to the concentration of the gold starting material. The provided polymer was prepared by free radical polymerization of Methacrylic acid using dodecanethiol as the phase transfer agent. The ^{1}H NMR of this polymer in DMSO had the following chemical shift peaks (δ, ppm): 0.9 (CH_3), 1.24 $(CH_2)_9$, 1.7 (CH_2), 2.4 (CH_2 from DDT) and 12.3 CO_2H. The molecular

weight values of this polymer (determined by GPC, values quoted as provided) were: $M_n = 4537$ gmol^{-1} and $M_w = 5483$ gmol^{-1}, $M_w/M_n = 1.21$.

The citrate reduction technique was first mentioned in chapter 1 (page 4) and was covered in experimental detail in chapter 3 [1, 2]. The citrate reduction synthesis is a single phase technique (thereby avoiding the necessity of using a phase transfer agent) which results in the formation of water soluble nanoparticles, typically in the 10-60 nm size range. These nanoparticles exhibit excellent stability due to the electrostatic stabilization of the metal cores provided by the citrate ligands. If the average core diameter and the size distribution of the products of the citrate synthesis could be controlled by to a greater extent (than simple variation of the citrate:gold ratio) by variation of the polymer:gold ratio it would be advantageous to the use of these nanoparticles in working applications.

Various mechanistic factors were considered during the synthesis of these nanoparticles including the possibility of competition between the polymer and the citrate to act as stabilizing ligands, in a similar manner to the replacement of citrate ligands with alkanethiol ligands [140, 141]. If the polymer acted as the only stabilizing ligand it is unlikely that the same degree of stabilization could be provided for nanoparticles with a core diameter of 20 nm and over due to the different stabilization mechanism by which the polymer ligands make use of (steric as opposed to the electrostatic stabilization provided by citrate ligands [141]). In order for the process to work it was anticipated that the polymer would act in tandem with citrate during the formation of the nanoparticles. The citrate ligands would provide sufficient electrostatic stability for larger nanoparticles while the presence of the polymer during synthesis would affect the polydispersity and size control of the products.

5.2.2 Experimental

Citrate stabilized gold nanoparticles were prepared based on a modified version of two previously described techniques (Chapters 5.2 and 3.4.1). To 20 mL of an aqueous solution of $HAuCl_4$ (84 mM) a given amount of the polymer (dodecanethioether terminated (poly)methacrylic acid) was added and allowed to mix for two hours. To this solution 2 mL of an aqueous solution of trisodium citrate dihydrate was added and the solution brought to the boil. After less than ten minutes the solution underwent a colour change from yellow to a deep red indicating the formation of gold nanoparticles. The nanoparticles were subsequently analysed by UV-visible absorption spectroscopy and TEM. It was interesting to compare the size of the produced nanoparticles with those produced under the same conditions in the absence of the polymer and to investigate the effect of varying the initial polymer concentration. The absorption spectrum for the sample (Figure 48) prepared in a 0.18 mM solution of PMMA-DDT shows a rather broad peak, centred at a wavelength higher than that seen in the spectrum of the particles prepared in the absence of the polymer.

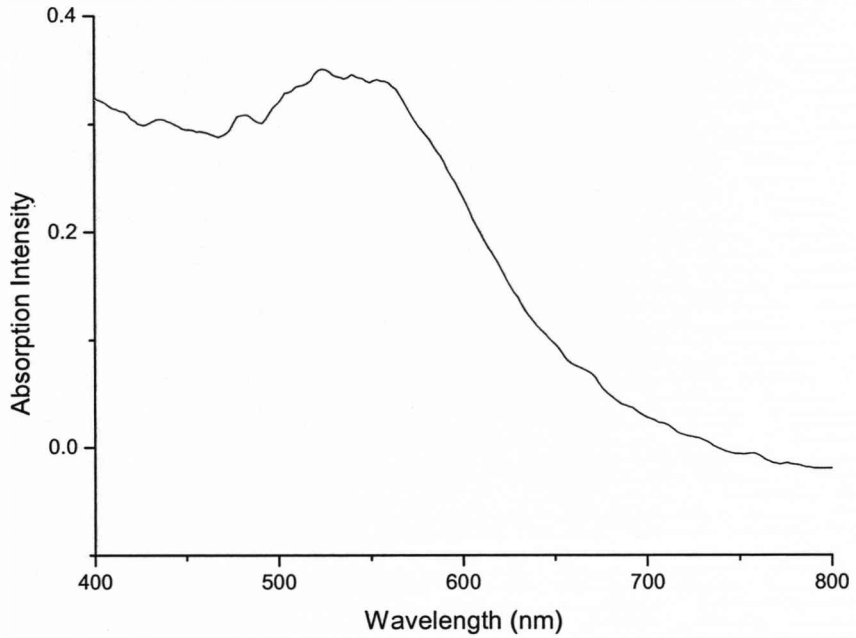

Figure 48. UV-visible absorption spectrum of the gold nanoparticles prepared via the citrate reduction in the presence of 0.18 mM PMMA-DDT.

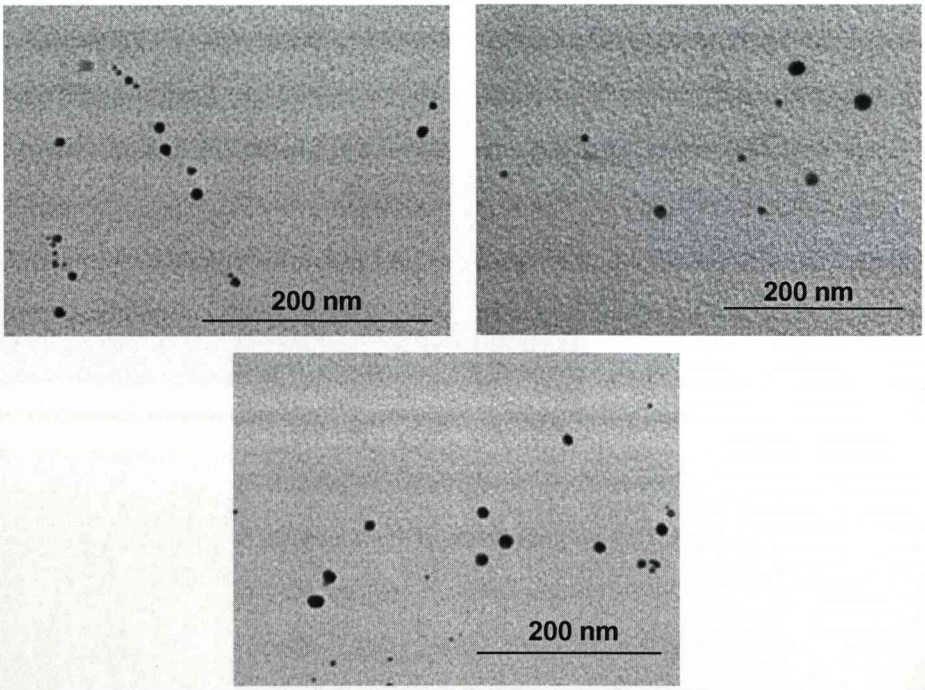

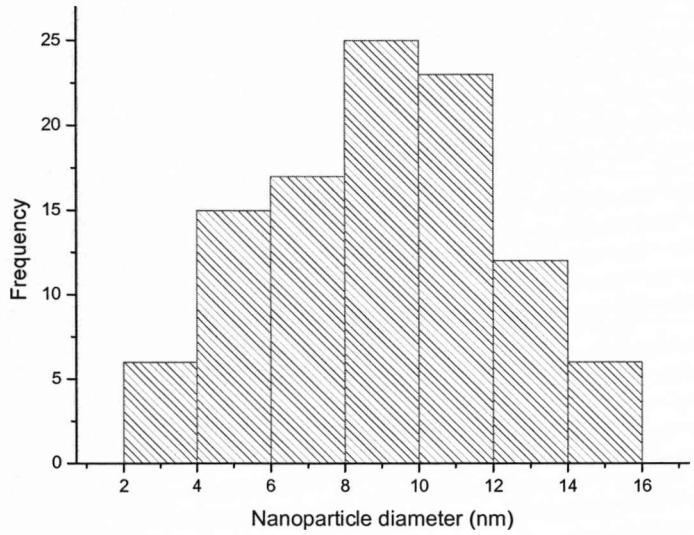

Figure 49. TEM images (and size distribution) of gold nanoparticles prepared via the citrate reduction in the presence of 0.18 mM PMAA-DDT. The scale bars on all spectra represents 200 nm.

Figure 49 shows three TEM images of samples of the nanoparticles prepared by the reduction of an aqueous solution of tetrachloroaurate with a solution of DDT-PMAA with a concentration of 0.18 mM. The images appear to show a variety of sizes of nanoparticles suggesting a lower degree of control over monodispersity than the gold nanoparticles prepared by the modified two-phase synthesis in the literature [57]. Analysis of the electron microscopy data shows a wide distribution of sizes is present in the sample.

Figure 50 shows the UV-visible absorption spectrum of the sample of nanoparticles prepared by the citrate reduction technique in an aqueous solution of tetrachloroaurate with a polymer concentration of 1.8 mM. The peak of the spectrum appears broader than that seen (see Figure 27 for comparison) for the sample prepared under the same conditions by the conventional citrate reduction, the peak is also centred on a lower frequency. This shift in peak frequencies and the increase in the bandwidth

of the peak would suggest that the average core diameter of the nanoparticles produced at this concentration of polymer is smaller than that for the nanoparticles prepared in a 0.18 mM solution of polymer. This is consistent with the effect of varying the polymer:gold ratio in the literature synthesis of gold nanoparticles in the presence of DDT-PMAA. In order to find more detailed information about the average core diameter and the distribution of sizes present in the sample, TEM images of the nanoparticles were captured.

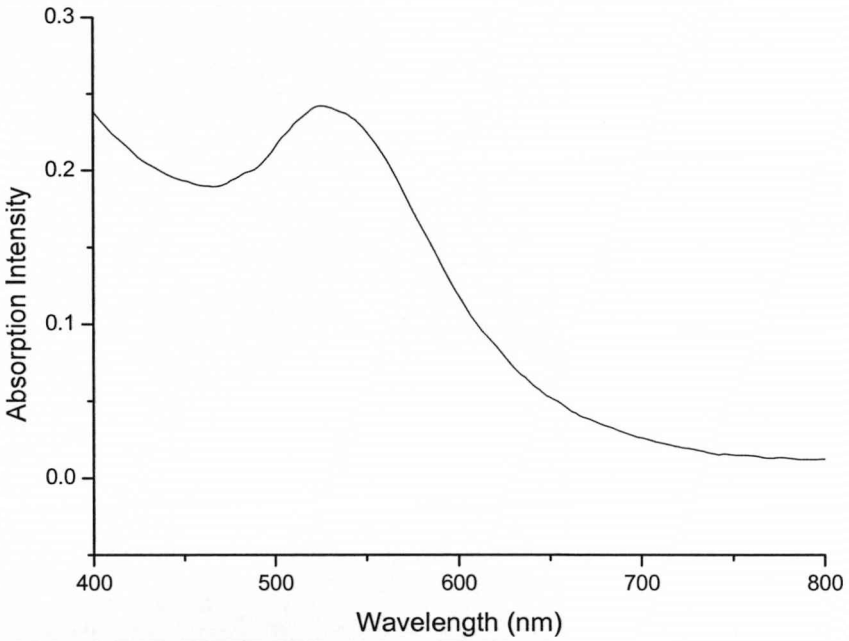

Figure 50. UV-visible absorption spectrum of the gold nanoparticles prepared via the citrate reduction in the presence of 1.8 mM DDT-PMAA.

The TEM images and the analysis of these images (Figures 51 & 52) show that there are a relatively wide range of diameter sizes present in the sample of nanoparticles produced in the 1.8 mM solution of DDT-PMAA. The nanoparticles do appear to be smaller than those produced with a lower concentration of polymer which explains why the peak in the absorption spectrum appears to be more typical of a sample of gold

nanoparticles in the 5-15 nm size range (ie. with a peak centred on around 520 nm). The average core diameter was determined as being 7.6 ± 3.1 nm.

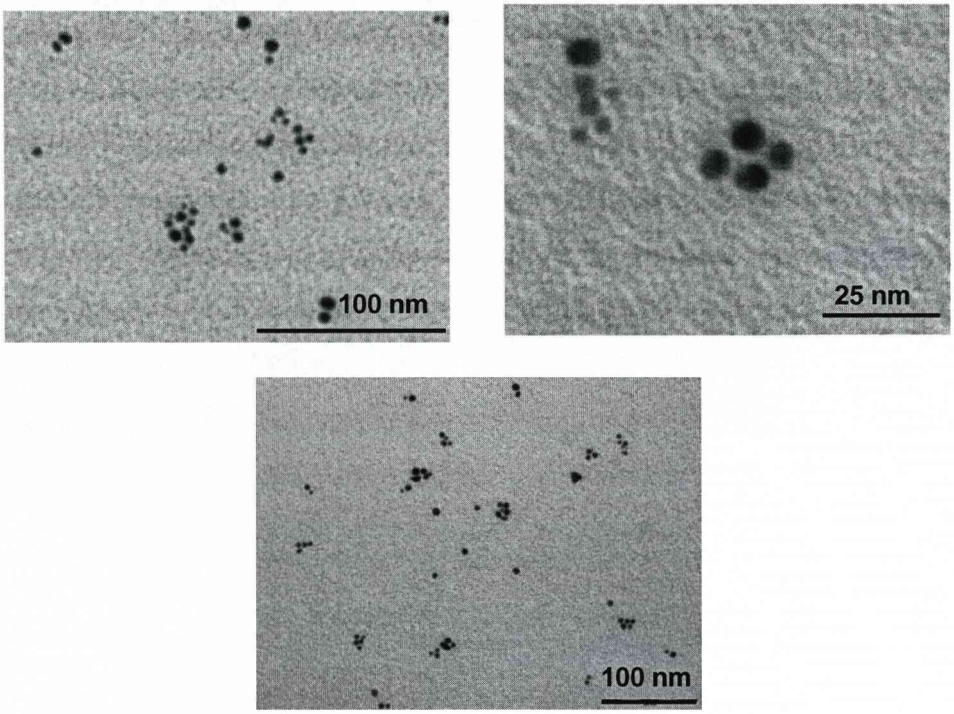

Figure 51. TEM images of the gold nanoparticles prepared via the citrate reduction in the presence of 1.8 mM DDT-PMAA. The scale bars represents 25 nm in the right spectrum and 100 nm in the top left spectrum.

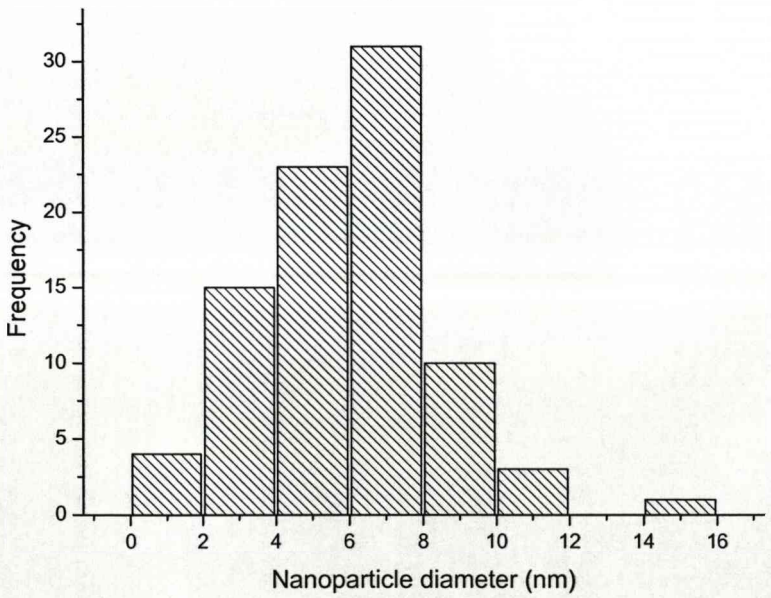

Figure 52 (previous page). ImageJ [126] analysis of the TEM images of the gold nanoparticles prepared via the citrate reduction in the presence of 1.8 mM DDT-PMAA.

Another sample of gold nanoparticles was prepared using this modified version of the citrate reduction technique. The concentration of polymer used was 0.03 mM, considerably lower than either of the concentrations previously used.

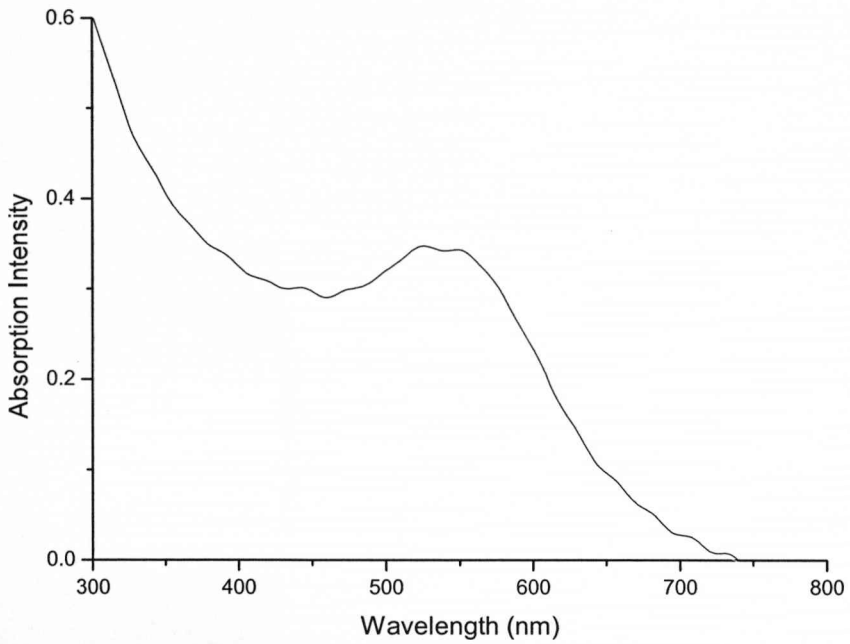

Figure 53. UV-visible absorption spectrum of the gold nanoparticles prepared via the citrate reduction in the presence of 0.03 mM DDT-PMAA.

When this concentration of polymer was used the absorption spectrum shows an unusually broad peak (Figure 53) centred on a wavelength higher than the 520 nm typical of nanoparticles in the 5-20 nm range. Figure 54 shows a selection of TEM images of the sample of nanoparticles prepared in a 0.03 mM solution of DDT-PMAA. The TEM

images (Figure 54 & 55) are unique amongst those obtained for the nanoparticles prepared by this technique. The nanoparticles are arranged in two-dimensional structures on the TEM grid with most nanoparticles exhibiting an approximately spherical shape with only a few of the larger nanoparticles deviating from that shape. It is likely that the dense arrangement of nanoparticles seen in these images occurs due to a high quantity of stable nanoparticles being produced in this synthesis. The average core diameter determined from an analysis of a representative area of a TEM image was found to be 6.0 ± 3.4 nm.

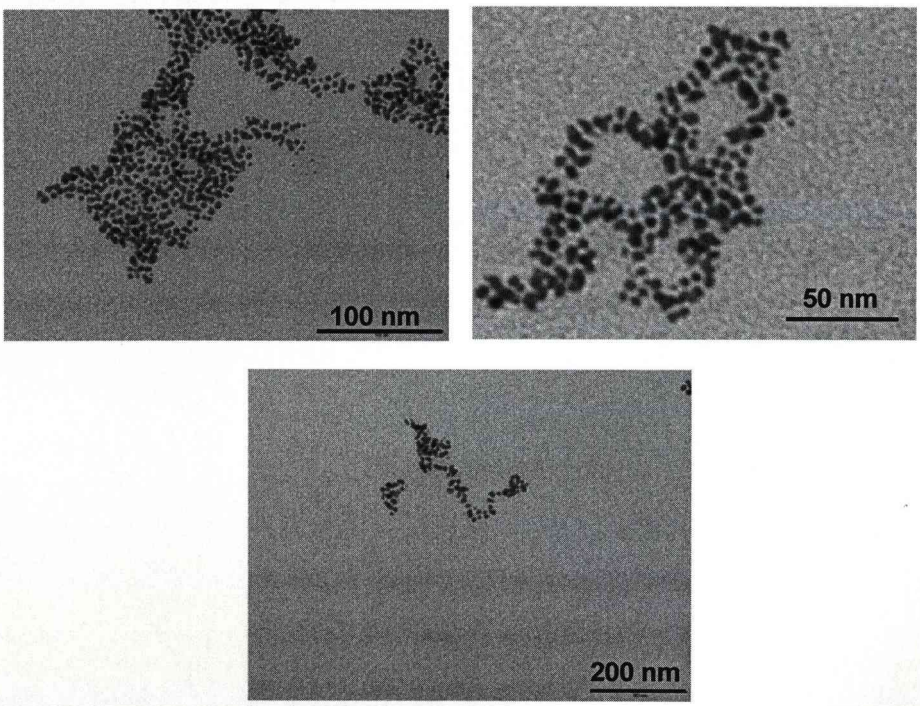

Figure 54. TEM images of gold nanoparticles prepared by the citrate reduction technique in a 0.03 mM aqueous solution of DDT-PMAA.

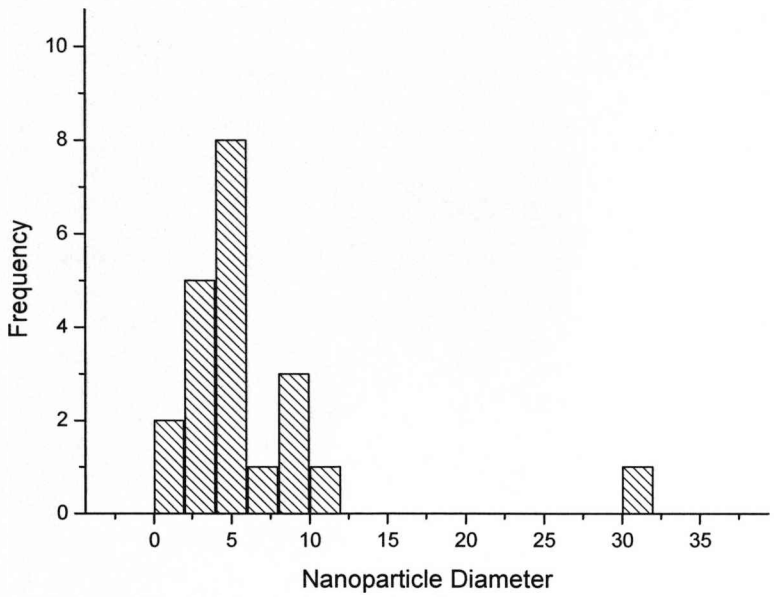

Figure 55. ImageJ [126] derived size distribution of gold nanoparticles prepared via the citrate reduction in a 0.03 mM aqueous solution of DDT-PMAA.

5.2.3 Summary

Contrary to expectations the nanoparticles prepared in a solution of the lowest concentration of polymer does not produce the largest gold nanoparticles. It seems that, in general, the degree of monodispersity imparted to nanoparticles synthesised by the citrate reduction technique in the presence of DDT-PMAA is not improved to the same extent as the two-phase synthesis but there is an improvement over that seen when gold nanoparticles are produced by the citrate reduction technique in the absence of DDT-PMAA.

As the stability of these large nanoparticles is not adversely affected by the addition of the polymer during synthesis it seems likely that citrate stabilization of nanoparticles prevails. It is possible that the polymer

plays a part in organising the nanoparticles into stable arrangements at an early stage of the reduction followed by functionalization of the surface by citrate ligands. This would result in the formation of citrate stabilized nanoparticles with slightly improved monodispersity. It is also possible that the combination of both PMAA-DDT and citrate ligands functionalize the nanoparticle. ^{1}H NMR studies of the products proved inconclusive, the polymer was detected in the product but this may have been unreacted polymer which hadn't been washed away during purification. Further analysis of the products would be necessary to determine which mechanism is most likely. Analysis by IR spectroscopy may show the presence of an Au-S bond in the product which would indicate the presence of PMAA-DDT at the surface of the nanoparticles. The results of such an analysis would have to be interpreted with care as it is possible that some polymer may remain in the final sample of nanoparticles especially given the difficulty of washing the sample (as citrate stabilised nanoparticles are water soluble).

It is possible that the low concentrations of polymer used were insufficient to provide an adequate surface coverage on the nanoparticles. For a sample of 7 nm gold nanoparticle we can assume there are around 1000 Au atoms on the surface of each particle (10% of the total number of gold atoms as determined from the core diameter using equation 8). Given the stoichiometry of the process (determined from the initial concentration of both polymer and gold starting material together with the number of surface sites) it is likely that the produced nanoparticles have a negligible coverage of polymer molecules which explains the weak effect on the size of the produced nanoparticles, at these lower polymer concentrations there would be less than one polymer molecule per nanoparticle.

It is possible that the application of this polymer in the synthesis of gold nanoparticles may produce monodisperse products if the concentration of polymer used was sufficient to provide sufficient surface coverage of the growing nanoparticles.

5.3 DDT-PMAA in the Synthesis of Ag Nanoparticles

5.3.1 Introduction

The synthesis of monodisperse metal nanoparticles in aqueous solutions of polymers has been previously demonstrated [57]. As mentioned at the start of the chapter, the use of DDT-PMAA and similar polymers during synthesis shows great potential for the production of monodisperse metal nanoparticles with average core diameters which can be controlled by variation of the initial concentration of polymer (with respect to the metal salt). In order to assess the scope for using this technique in conjunction with solubility testing, a short study on the effect of DDT-PMAA on the synthesis of silver nanoparticles was performed. The synthesis of silver nanoparticles by reduction with sodium borohydride was studied at a range of different polymer concentrations (at a fixed silver nitrate concentration) along with a control experiment under the same conditions but with a complete absence of the polymer. Alkanethiol stabilized silver nanoparticles are well known and can be characterized by their colourful solution and strong plasmon band absorptions [86]. The Ag-S bond is strong enough to allow the effective surface coverage (and subsequent steric stabilisation) of silver nanoparticles by alkanethiol ligands so it was predicted DDT-PMAA would bind to the surface in the same way.

5.3.2 Experimental

20 mL of a 0.5 mM aqueous solution of silver nitrate was prepared; to this a given amount of polymer (DDT-PMAA) was added to make the solution up to the required concentration of polymer. 2 mL of an aqueous solution of sodium borohydride was added to the solution. The solution initially turned yellow, at some concentrations a darker yellow/brown colour was observed later.

The first experiment used an aqueous solution of silver nitrate (as described above) and 0.03 mM of DDT-PMAA. The UV-Visible absorption spectrum shows a broad peak centred on a wavelength of 420 nm (Figure 58). The TEM images of the nanoparticles produced during this synthesis are presented in Figure 56. Analysis of the TEM images (Figure 57) shows a less monodisperse sample than obtained using the same concentration of polymer in the synthesis of gold nanoparticles. The average core diameter was determined as being 3.1 ± 2.7 nm.

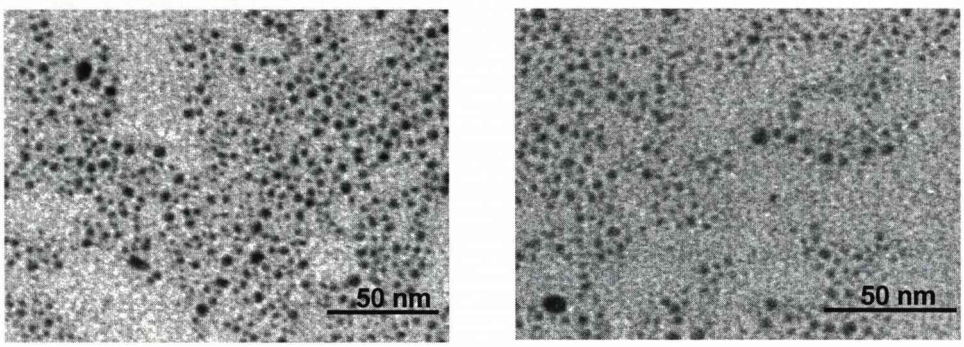

Figure 56. TEM images of the silver nanoparticles prepared via the $NaBH_4$ reduction in the presence of 0.03 mM DDT-PMAA.

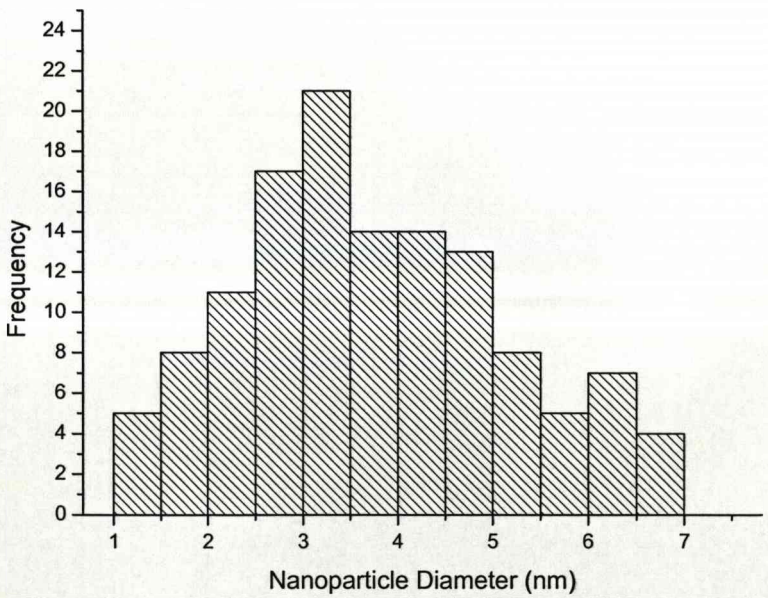

Figure 57 (previous page). ImageJ [126] size distribution of silver nanoparticles prepared via the $NaBH_4$ reduction a 0.03 mM solution of DDT-PMAA.

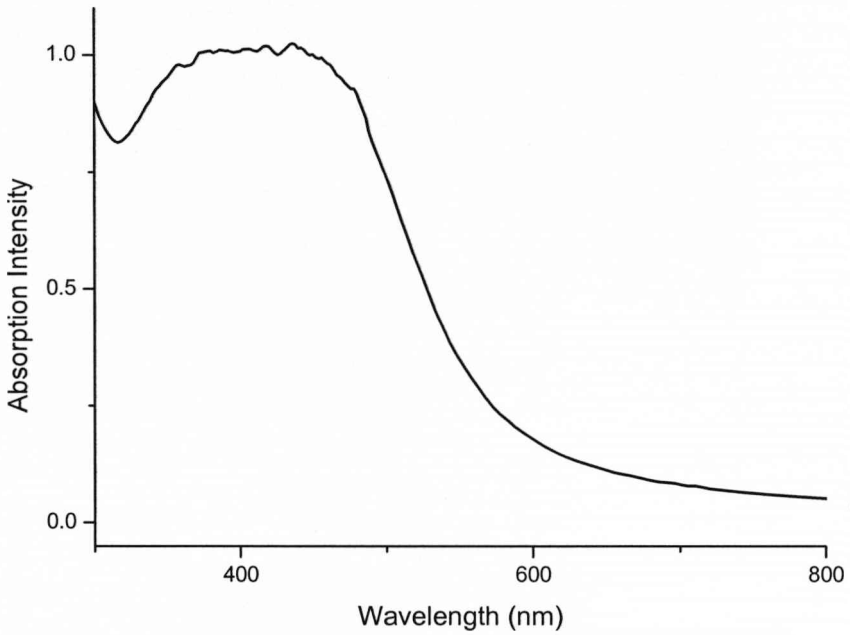

Figure 58. UV-visible absorption spectrum of the silver nanoparticles prepared via the $NaBH_4$ reduction in a 0.03 mM aqueous solution of DDT-PMAA.

The series of syntheses was continued with the preparation of silver nanoparticles in a 0.18 mM aqueous solution of the polymer. The UV-visible absorption spectrum is presented in Figure 59 and shows a relatively sharp peak, again centred at a wavelength of approximately 420 nm.

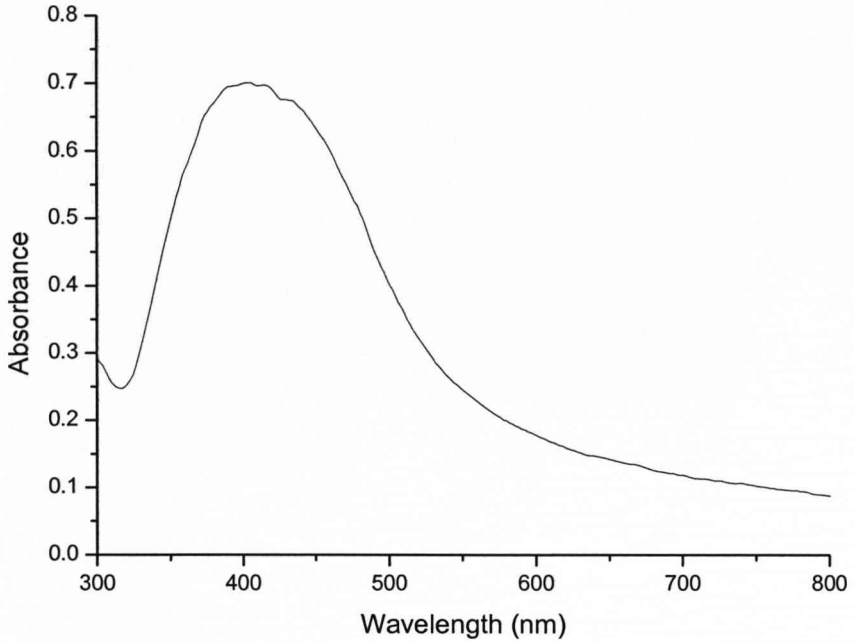

Figure 59. UV-visible absorption spectrum of the silver nanoparticles prepared via the $NaBH_4$ reduction in a 0.18 mM aqueous solution of DDT-PMAA.

The TEM images (Figure 60) of these nanoparticles shows a narrow size distribution with an average core diameter of 1.9 ± 0.8 nm (Figure 61). The sample was also analysed by DLS (Figure 62) which calculated an average core diameter of 8.8 nm from the mass distribution and 9 nm from the intensity distribution.

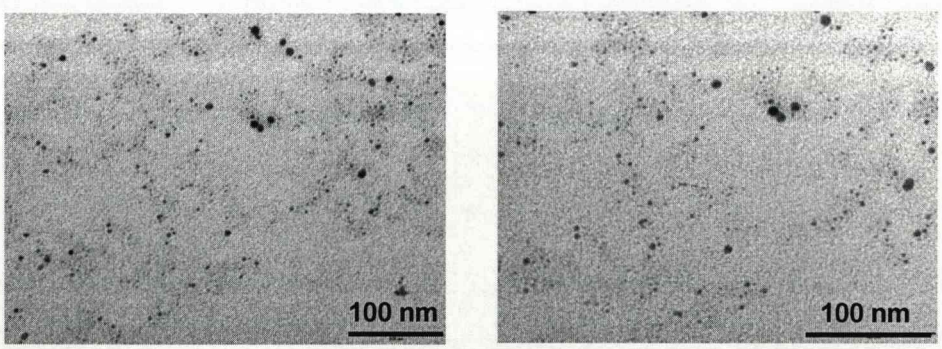

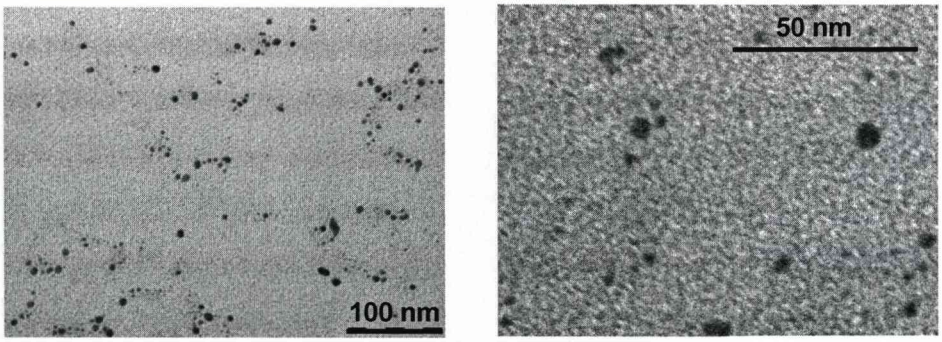

Figure 60. TEM images of silver nanoparticles prepared via the $NaBH_4$ reduction in a 0.18 mM DDT-PMAA aqueous solution.

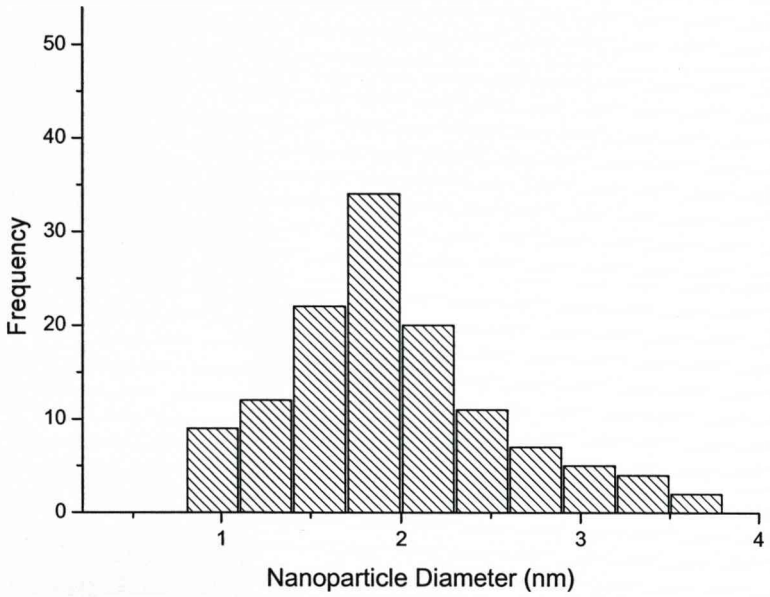

Figure 61. Analysis of the TEM images of the silver nanoparticles prepared via the $NaBH_4$ reduction in the presence of 0.18 mM DDT-PMAA.

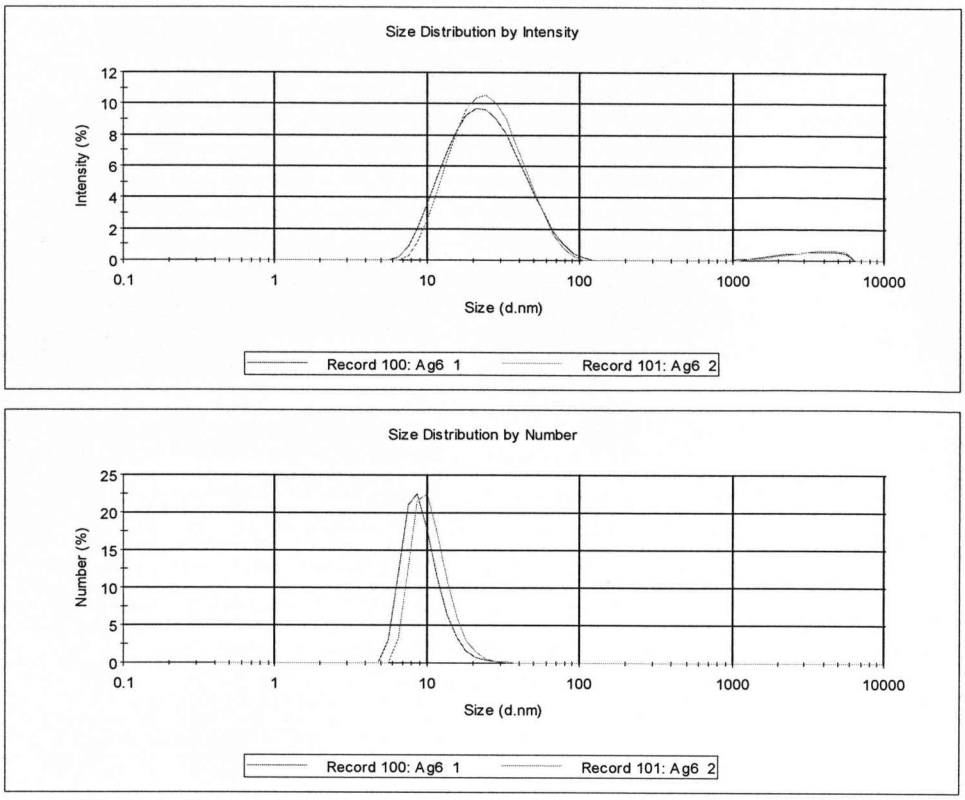

Figure 62. DLS Analysis of the silver nanoparticles prepared via the $NaBH_4$ reduction in the presence of 0.18 mM DDT-PMAA.

The synthesis was repeated with an initial polymer concentration of 0.001 mM. The product of this solution was a dark yellow/brown solution, the UV-visible absorption spectrum shows a broad peak (Figure 63) at a maximum wavelength of around 400 nm. When the solvent was evaporated the dry particles would not redissolve in an excess of solvent. It is possible that the stability of the nanoparticles decreases as the polymer concentration is reduced due to a lower surface coverage of the metal core and less effective steric stabilization of the core against aggregation. This effect is demonstrated by the inability of the solvent to reprecipitate the nanoparticles following evaporation of the solvent.

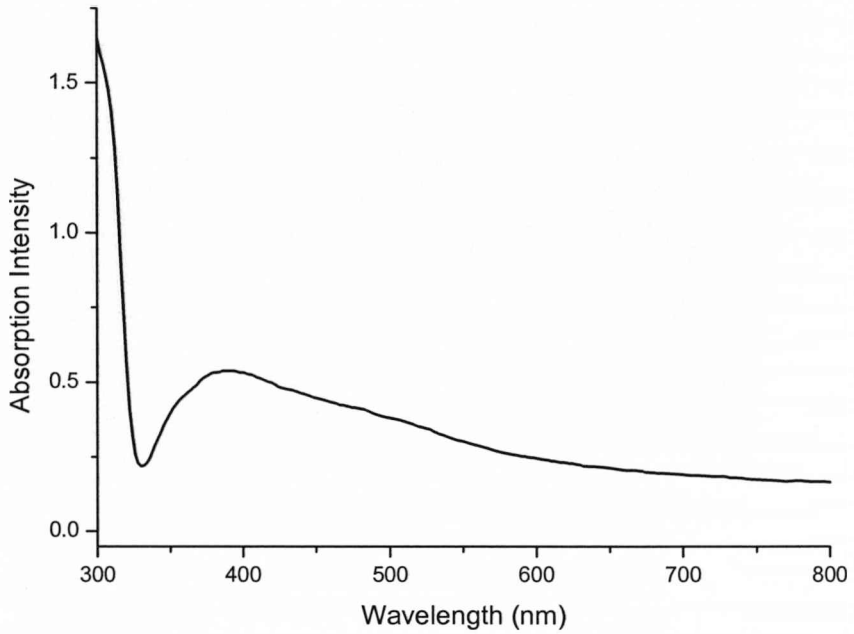

Figure 63. UV-visible absorption spectrum of the silver nanoparticles prepared via the $NaBH_4$ reduction in the presence of 0.001 mM DDT-PMAA.

There is a small degree of inconsistency in the average core diameters determined from TEM (Figure 64) and DLS analysis (Figure 65) of this sample of nanoparticles. The number intensity distribution of the DLS results shows that the average core diameter is 2.78 nm whereas the analysis of the TEM images (Figure 66) suggests that the average core diameter is higher at 3.39 nm. However, this is reasonable agreement from these very different techniques.

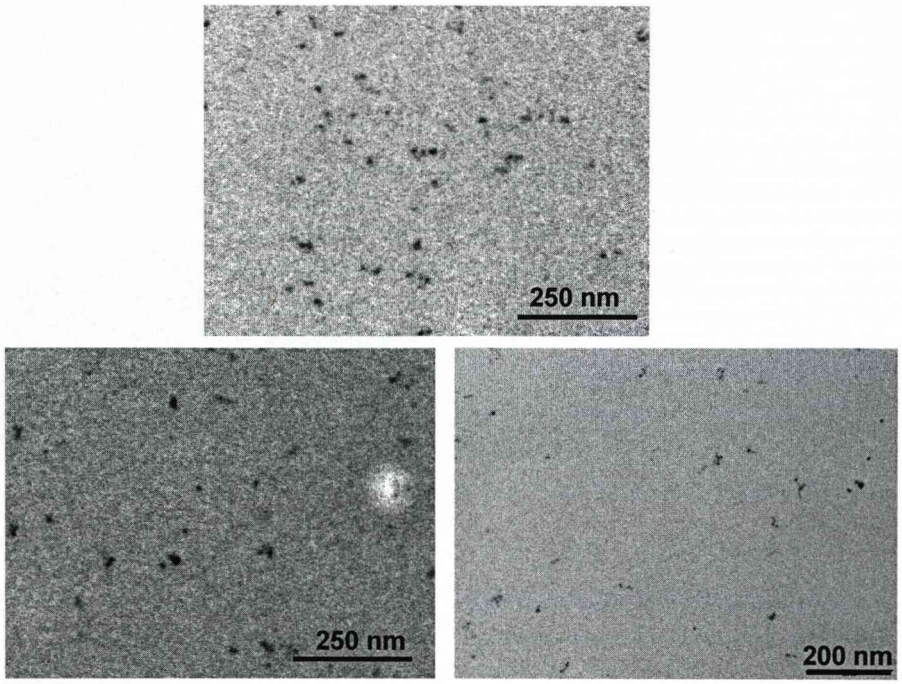

Figure 64. TEM images of the silver nanoparticles prepared via the $NaBH_4$ reduction in the presence of 0.001 mM DDT-PMAA.

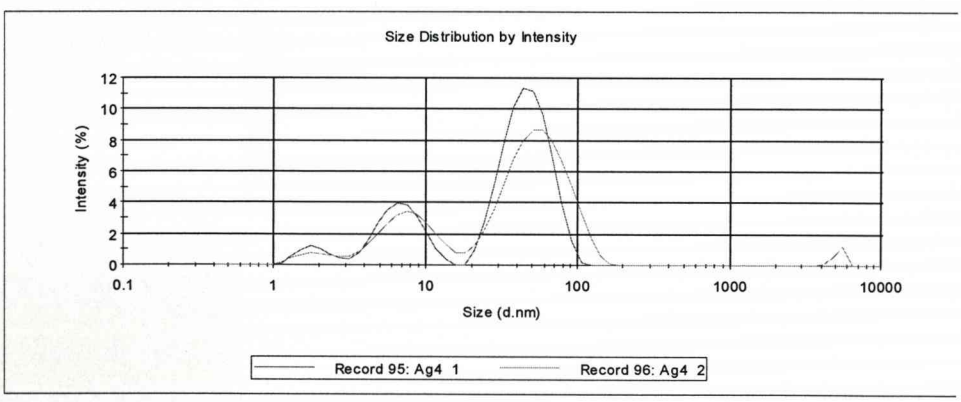

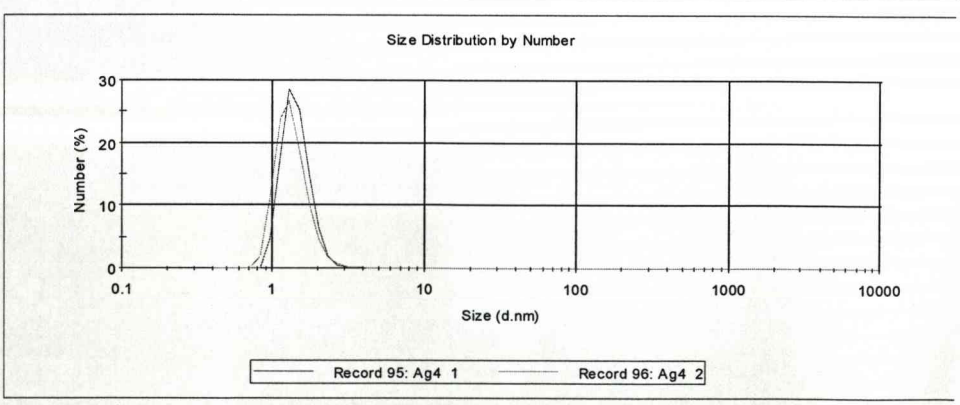

Figure 65 (previous page). DLS analysis of the silver nanoparticles prepared via the $NaBH_4$ reduction in the presence of 0.001 mM DDT-PMAA.

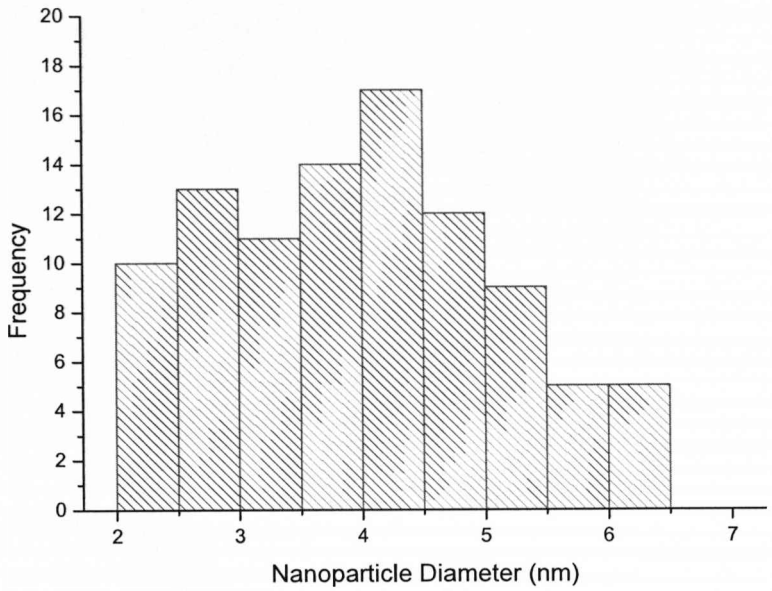

Figure 66. Analysis of the TEM images of the silver nanoparticles prepared via the $NaBH_4$ reduction in the presence of 0.001 mM DDT-PMAA.

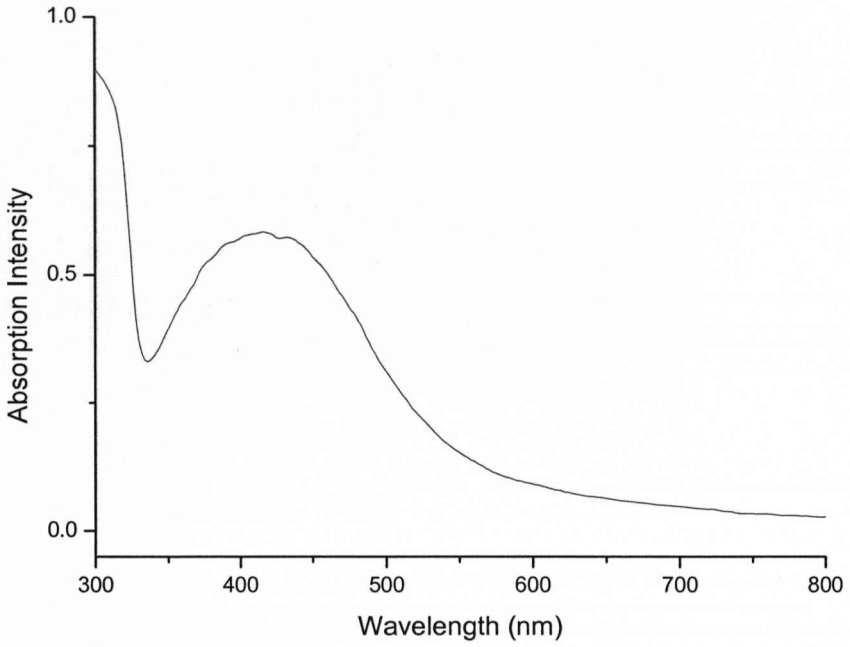

Figure 67. UV-visible absorption spectrum of the silver nanoparticles prepared via the $NaBH_4$ reduction in the presence of 1.8 mM DDT-PMAA.

The synthesis was repeated at an initial polymer concentration of 1.8 mM. The UV-visible absorption spectrum (Figure 67) shows a familiar peak centred around 420 nm). The DLS analysis (Figure 70) suggests that the average core diameter of the nanoparticles produced is larger than those prepared in the presence of less concentrated solutions of the polymer. The average core diameter proposed by the DLS analysis is 2.59 nm, the TEM image analysis (Figure 68 & 69) is in reasonable agreement with the DLS value, giving a value of 1.8 ± 1.0 nm.

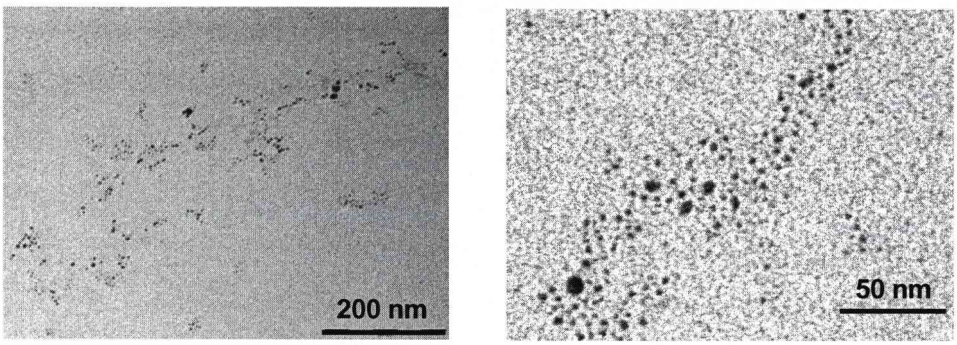

Figure 68. TEM images of the silver nanoparticles prepared via the $NaBH_4$ reduction in the presence of 1.8 mM DDT-PMAA.

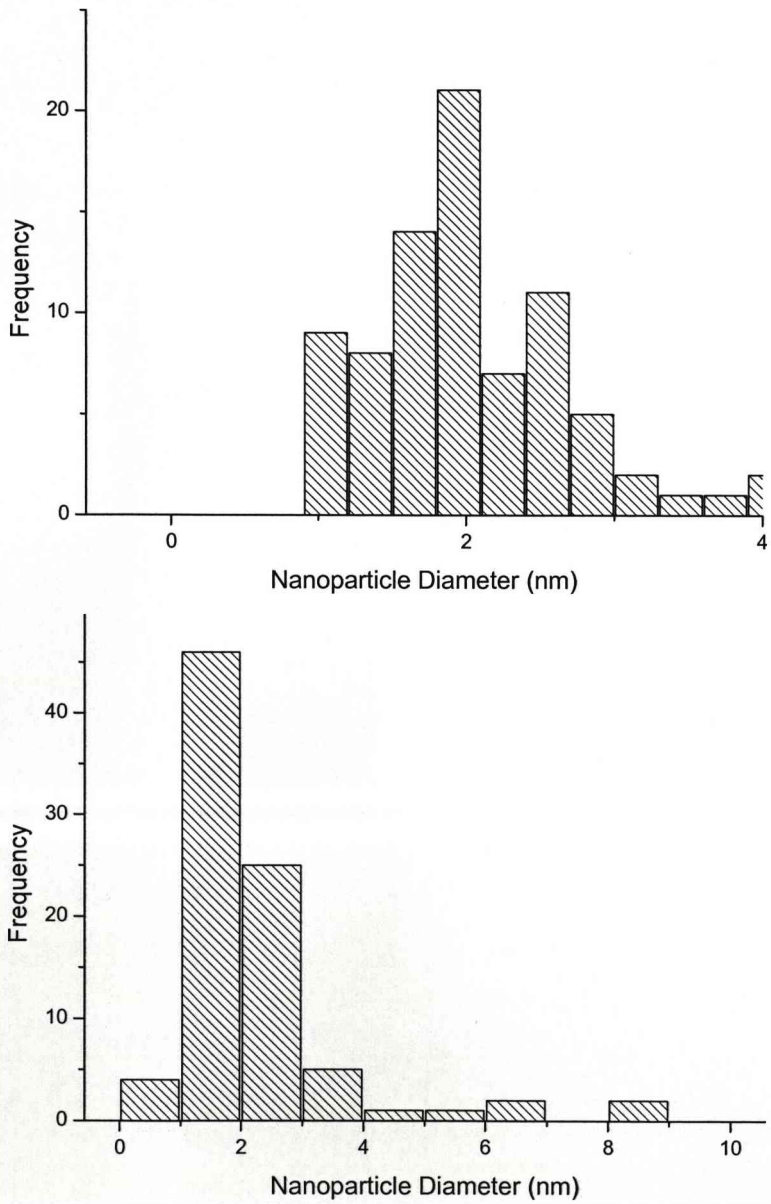

Figure 69 (previous page). Analysis of the TEM images of the silver nanoparticles prepared via the $NaBH_4$ reduction in the presence of 1.8 mM DDT-PMAA.

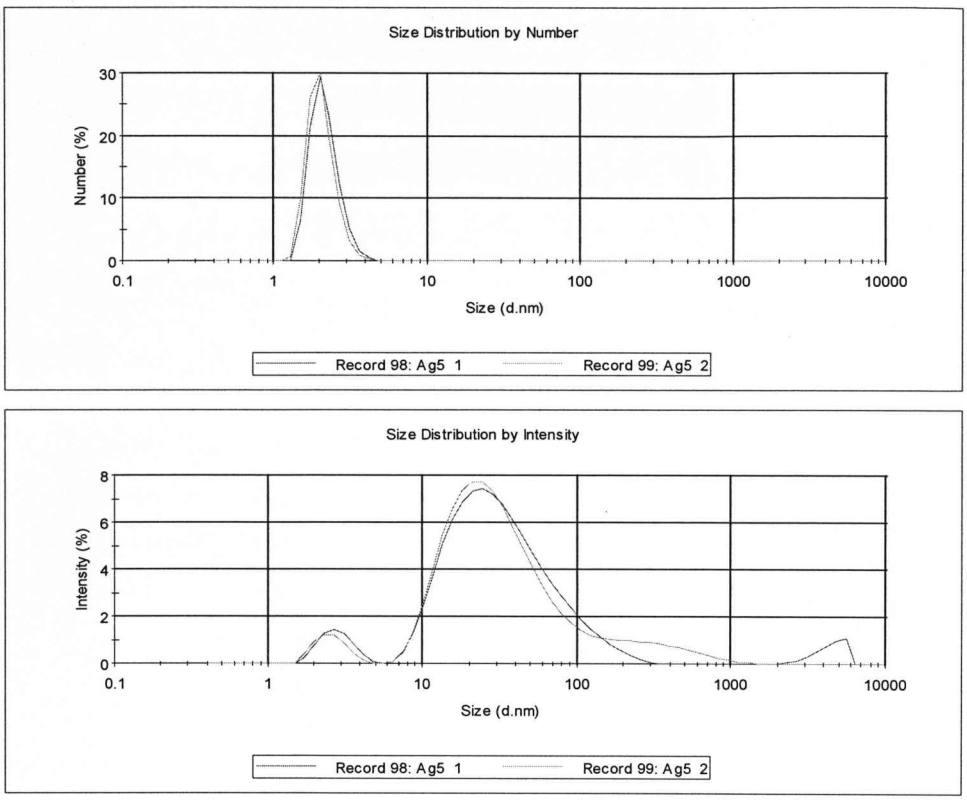

Figure 70 (previous page). DLS analysis of the silver nanoparticles prepared via the $NaBH_4$ reduction in the presence of 1.8 mM DDT-PMAA.

5.4 Summary

PMAA-DDT Concentration (nM)	1)Average core diameter (nm)	2)Average Core Diameter (nm)
0.001	3.39 ± 2.1	2.78
0.03	3.10 ± 2.7	Unmeasured
0.18	1.75 ± 0.80	8.8
1.8	1.80 ± 1.0	2.15

Table 2. Summary of the average core diameters of Ag nanoparticles produced following reduction in $NaBH_4$ in the presence of PMAA-DDT, 1 is the diameter calculated from TEM analysis and 2 is the diameter determined from DLS (number distribution).

Table 2 is a summary of the results from this sub-chapter. This series of experiments shows a similar trend in the variation of average core diameter with polymer concentration to the published work [33, 57] on gold nanoparticle synthesis. The lower the concentration of polymer used (at a fixed concentration of silver nitrate) the higher the average core diameter of the nanoparticle produced. It has been stated that this may be due to a lower degree of steric protection of the growing nanoparticle due to the lower abundance of the polymer in the reaction mixture and, therefore a lower surface coverage on the nanoparticle [57]. Higher initial concentrations of polymer with respect to silver nitrate result in the formation of smaller silver nanoparticles, possibly due to the more effective steric protection of the growing silver particles. The polydispersity of the reaction with low concentrations of polymer is quite disappointing and is not a substantial improvement on degrees of polydispersity reported in conventional synthesis of silver nanoparticles. At higher initial polymer concentrations (again, at a fixed concentration of silver nitrate) the monodispersity shows a significant improvement. It is possible that further investigation of this process may show it to be as

useful to the preparation of monodisperse samples of silver nanoparticles as it is to their gold analogues.

It is again likely that the lower concentrations of polymer only provide a very small level of surface coverage meaning that the nanoparticles produced differ only slightly from those produced in the absence of the polymer.

On a closing note it is worth highlighting the fact that there is little variation between the final two core diameters in spite of the fact that there is a significant variation in the polymer concentration between these two experiments. It is possible that a minimum stable nanoparticle size exists for this process and smaller nanoparticles will not readily form at any concentration below this size. For the silver-DDT-PMAA synthesis this point appears to have been reached at around 1.70-1.80 nm.

Chapter Six

The Synthesis and Solubility Behaviour of Near-Monodisperse Gold Nanoparticles

6.1 Introduction

As established in earlier chapters, one of the primary aims of this project was the determination of the solubility of gold nanoparticles with a range of core diameters in supercritical ethane. As stated earlier, accurate solubility testing requires the isolation of highly monodisperse fractions of gold nanoparticles. Synthetic techniques used earlier in the study (including the two-phase [4] and Turkevich-Frens [1, 2] techniques) can lead to the preparation of inhomogeneous samples of nanoparticles (varying ranges of polydispersity have been reported [4, 26, 37, 53, 142]). In order to determine the solubility of such samples an estimate of the quantity of material which had dissolved in each experiment would have to be made. This would be difficult to determine from UV-Visible absorption analysis of the dissolved samples as the spectra would consist of a resultant absorption arising from the individual plasmon responses of the various nanoparticle size fractions present in the sample. Additionally, the distinct solubility behaviour of metal nanoparticles of different sizes (which was discussed in greater detail in Chapter 4) prevented the accurate calculation of solubility for samples of polydisperse nanoparticles. Elemental analysis data for these particles showed the total weight percentage of gold atoms present in a sample but, as the size and relative proportion of the metal clusters present in the sample was not known, the percentage of gold atoms corresponding to each individual cluster size could not be determined. MALDI-TOF mass spectroscopy has been used to determine some qualitative information about the clusters present in samples of nanoparticles but this is an unreliable technique for obtaining the relative abundances of these clusters due to the variable results obtained by the technique depending on the precise way the spectrometer laser beam strikes the sample.

Because of the difficulties outlined above it was desirable to synthesise monodisperse samples of metal nanoparticles for the solubility

measurements. As discussed in earlier chapters, various techniques have been used to prepare stable samples of highly monodisperse nanoparticles. This study has demonstrated the viability and versatility of using supercritical fluids in separating size fractions from a polydisperse sample of gold nanoparticles prepared via a conventional synthetic technique. Due to the limitations of the project and the apparatus available the ability to fully fractionate a sample was not demonstrated and the quantities of monodisperse product which were obtained were insufficient to sustain the needs of a solubility study. A simple and fast synthetic technique to prepare sufficient quantities of monodisperse samples of gold nanoparticles was needed.

In order to produce highly monodisperse gold nanoparticles, the polymer assisted synthesis described in the previous chapter was used [33, 57]. For the preparation of alkanethiol stabilised nanoparticles the reaction conditions used in the literature study were recreated. Some sample were prepared using some of the polymer:gold ratios quoted in the literature and some were prepared with different ratios.

The first part of this chapter covers the synthesis of highly monodisperse alkanethiol stabilised gold nanoparticles and the subsequent characterization of these nanoparticles. Later sections focus on the solubility measurements, including some consideration of the Henry's Law constants determined from these studies compared with those obtained from theory.

6.2 Experimental

6.2.1 Nanoparticle Synthesis

The polymer (dodecanethiol-terminated poly(methacrylic acid, DDT-PMAA) used for this project was generously provided by the M. Brust and A. I. Cooper research groups. Most of the early work made use of DDT-PMAA, basic details of the synthesis of this polymer can be found

in Chapter 5.2, further details can be found in the supporting information of the original article [57].

In order to prepare monodisperse gold nanoparticles 20 mL of a 0.5 mM aqueous solution of hydrogen tetrachloroaurate was prepared. A specific amount of the polymer was added to this solution (see Table 3) and allowed to mix under vigorous stirring. 2 mL of an aqueous solution of the reducing agent ($NaBH_4$, 50 mM) was added to the solution, the mixture was left under agitation for 2 hours. The resulting colourful aqueous solutions of gold nanoparticles were then analysed by UV-visible absorption spectroscopy.

The nanoparticles were then transferred from aqueous to organic solvent by the addition of 20 mL of an ethanolic solution of dodecanethiol and stirred overnight. Following stirring the nanoparticles were found floating on the surface of the solution and could be extracted by n-hexane. The particles were then washed at least three times with distilled water to remove any excess polymer from the extracted material. Any remaining water was subsequently removed by filtering the solution of nanoparticles over anhydrous sodium sulphate. The solution was reduced to several mL by rotary evaporation and the excess dodecanethiol was removed by thoroughly washing the solution with ethanol. The particles were not subject to any additional purification. It is possible that some polymer remained bound to the particles as the polymer peak was detected in ^1H NMR analysis.

Concentration of polymer in initial solution (mM)	Particle diameter (nm)
0.006	4.0 ± 0.1
0.03	3.0 ± 0.1
0.18	2.5 ± 0.3
0.6	2.0 ± 0.2
1.8	1.8 ± 0.3
3.6	1.5 ± 0.2

Table 3 (previous page). Summary of particle diameters of nanoparticles produced using the technique described above with the given concentrations of polymer as determined by M. Brust and A. I. Cooper research groups [57].

Following purification in ethanol the nanoparticles were filtered, dried and redissolved in n-hexane solution for storage and analysis. The UV-visible absorption spectrum for each sample was recorded and a selection of TEM images for the different nanoparticles was also obtained by evaporating a drop of the solution onto a copper mesh grid. The nanoparticles were also analysed by DLS to provide a complementary analysis to TEM.

6.2.2 Characterization

In order to prepare 2.5 nm gold nanoparticles the polymer concentration in the original solution was 0.18 mM as specified in earlier work on the subject.

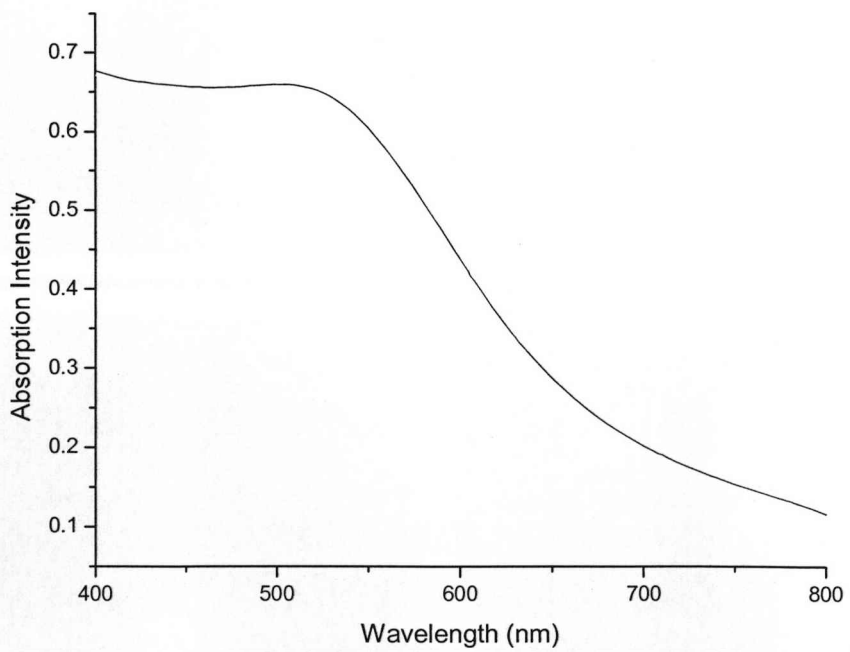

Figure 71 (previous page). UV-visible absorption spectrum of the sample of gold nanoparticles synthesized with 0.18 mM DDT-PMAA.

The UV-Visible absorption spectrum (Figure 71) is similar to that obtained in the synthesis using the same concentration of polymer in the published work [57]. In order to establish a value for the core diameter and the degree of polydispersity of sizes of the nanoparticles in the sample, a drop of the solution was placed onto a copper mesh grid and allowed to dry (as described in Chapters 3 and 4). This grid was then placed into the sample holder of the TEM and a series of images of different parts of the surface was captured (Figure 72).

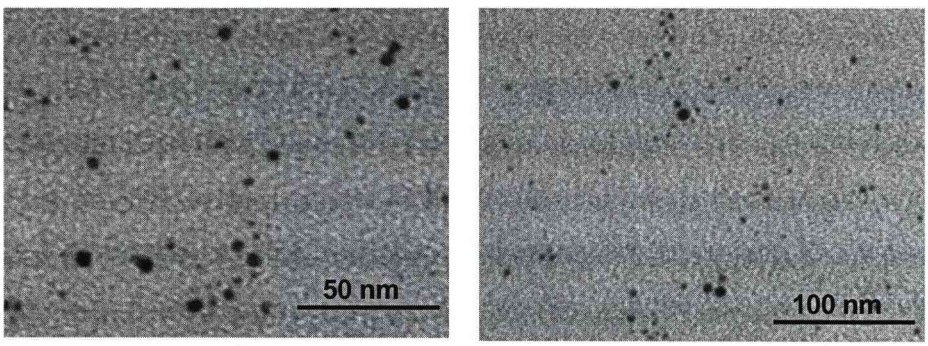

Figure 72. A selection of TEM images of the gold nanoparticles produced in a 0.18 mM solution of DDT-PMAA obtained at different magnifications.

The size distribution histogram determined by ImageJ [126] analysis of one of the TEM images is presented in Figure 73. This data shows that the average core diameter was slightly larger than that expected (from the literature [57]) and that the degree of polydispersity may have been larger than anticipated for this type of synthesis. It is possible that the distribution obtained from the analysis of the TEM images was flawed due to the possibility that the images are not representative of the bulk sample in spite of best efforts (i.e. multiple measurements over different areas of

the grid). It is also worth mentioning the effect of polymer polydispersity on the distribution of sizes in the product. It has been shown [33, 57] that the most monodisperse polymers result in the highest degrees of size control and monodispersity in the product. The sample of polymer used in this study is significantly more polydisperse than that which appeared in the literature and it is highly likely that the greater range of polymer sizes present in each synthesis would lead to a range of nanoparticle diameters due to inhomogeneous surface coverage or the particles.

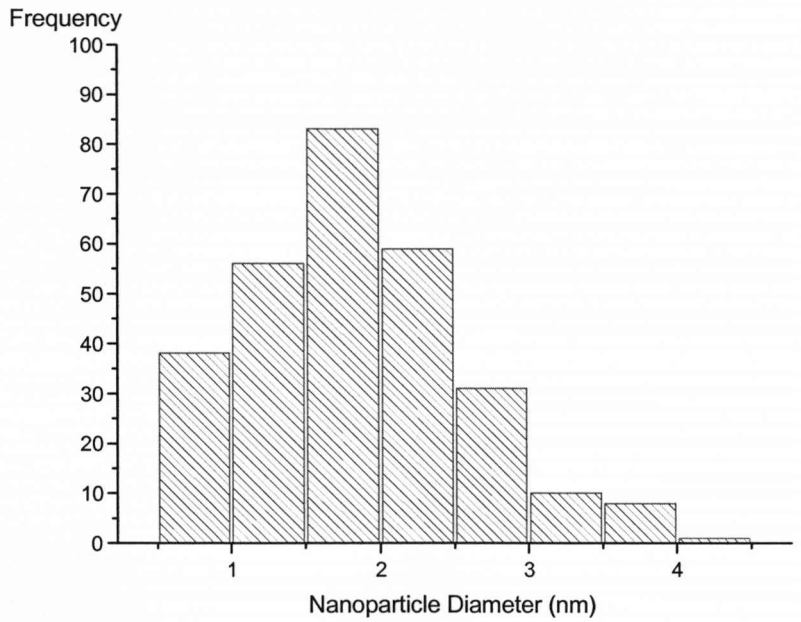

Figure 73. Size distribution histogram of the nanoparticles present in TEM images of the nanoparticles synthesised in a 0.18 mM solution of DDT-PMAA.

Further analysis of the sample was conducted by determination of the average core radius of a sample of the aqueous solution of nanoparticles by DLS. The aim of this analysis was to support the findings of the TEM analysis presented above. DLS has several advantages over analysis by TEM including the ability to analyse a bulk sample of the nanoparticles in solvent whereas TEM relies on a much smaller sample

size which must be dried before analysis (which may result in aggregation or spacing effects which do not occur when the nanoparticles are in solution).

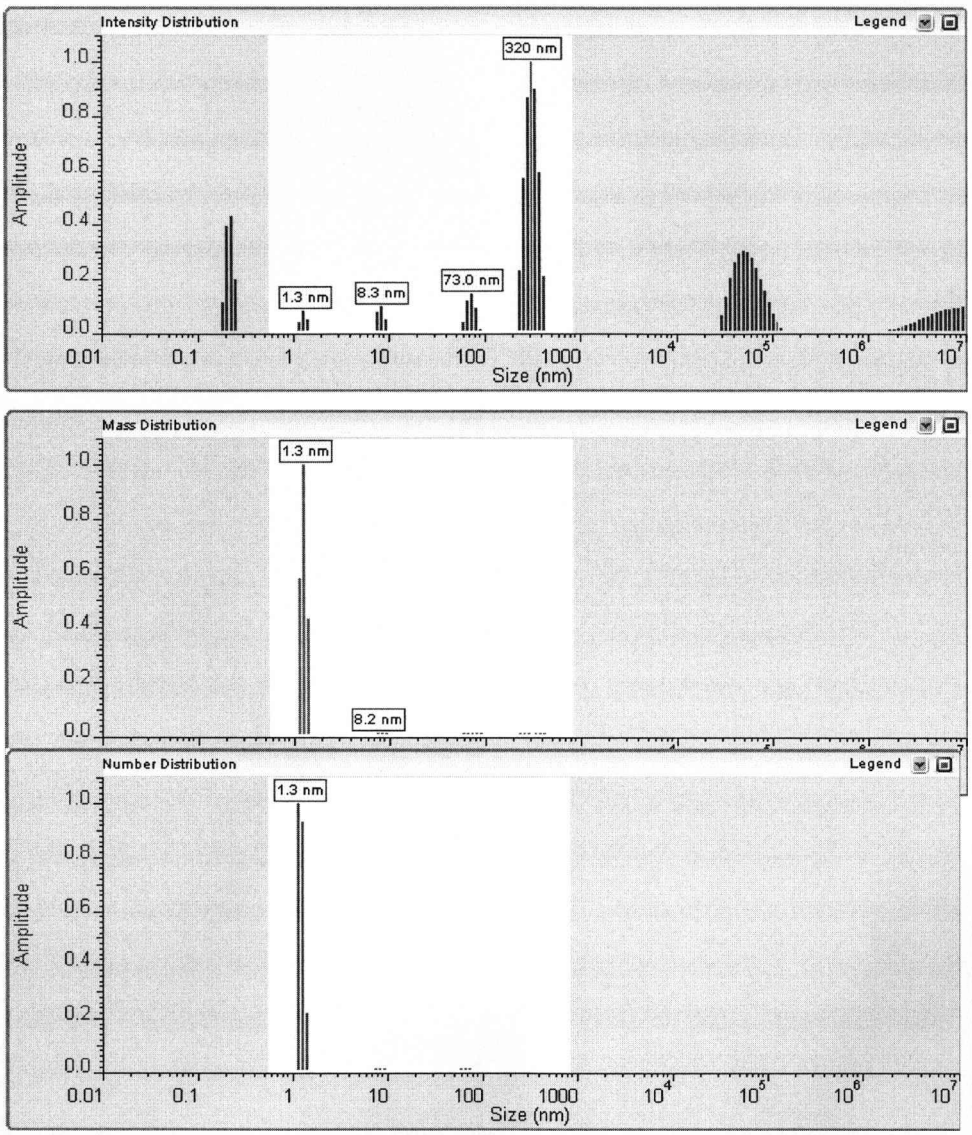

Figure 74. DLS analysis of gold nanoparticles prepared in a 0.18 mM solution of DDT-PMAA. From top to bottom: the intensity, mass and number distributions are presented.

The mass and number distributions obtained from DLS analysis (Figure 74) suggest that the particles in solution had an average core radius of 1.3 nm, corresponding to a diameter of 2.6 nm. This was slightly larger than the average diameter determined from the analysis of the TEM image

(2.1 ± 1.1 nm) but closer to the core diameter expected from the synthesis with this concentration of polymer from the published results [57]. The summary of results from the DLS analysis shows that the average radius from the mass distribution was 1.30 ± 0.09 nm and from the number distribution is 1.26 ± 0.09 nm. It is entirely reasonable that analysis by DLS and TEM will result in different values of average core diameters due to the considerable differences in the state of the sample during analysis.

The same synthetic technique was repeated with an initial DDT-PMAA concentration of 0.3 mM. This concentration was not amongst those quoted in the original investigation [57] so it was of interest to determine the core diameter and polydispersity of the nanoparticles produced under these conditions.

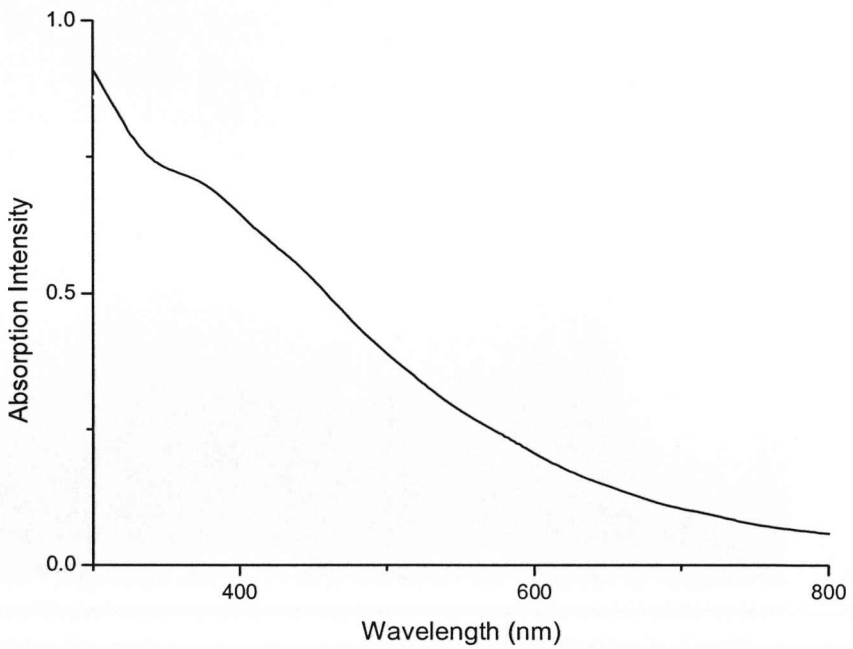

Figure 75. UV-visible absorption spectrum of the sample of gold nanoparticles synthesized with 0.3 mM DDT-PMAA.

Figure 75 shows the UV-visible absorption spectrum for the sample of nanoparticles synthesised under these conditions. A clear difference was

seen in the shape of the curve compared to that obtained from the synthesis with the lower concentration of polymer (0.18 mM). The characteristic plasmon band absorption of gold nanoparticles with a core diameter over around 2 nm was completely absent from the spectrum in figure 5 which suggested that the particles produced were significantly smaller than those obtained from those synthesised at lower polymer concentration. Further, the absence of the plasmon band shows that the particles produced under these conditions had an average core diameter below the point at which metal nanoparticles exhibit metallic behaviour (i.e. the free electron structure) gives way to a discrete electronic structure, commonly associated with very small nanoparticles [19, 111, 138]. As a consequence of this electronic rearrangement the plasmon band absorption observed in larger nanoparticles is completely lost.

These observations are consistent with the findings of the publication [57] which stated that the average core diameter of nanoparticles produced decreases as the initial concentration of polymer is increased with respect to the concentration of the gold starting material. It seems somewhat surprising that such a small variation in PMAA concentration would lead to such a larger variation in physical properties. A similar variation was observed in the earlier published work [57] on the subject but a decrease in average core diameter 2.5 to 2.0 nm was observed for a variation in initial concentration from 0.18 to 0.6 mM. The results from this study suggest an even larger decrease in average core diameter for a smaller variation in polymer concentration. The average core diameter and the size distribution of the nanoparticles were then determined from analysis of TEM images (Figures 76 & 78) and DLS measurements (Figure 77) for these particles.

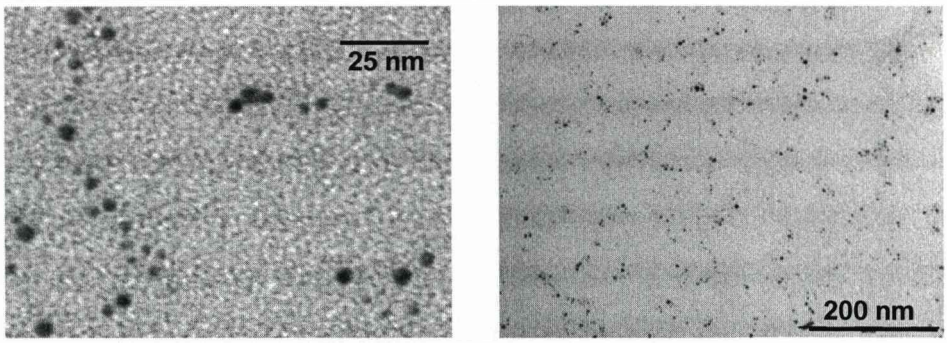

Figure 76. A selection of TEM images of the gold nanoparticles produced in a 0.3 mM solution of DDT-PMAA. The scale bars read 25 nm for the image on the left and 200 nm for the image on the right.

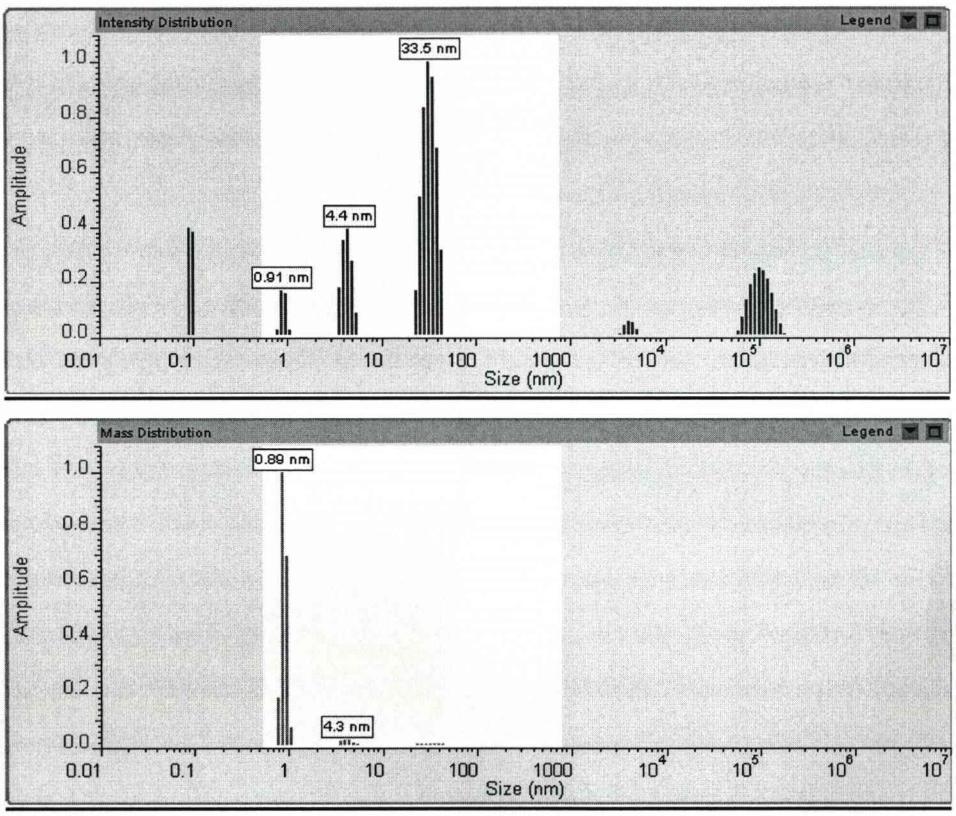

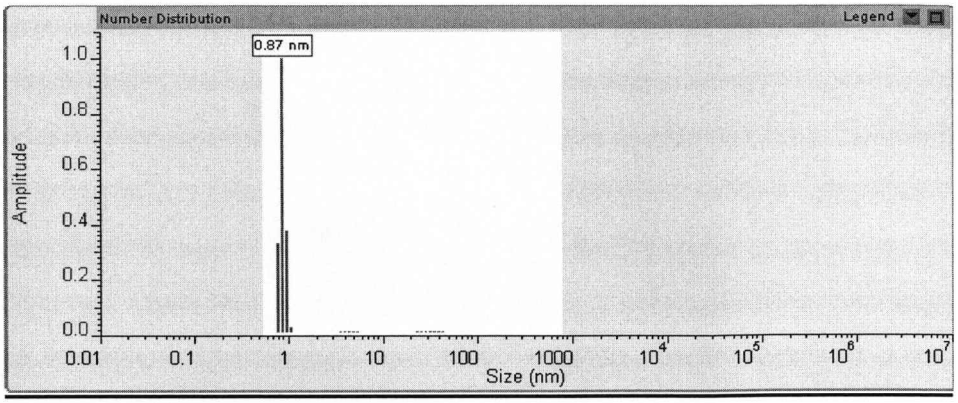

Figure 77. DLS analysis of gold nanoparticles prepared in a 0.3 mM solution of DDT-PMAA. From top to bottom: the intensity, mass and number distributions are presented.

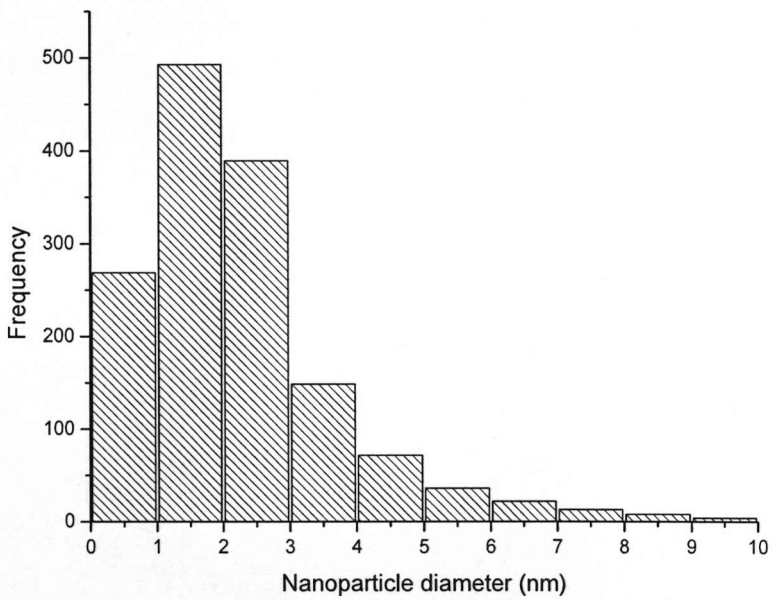

Figure 78. ImageJ [126] core diameter distribution histogram of alkanethiol stabilized gold nanoparticles prepared by reduction of gold tetrachloroaurate in a 0.3 mM solution of DDT-PMAA.

From the DLS mass and number analysis the nanoparticles produced at these conditions appeared to be relatively monodisperse (compared to those synthesized by the two-phase technique in Chapter 3)

with an average core radius of 0.87 ± 0.3 nm (from the number distribution), equal to a diameter of 1.74 ± 0.6 nm, which was consistent with the lack of plasmon band absorption at around 520 nm in the UV-visible absorption spectrum. A number of other peaks were seen in the intensity distribution of the sample - included for completeness. As larger particles scatter light to a much greater extent than small particles large peaks are usually detected corresponding to small concentrations of dust impurities, aggregates or artefacts from within the cuvette. It is possible that the peak at radius of 4.4 nm in the intensity distribution and 4.3 nm in the mass distribution correspond to a stable cluster of gold atoms. The size distribution histogram determined from analysis of the TEM images agree well with the findings of the DLS analysis, the average core diameter was determined as being 1.9 ± 1.4 nm.

Both the mass and number distribution analysis resulted in an average core radius of 0.86 nm with a standard deviation of 0.6 nm. This suggested a larger degree of polydispersity in the sample than reported in the published study. The size distribution appeared to be a considerable improvement over that achieved from conventional synthetic techniques; the variation with the size distribution in the published study is likely to be due to variations in the quality of the polymer used in the synthesis.

The same technique was used with an initial concentration of dodecanethiol ether terminated PMAA of 0.006 mM. Using this initial concentration resulted in the formation of gold nanoparticles with an average core diameter of 4.0 nm in the original study.

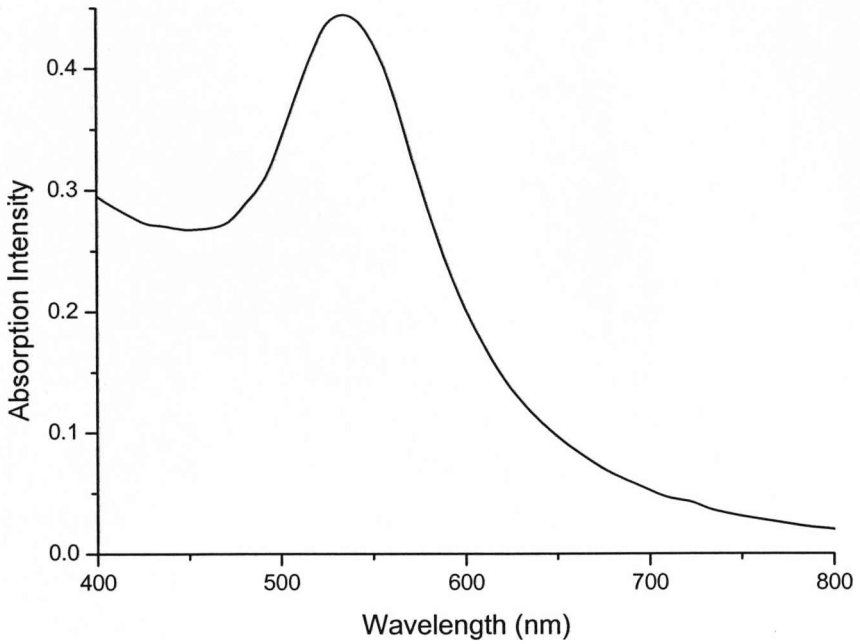

Figure 79. UV-visible absorption spectrum of the synthesis of a sample of gold nanoparticles using an initial DDT-PMAA concentration of 0.006 mM.

The result of the synthesis using an initial polymer concentration of 0.006 mM is consistent with that obtained in the literature with a prominent plasmon band absorption appearing at a wavelength of approximately 520 nm in the absorption spectrum (Figure 79). The deep red colour of this sample also corresponds to that of a solution of nanoparticles of the size expected to be formed at this concentration of polymer. As before the synthesised nanoparticles were analysed by TEM (Figure 80) in order to obtain the average core diameters and size distribution of the particles.

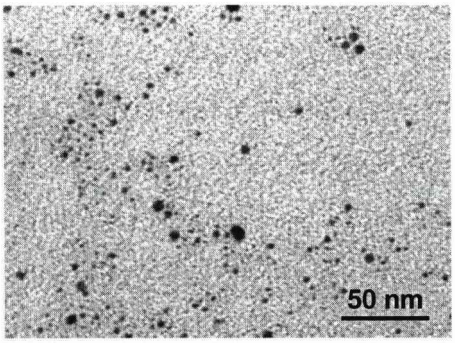

Figure 80. TEM image of the gold nanoparticles produced in a 0.006 mM solution of DDT-PMAA. The scale bar reads 50 nm.

DLS analysis (Figure 81) was also performed on an aqueous solution of the sample in order to obtain independent measurements of the core diameter and size distribution.

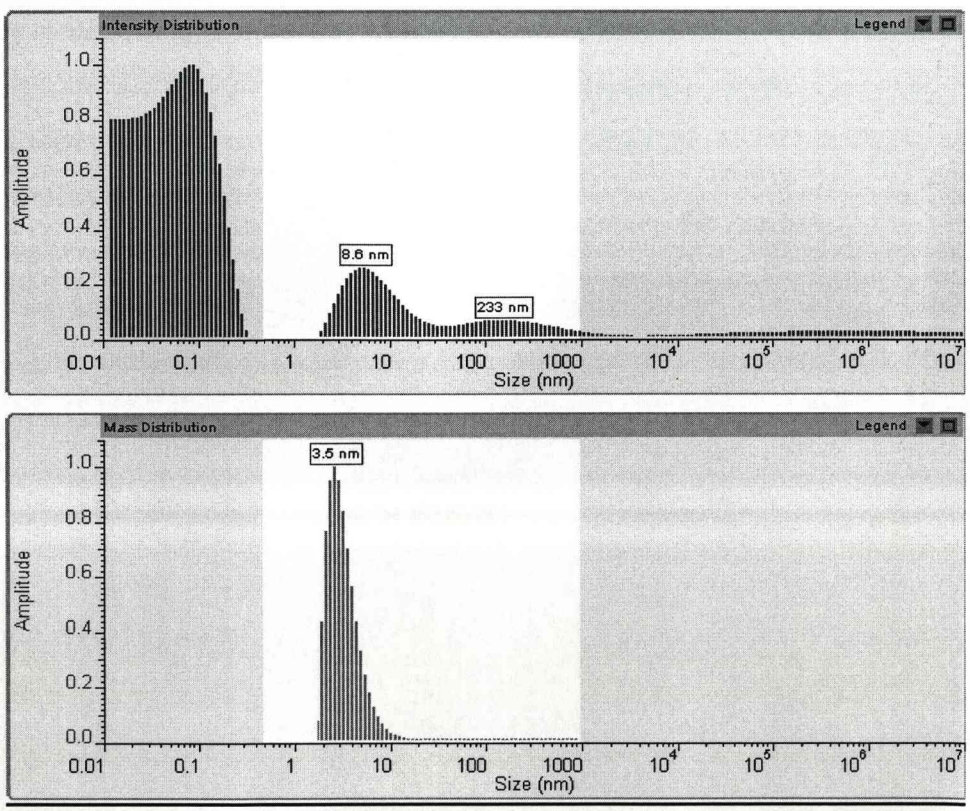

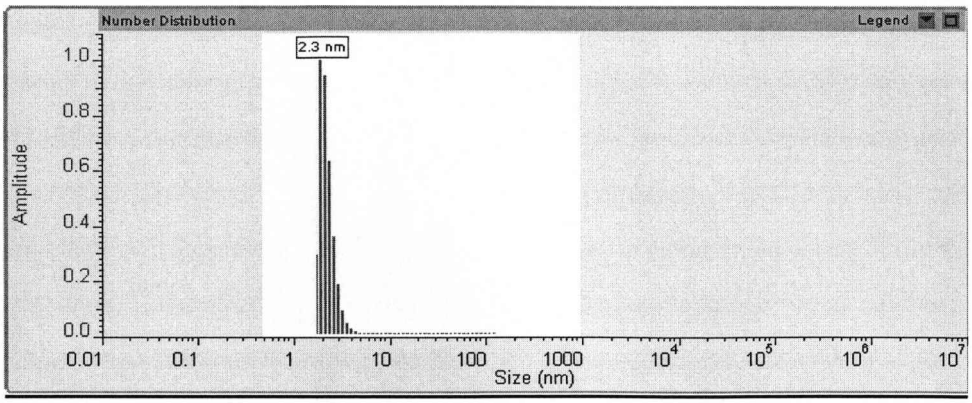

Figure 81. DLS analysis of the gold nanoparticles produced in a 0.006 mM solution of DDT-PMAA.

The DLS analysis indicates that the particles prepared at these concentrations are less monodisperse than the other samples of nanoparticles prepared by this technique. There is also some variation in the values of average core radius determined by the mass and number distributions. The mass distribution suggests that the average core radius is 3.5 ± 1.68 nm, i.e. it has a significant degree of polydispersity. The number distribution from DLS suggests that the average core radius is 2.29 ± 0.42 nm.

The determined core size is consistent with the general trend of increasing core diameter of products with decreasing polymer:gold ratio established in the literature and earlier experimental runs [57]. This is possibly due to enhanced protection of the nanoparticle core during the growth and nucleation stages when a higher concentration of polymer is present.

From this study it appears that the experiments using relative higher concentrations of polymer in the synthesis of nanoparticles results in more monodisperse, smaller nanoparticles, this is again consistent with the findings in the literature [57].

6.2.3 Effect of Polydispersity

The effect of the higher than anticipated polydispersity of the produced nanoparticles on the concentration values determined from absorption spectroscopy data was investigated. As the calculation of extinction coefficient (which is then used to determine concentration from the absorption spectrum using the Beer-Lambert Law) requires a single value of core diameter and the samples prepared by the above synthetic procedure have a distribution of sizes the extinction coefficient value is likely to be inaccurate. As an example of this the data from the TEM images in figure 72 was considered.

The mean (μ) value of the particle size and the standard deviation (σ) were determined from the data used to produce figure 82. These values (μ = 1.85 nm, σ = 1.74 nm) were used to obtain a normal distribution which was subsequently transformed into a probability density function (pdf). Figure 82 shows this pdf function plotted against the original data (scaled so that the area of the histogram bars sum to unity). The computer programme Mathematica was used to carry out these calculations.

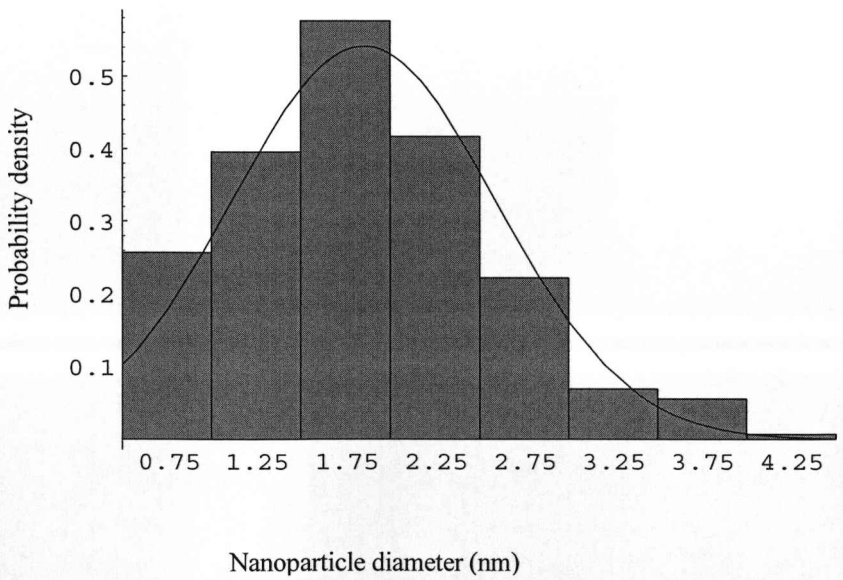

Figure 82 Probability density function of the distribution of core sizes of gold nanoparticles synthesised in a 0.18 mM solution of DDT-PMAA.

The pdf function was then integrated between the mean and ± 0.5 times the standard deviation. The procedure was then repeated integrating between the mean and ± 1 standard deviation. In the first case 38.3 % of the particles in the distribution were within half a standard deviation of the mean, for the second case 68 % of particles were within one standard deviation of the mean. The first case covers essentially only the particle size that occurs with the highest frequency.

For a pure sample, the Beer-Lambert law can be expressed as $I=I_0 10^{-\varepsilon cl}$ where I is the intensity of light which is transmitted through the sample and I_0 is the intensity of the incident light. When there is a mixture of components the law can be stated as $I=I_0 10^{-(\varepsilon 1c1l+\varepsilon 2c2l\ldots)}$. The effect of each component on the resultant absorption can therefore be considered as being additive (determined by the contribution from each of the $\varepsilon_i c_i l$ terms). In general for a mixture where the absorbance $A = I_o/I$ is known for a mixture and each of the extinction coefficient values the concentration terms cannot be calculated since there are two unknown quantities in the equation. However, as the components differ only in size it seems reasonable to assume that the components do add together in a linear manner, in proportion to their concentrations so A has contributions from each component in proportion to that found in the normal distribution. For this example $A_{506nm} = 0.67$ and the mean core diameter is 1.85 nm so the concentration of the most predominant size nanoparticle can be found from the area obtained from the integration performed earlier. The concentration of these particles from the first integration (which is likely to only include the highest frequency size nanoparticles) was 6.70×10^{-7} moldm^{-3} and the second integration was 1.19×10^{-6} moldm^{-3} (which is likely to include the highest frequency size and the next two closest sizes from the histogram) compared to 1.75×10^{-6} moldm^{-3} by assuming the sample is monodisperse.

In order to perform this type of calculation for every solubility measurement it would be necessary to obtain TEM data for every sample recovered from the pressure vessel as a distribution of sizes would be

needed for every measurement (due to the likely effects of size-selective solubility in supercritical ethane). As this measurement was impossible due to the small quantities of dissolved nanoparticles recovered from the high pressure vessel there is no data available to create the distribution. Consequently, to do further calculations it is necessary to either assume that the sample is monodisperse or assume that the distribution of sizes is the same in every dissolved sample. As it is highly likely that the distribution varied for the above reason it was decided to base the calculations on the original measured diameter. It would be beneficial to have an in-situ measurement of particle diameter (such as in-situ DLS) which would allow the variation of size distribution with fluid density to be constantly monitored.

6.3 Solubility Measurements

6.3.1 Experimental and Results

Two samples of monodisperse alkanethiol stabilized gold nanoparticles with core diameters of 2.5 and 4.2 nm were prepared by the two-phase reduction of tetrachloroaurate ions in the presence of DDT-PMMA (further detail is available in section 6.2) for the determination of the solubility of gold nanoparticles in supercritical ethane. Solubility data was obtained by placing a standard volume of a solution of the alkanethiol stabilized gold nanoparticles in the pressure vessel; supercritical ethane was then added to the vessel at the desired pressure. The nanoparticles were kept in the vessel for 18 hours (using a magnetic flea for agitation) and the general procedure for recovery of the dissolved and undissolved sample at the end of the experiment was the same as that described in earlier chapters (Chapters 3 & 4). The experiment was repeated over a range of pressures for each size of nanoparticles. The analysis of the recovered samples was based on the use of UV-visible absorption

spectroscopy. This study was the first attempt to quantifying the solubility of metal nanoparticles in a supercritical fluid.

In order to calculate the solubility of the two different sizes of dodecanethiol stabilized gold nanoparticles the UV-Visible absorption spectra of the undissolved samples (as well as TEM and DLS size measurements of the nanoparticles) were analysed. The extinction coefficients at 506 nm for the two different sizes were calculated using the previously described technique (see Chapter 4) [139] and the concentrations were determined from the absorption values at that wavelength. The molecular weight of gold nanoparticles was determined from TEM images by finding the average size and determining the number of core atoms by assuming the particles are spherical, ligand coverage was determined from the literature [57].

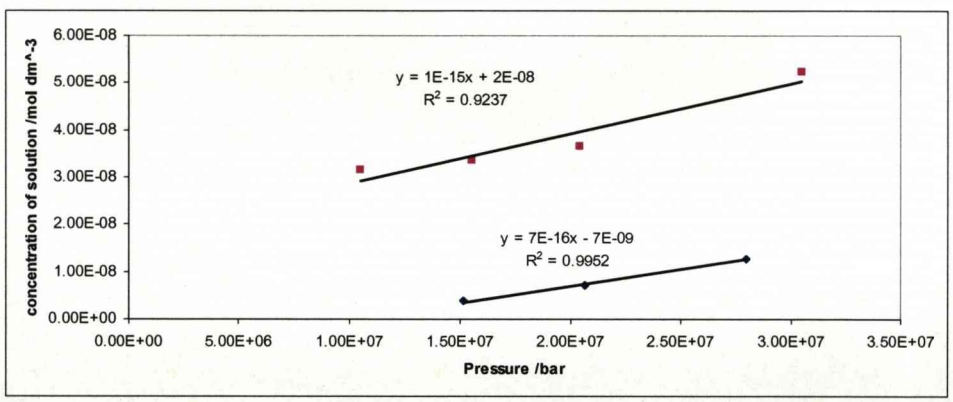

Figure 83. Plot of concentration of nanoparticles dissolved versus supercritical ethane pressure for both sizes of nanoparticles: 2.5 nm (purple) and 4.2 nm (blue).

Figure 83 shows the relationship between the concentration of gold nanoparticles dissolved and supercritical ethane pressure for both sizes of nanoparticles studied. Both plots clearly show a linear relationship, concentration of nanoparticles dissolved increases with pressure. As expected the 2.5 nm nanoparticles dissolve in greater concentrations at equivalent pressures, this is due to the relationship between Gibbs energy

of solubilisation and core diameter which was discussed at the end of Chapter 4. From the plot an estimate of the solubility can be obtained giving 5×10^{-18} mol.bar^{-1} for the 2.5 nm nanoparticles and 3.5×10^{-18} mol.bar^{-1} for the 4.2 nm nanoparticles.

P (Pa)	C_{atoms} (mol/dm^3)
2.04E+07	1.77E-05
1.56E+07	1.62E-05
1.05E+07	1.52E-05

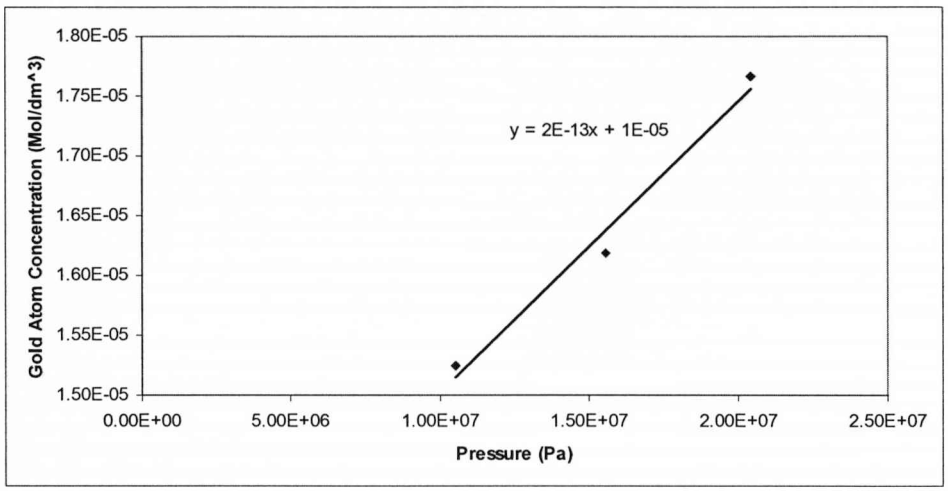

Figure 84. The solubility of gold nanoparticles in 2.5 nm dodecanethiol stabilised gold nanoparticles in terms of a plot of concentration of gold atoms (in 2.5 nm nanoparticles) dissolved in supercritical ethane versus pressure of supercritical ethane.

P (Pa)	c_{atoms} (mol/dm^3)
2.80E+07	2.92E-05
2.06E+07	1.63E-05
1.52E+07	8.76E-06

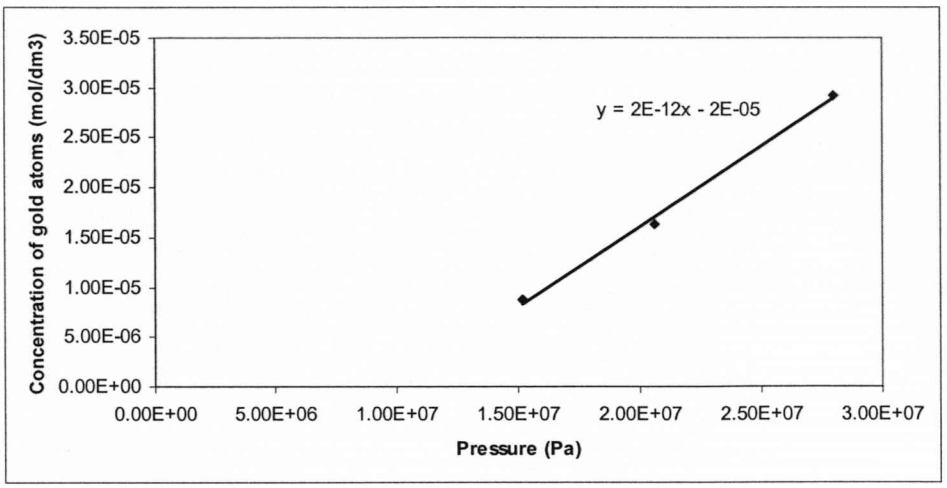

Figure 85. The solubility of gold atoms in 4.2 nm dodecanethiol stabilised gold nanoparticles plotted in terms of a plot of concentration of gold atoms dissolved versus supercritical ethane pressure.

Figure 84 and 85 show the concentrations of gold atoms dissolved in supercritical ethane at a range of pressures. This concentration was calculated from the concentration of dissolved gold nanoparticles and a simple estimate of how many atoms are present in each nanoparticle [139]. In order to determine whether metal nanoparticles can be described by Scaled Particle theory, a Henry's Law treatment of solubility data was performed and the experimental results compared with Scaled Particle Theory calculations. Scaled Particle Theory can be used to calculate Henry's Law constants by determining the free energy associated with opening a cavity in the solvent to accommodate the solute and the free energy of the interaction between solute and solvent molecules.

Henry's Law is usually used to describe the solubility of gases dissolving in a liquid solvent. It was assumed in the current work that metal nanoparticles dissolving in a supercritical fluid show this type of solubility behaviour in the low solute mole fraction range. The first stage was to construct a Henry's Law plot of nanoparticle partial pressure (found from the product of solute mole fraction and total pressure) against mole fraction of nanoparticles dissolved. The gradient of such a plot is equal to

the Henry's Law constant (K_H from the equation $p_A = K_H x_A$ where x_A is the mole fraction of nanoparticles in solution and p_A is the partial pressure of the solute) for the nanoparticles.

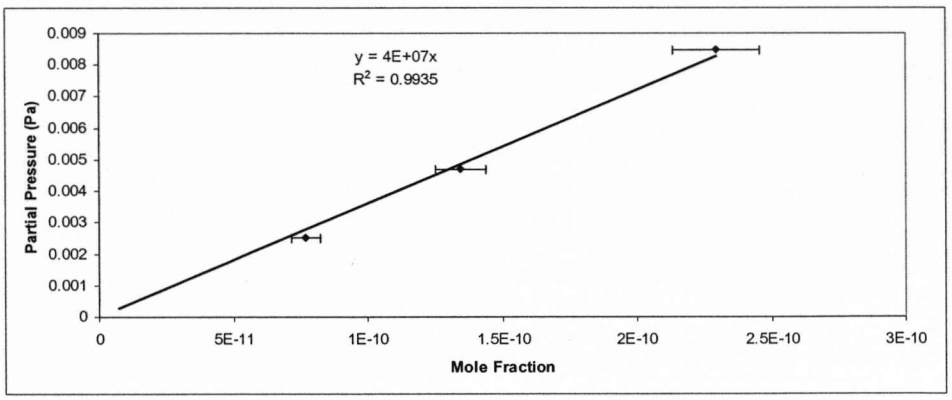

Figure 86. Henry's Law plot of nanoparticle partial pressure versus mole fraction for 4.2 nm dodecanethiol stabilised gold nanoparticles.

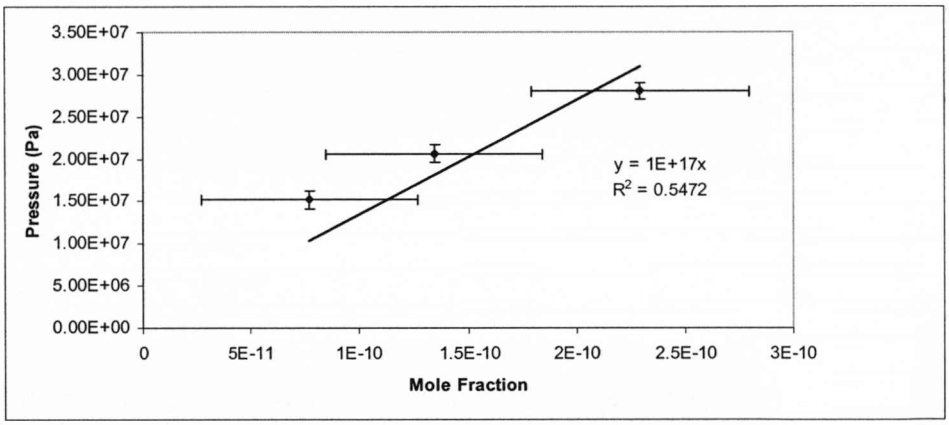

Figure 87. The solubility of 4.2 nm dodecanethiol stabilised gold nanoparticles shown as a plot of pressure of supercritical ethane versus mole fraction of nanoparticles.

The plot of pressure versus mole fraction (Figure 87) shows an approximately linear relationship which passes though the origin (as expected, the dissolved solid mole fraction should be zero when the ethane pressure is zero). This plot gives an indication of the relationship between total amount of nanoparticles dissolved and pressure of fluid (at constant temperature). As the temperature was constant throughout this experiment

we can use Figure 87 to qualitatively verify the fact that solubility increases approximately proportionally with solvent density. K_H was found from the gradient of the plot of mole fraction versus partial pressure of the solute (Figure 86). The partial pressure of the nanoparticles at each pressure was determined from the measured concentration together with a simple calculation to determine the number of atoms in each nanoparticles (from the average core diameter, determined earlier by TEM and DLS analysis) and by assuming ideal gas behaviour for the nanoparticles in solution which is a reasonable assumption to make in the region where the linear relationship between density of the supercritical fluid and the logarithm of mole fraction of solute is obeyed (see the last two figures in the chapter). For 4.2 nm dodecanethiol stabilised gold nanoparticles in supercritical ethane, the K_H value is found to be 4×10^7 Pa.

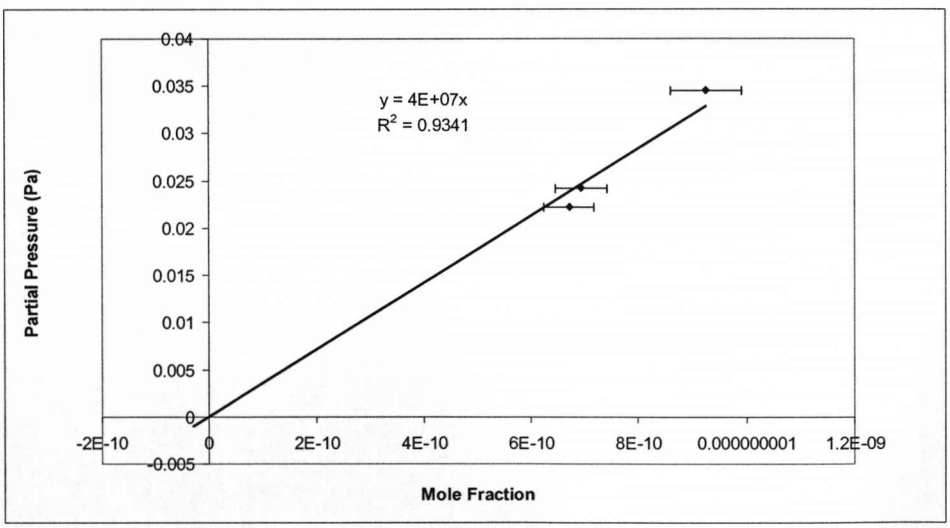

Figure 88. Henry's Law plot of nanoparticle partial pressure versus mole fraction for 2.5 nm dodecanethiol stabilised gold nanoparticles.

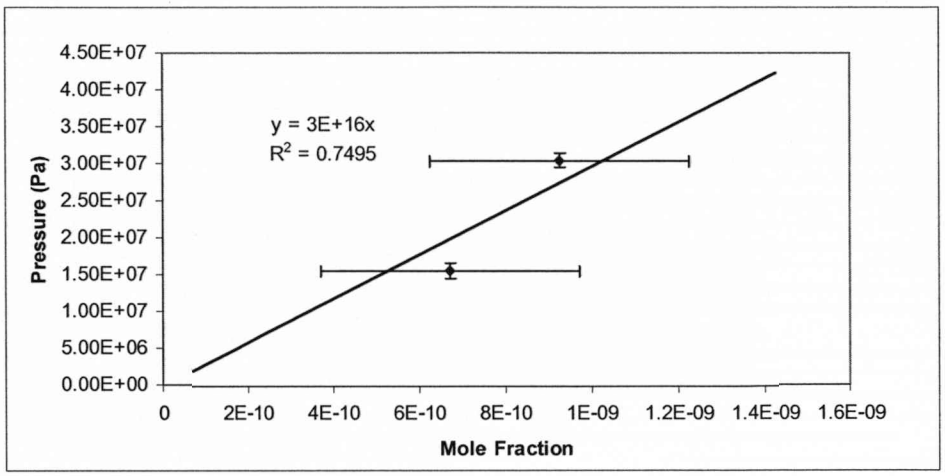

Figure 89. The solubility of 2.5 nm dodecanethiol stabilised gold nanoparticles expressed as a plot of pressure of supercritical ethane versus mole fraction of nanoparticles.

The Henry's Law constant for 2.5 nm dodecanethiol stabilised gold nanoparticles (found from the gradient of figure 88) was found to be 4×10^7 Pa. Figure 89 shows a plot of the solubility (in terms of fluid pressure versus mole fraction) of the 2.5 nm nanoparticles, the plot shows that the mole fraction of particles dissolved increases approximately linearly with increasing pressure (and, therefore solvent density). The plot passes through the origin as no material is dissolved at a supercritical fluid pressure of 0 bar.

The measured Henry's Law constants for the two sets of particles were used to calculate the core diameters of the nanoparticles using Scaled Particle Theory [61]. The values of core diameter were 19 and 22 nm compared to 2.5 and 4.2 nm from experimental measurements.

In order to justify this inconsistency we must consider the free energy associated with transferring a particle from a solid state into the fluid. The free energy is made up of three terms: the first term takes into account the energy to extract a particle from the solid; the next term is due to the free energy needed to open a cavity within the fluid for the solute to occupy and the third term takes into account the free energy arising from

the curvature of this cavity. Since this system has a solid in equilibrium with a fluid the first term must be taken into account whereas a scaled particle theory consideration of the process does not include this term.

The solubility of the nanoparticles in supercritical ethane is very low compared to that of liquid hydrocarbon at ambient conditions but this is to be expected due to the density of supercritical ethane at a pressure of 300 bar is approximately half that of toluene at ambient conditions. Given the strong colours of these solutions we expected solubilities to be higher but it seems that even at very low concentrations these solutions retain the characteristic red colour.

Another model was found which specifically relates to the solubility behaviour of a solid-supercritical fluid system in the low mole fraction range. According to Harvey, [143] in such a system a plot of logarithm of the solubility expressed as mole fraction of solid versus solvent density (of the supercritical fluid) at a fixed temperature is a straight line over a wide range of densities. Theoretical studies by Ewald *et. al.* [144] predict a linear relationship at low concentrations due to independent clustering of molecules of one component around molecules of the other. This behaviour is not observed at higher densities due to the fact that gases deviate from perfect behaviour (so at higher densities this effect becomes more pronounced) and additional intermolecular forces between gas molecules at higher densities. Figure 90 shows this plot for a sample of 4.2 nm gold nanoparticles in supercritical ethane at a number of pressures (at constant T = 318 K).

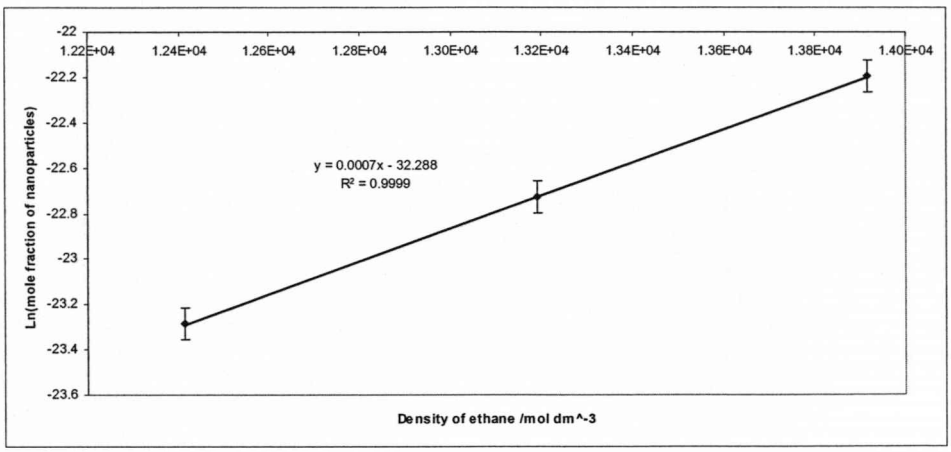

Figure 90. A plot of the logarithm mole fraction of gold nanoparticles versus supercritical fluid density for 4.2 nm monodisperse gold nanoparticles stabilised by dodecanethiol.

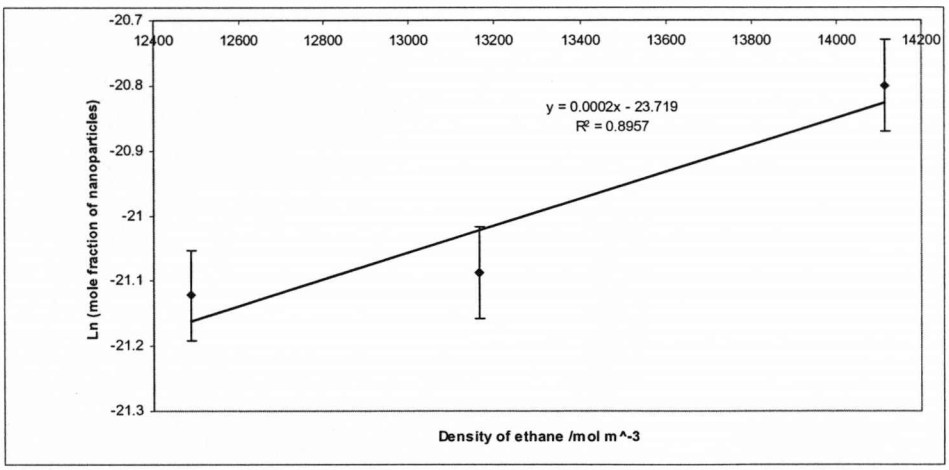

Figure 91. A plot of the logarithm of mole fraction of gold nanoparticles versus supercritical fluid density versus for 2.5 nm monodisperse gold nanoparticles stabilised by dodecanethiol.

The experimental data agrees well with the predicted behaviour of small solid particles in a gas. The plot of fluid density versus logarithm of mole fraction (Figure 90 & 91) also agrees with the predicted trend, there is a linear relationship between the logarithm of the mole fraction of solid and the ethane density for both sizes of nanoparticle.

6.3.2 Closing Remarks

The solubility testing of dodecanethiol stabilised gold nanoparticles has shown that the solubility of both samples of nanoparticles were too low to allow the technique to be used for the industrial scale fractionation of polydisperse samples of nanoparticles. Further work in this area may be useful for developing an understanding of the nature of intermolecular forces between nanoparticles and supercritical fluids. This is the first time the solubility of gold nanoparticles in supercritical ethane has been investigated and the results obtained support the widely held theory that this technique is unsuitable for large scale fractionations.

6.4 Summary

The synthesis of dodecanethiol stabilised gold nanoparticles with improved degrees of monodispersity has been demonstrated in this chapter. The synthesis was repeated using a number of different polymer:gold ratios and the effect on the average core diameter and the degree of monodispersity was recorded (by measurement of the average core diameter and distribution of sizes by both TEM and DLS). The trends observed were consistent with those recorded in the published work on the subject. The average core diameter of the nanoparticles produced decreased in general as a function of increasing polymer:gold ratio. The monodispersity also seems to increase with increasing polymer concentration; this is possibly due to the decreased control over the growth of each nanoparticle at early stages due to a lesser surface coverage.

The solubility studies of these nanoparticles show that when mole fraction of dissolved gold nanoparticles is low the natural log of the mole fraction of solid dissolved versus the density of the supercritical ethane does obey a linear relationship as predicted by the literature [143, 144] and

that scaled particle theory does not accurately predict the solubility behaviour of metal nanoparticles in supercritical fluids, this is possibly due to the explanation given in the above section (ie. that a scaled particle consideration does not taken into account the free energy required to transfer a particle from the solid state into the fluid).

Chapter Seven

Summary and Future Work

7.1 Separation Techniques

This project demonstrated the potential of using supercritical fluids to isolate a series of size fractions from a polydisperse sample of metal nanoparticles. Although the results appear to indicate that samples of synthesized nanoparticles with degrees of polydispersity in the region of several nanometres can be separated to an extent, a greater understanding of the pressures necessary to isolate specific size fractions is necessary. In spite of the fact the complete separation of the sample into a series of size fractions was not possible using this experimental set-up, this was the first demonstration of the application of supercritical fluids in the size separation of a single sample of polydisperse gold nanoparticles. Earlier applications of similar techniques made use of supercritical fluids to separate bimodal mixtures of nanoparticles with a large difference in average core diameter (and therefore, a much larger degree of polydispersity than any of the samples studied in this experiment).

The separation of fractions so close in size demonstrates that the solubility of small gold nanoparticles varies greatly with small changes in size. The explanation for this variation is provided by size dependence of the Gibbs energy of solubilisation and a consideration of the electronic behaviour of metal nanoparticles. The metal nanoparticles studied had core diameters which crossed the size range in which the free electron model ceases to accurately describe the electronic behaviour and a series of discrete electronic states occur as a consequence of the confinement of the electronic wavefunction. The gap between successive quantum levels is known as the Kubo gap (see equation 1, chapter 1), as the size of the Kubo gap becomes comparable to the thermodynamic energy (kT) of electrons energy levels become separated into discrete states. This discreteness in small nanoparticles results in a marked decrease in the polarizability of these particles which results in a sudden decrease in the Gibbs energy of solubilisation.

As a consequence of the variation of solubility of metal nanoparticles (described above) and the unique properties of supercritical fluids, separation of size fractions from a polydisperse sample is possible. As supercritical fluids are compressible they exhibit very large changes in density for only small variations in pressure. This allows the solubility of the fluid to be 'tuned' by variation of pressure. It is also worth noting that supercritical fluids are, in general, less dense than liquid solvents. This means that they are less viscous than equivalent liquid solvents and therefore diffuse much more efficiently [59].

In order to perform more precise fractionation some fundamental additional research is needed. Ideally solubility data for a wide size range of gold nanoparticles in supercritical fluids should be collected. With this information specific size fractions could be removed more effectively. As the precise pressures required to dissolve specific size fractions were unknown during this investigation, it was difficult to fully extract one size fraction without taking part of another. This is a potential problem of a scaled up version of this process, it seems likely that the solubility of each individual size fraction overlap will overlap at certain pressures (i.e. two fractions will both be soluble at the same pressure) which means that a complete separation would never be possible. It is also possible that at this 'overlap' point the solubility of the larger fraction would be so low that the overall polydispersity of the isolated fraction would be small. A degree of polydispersity in the range of ± 0.1-0.5 nm would be a considerable improvement on many of the existing synthetic and separation procedures which would justify further research into the technique.

Other considerations have to be taken into account of a modified version of this process including the fact that any fractionation of a single polydisperse sample must start with the isolation of the most soluble (i.e. smallest) fraction followed by the next most soluble fraction and so on. Also in order to perform this process on a larger scale a new approach may be necessary as the experimental set-up used in this investigation would be

difficult to modify for large scale use. One of the primary issues is the need to extract dissolved nanoparticles which precipitate during depressurization. Any new technique used for this process must improve the efficiency of this step in particular. The process is likely to be made more efficient by the addition of agitation to the pressure vessel. Agitation was used in the solubility measurements during this project in order to ensure that all soluble nanoparticles did indeed dissolve.

The characterization of the dissolved nanoparticles was performed by a number of techniques. The size distribution was determined by using both TEM and DLS. Access to DLS facilities was limited during this project, in particular at the early stages. It would be useful to fully incorporate DLS analysis into the characterization of dissolved fractions recovered from any attempt at performing a fractionation experiment. It would be particularly interesting to compare the results of DLS analysis of samples with the size distributions obtained from the analysis of TEM images. One of the greatest difficulties throughout this project was the lack of in-situ characterization facilities in the high pressure apparatus. Other groups have incorporated view cells which allow in-situ UV-visible absorption spectra measurements to be performed. Due to the relationship between the average core diameter of the nanoparticles and the shape of the absorption curve and that between the amount of nanoparticles dissolved and the intensity of the absorption curve it would be extremely useful to be able to analyse these spectra during the experiment.

7.2 Synthetic Techniques

The other technique used to produce monodisperse samples of metal nanoparticles was based on a new synthetic approach devised by the Brust and Cooper groups [57]. The technique had already been demonstrated for a range of gold:polymer ratios and the work carried out in this investigation showed the effect of applying some different

gold:reducing agent ratios. The same general trend was observed with respect to the size of gold nanoparticles produced.

The analysis of the nanoparticles produced was performed by a variety of techniques but the determination of the average core diameter and distribution of sizes was again recorded by both DLS and analysis of TEM images. Although some greater degrees of polydispersity were observed than those in the published work it is worth noting that this technique results in samples which are significantly more monodisperse than those produced by the conventional form of the two-phase synthesis. It is likely that the difficulty in reproducing the monodispersity seen in the published work was partly down to differences in the sample of polymer used in the synthesis. It was shown in a later publication that higher molecular weight forms of polymers resulted in more polydisperse metal nanoparticles being produced, the influence of the molecular weight of the polymer and the end group must be considered due to the effect on the metal nanoparticle product [33].

The nanoparticles produced by this synthetic technique were then used for the measurement of solubility of metal nanoparticles, this was a time consuming process. The synthetic procedure and characterization took more time than expected due to the lack of availability of several resources (notably DLS and TEM facilities). Setting up the high pressure apparatus for the solubility measurements was another lengthy process. A standard amount of the nanoparticles had to be evaporated in a glass vial without heating (low temperature evaporation was attempted using a vacuum oven near the end of the investigation), once the sample was ready it had to be placed into the high pressure apparatus. Because of the difficulties in setting up the apparatus (as described in Chapter 3) each experimental run required several days to set up and occasionally had to be aborted due to the occurrence of leaks in the pressure vessel or elsewhere in the pipework. Once the apparatus had been set up two days of experimental work and apparatus were required for each sample tested. Due to the cumbersome

nature of this process the number of samples tested was greatly restricted. It would be desirable to continue the study over a much wider range of sizes. The results of such an investigation could be used to support any investigation into the use of supercritical fluids in the fractionation of polydisperse samples of gold nanoparticles.

The synthesis of silver nanoparticles by the two-phase reduction in the presence of DDT-PMAA was demonstrated. This technique allowed size control of the nanoparticles produced by variation of the initial polymer:silver nitrate ratio. The nanoparticles produced in the presence of higher relative concentrations of polymer showed reasonable degrees of monodispersity. This benefit was lost when low concentrations of polymer were used; degrees of polydispersity were equal to or worse than those seen in conventional synthesis of silver nanoparticles. It would be interesting to see the outcome of further study into this process as if the process could be refined (by using different polymer:silver nitrate ratios or using a lower molecular weight polymer) monodisperse silver nanoparticles of desired core diameters could be produced.

7.3 Solubility Measurements

Due to the excessive time taken to set up the high pressure apparatus solubility measurements were only ever recorded for two samples of gold nanoparticles. It was obvious at an early stage that the nanoparticles produced were not suitable for solubility measurements due to the polydispersity (which meant that there were a number of different size fractions of nanoparticles present, each with a different solubility) of all nanoparticles produced. These nanoparticles were separated to an extent in supercritical fluid but due to the lack of measurements and the scale of the original synthesis it was impossible to produce samples with the degree of monodispersity and in the amounts necessary for such a study. The plan to conduct solubility measurements was deferred until a technique to

produce large enough quantities of metal nanoparticles with higher degrees of monodispersity had been developed.

The technique that was eventually used to produce monodisperse nanoparticles was the reduction of tetrachloroaurate by sodium borohydride in the presence of DDT-PMAA (see above). This technique produced samples of nanoparticles with significant improvements in degrees of monodispersity compared to those compared by conventional synthetic techniques (e.g. Citrate reduction and two-phase reduction) and those isolated from polydisperse samples by separation in supercritical fluids (synthesis with DDT-PMAA also produced the nanoparticles in a far greater quantity than that produced by separation of a sample in supercritical fluid). The most monodisperse of these samples were used for the solubility measurements.

A number of readings were made for each sample at a range of pressures between 50 and 300 bar. In order to ensure saturation pressure would not be exceeded a simple experiment was performed using double the normal amount of the nanoparticles at a pressure at the top end of the range investigated. Unfortunately several of the experiments were unsuccessful and due to severe time constraints not all experiments could be repeated.

7.4 Closing Remarks

Overall this study has shown some of the difficulties in obtaining solubility data for samples of alkanethiol stabilized gold nanoparticles and the various synthetic and separation technique that may be used to prepare such monodisperse samples.

This study included the first known demonstration of the separation of a single polydisperse sample (rather than a bimodal mixture) of alkanethiol stabilized gold nanoparticles using supercritical ethane as well

as the first known solubility measurements on monodisperse samples of gold nanoparticles in supercritical ethane.

As mentioned in the above sections this study has left several areas open for further research, in particular the refinement of the separation of polydisperse samples of gold nanoparticle using supercritical fluids. If further research revealed a good degree of size-selective solubility it is possible that the technique could be used on a larger scale if several improvements were made to the experimental set-up.

It would be interesting to see the results of solubility studies on a wider range of metal nanoparticles. In order to do this it is likely that a lot of time would and resources would be needed due to the various labour intensive processes involved in this type of measurement.

In closing, this study has shown the potential of using supercritical fluids to fractionate samples of polydisperse nanoparticles and outlined many of the difficulties that must be overcome before this is a practical reality. The study also demonstrated an approach to the determination of the solubility of metal nanoparticles in supercritical ethane and showed that the solubility behaviour of these particles followed some expected trends.

REFERENCES

1. Turkevich, J., P.C. Stevenson, and J. Hillier, Discussions of the Faraday Society, 1951. **11**: p. 55 - 75.
2. Frens, G., Physics Letters A, 1973. **A 44**(3): p. 208-210.
3. Schmid, G., R. Pfeil, R. Boese, F. Bandermann, S. Meyer, G.H.M. Calis, W.A. Vadervelden, Chemische Berichte-Recueil, 1981. **114**(11): p. 3634-3642.
4. Brust, M., M. Walker, D. Bethell, D.J. Schiffrin, R. Whyman, Chem. Commun., 1994(7): p. 801-802.
5. Wang, Y. and N. Herron, J. Phys. Chem., 1991. **95**(2): p. 525-532.
6. Haase, M., H. Weller, and A. Henglein, J. Phys. Chem., 1988. **92**(16): p. 4706-4712.
7. Haase, M., H. Weller, and A. Henglein, J. Phys. Chem., 1988. **92**(2): p. 482-487.
8. El-Sayed, M.A., Acc. Chem. Res., 2001. **34**(4): p. 257-264.
9. Zhang, J.Z., Acc. Chem. Res., 1997. **30**(10): p. 423-429.
10. Alivisatos, A.P., J. Phys. Chem., 1996. **100**(31): p. 13226-13239.
11. Murray, C.B., C.R. Kagan, and M.G. Bawendi, Science, 1995. **270**(5240): p. 1335-1338.
12. Heath, J.R., Science, 1995. **270**(5240): p. 1315-1316.
13. Kamat, P.V., Progress in Reaction Kinetics, 1994. **19**(3): p. 277-316.
14. Alivisatos, A.P., A.L. Harris, N.J. Levinos, M.L. Steigerwald, L.E. Brus, J. Chem. Phys., 1988. **89**(7): p. 4001-4011.
15. Chestnoy, N., T.D. Harris, R. Hull, L.E. Brus, J. Phys. Chem., 1986. **90**(15): p. 3393-3399.
16. Brus, L., Ieee Journal of Quantum Electronics, 1986. **22**(9): p. 1909-1914.
17. Chen, S.W., R.S. Ingram, M.J. Hostetler, J.J. Pietron, R.W. Murray, T.G. Schaaff, J.T. Khoury, M.M. Alvarez, R.L. Whetten, Science, 1998. **280**(5372): p. 2098-2101.
18. Chen, S.W., R.W. Murray, and S.W. Feldberg, J. Phys. Chem. B, 1998. **102**(49): p. 9898-9907.
19. Clarke, N.Z., C. Waters, K.A. Johnson, J. Satherley, D.J. Schiffrin, Langmuir, 2001. **17**(20): p. 6048-6050.
20. Mellor, J.W., *A Comprehensive Treatise on Inorganic and Theoretical Chemistry*. 1923, London: Longmans, Green and Co.

21. Kerker, M., Journal of Colloid and Interface Science, 1985. **105**(2): p. 297-314.
22. Faraday, M., *Philosophical Transactions*. Vol. 147. 1857, London: Royal Society of Chemistry. 145-181.
23. Mie, G., Ann. Phys., 1908. **25**: p. 328.
24. *The Lycurgus Cup*. 2007 cited; Available from: http://www.thebritishmuseum.ac.uk/explore/highlights/highlight_objects/pe_mla/t/the_lycurgus_cup.aspx.
25. Brust, M., J. Fink, D. Bethell, D.J. Schiffrin, C. Kiely, Chem. Commun., 1995(16): p. 1655-1656.
26. Hostetler, M.J., J.E Wingate, CJ. Zhong, J.E. Harris, R.W. Vachet, M.R. Clark, J.D. Londono, S.J. Green, J.J. Stokes, G.D. Wignall, G.L. Glish, M.D. Porter, N.D. Evans, R.W. Murray, Langmuir, 1998. **14**(1): p. 17-30.
27. Templeton, A.C., M.P. Wuelfing, and R.W. Murray, Acc. Chem. Res., 2000. **33**(1): p. 27-36.
28. Ingram, R.S., M.J. Hostetler, and R.W. Murray, J. Am. Chem. Soc., 1997. **119**(39): p. 9175-9178.
29. Chen, S., Langmuir, 1999. **15**(22): p. 7551-7557.
30. Chen, S. and R.W. Murray, Langmuir, 1999. **15**(3): p. 682-689.
31. Hostetler, M.J., S.J. Green, J.J. Stokes, R.W. Murray. J. Am. Chem. Soc., 1996. **118**(17): p. 4212-4213.
32. Hussain, I., Z.X. Wang, A.I. Cooper, M. Brut, Langmuir, 2006. **22**(7): p. 2938-2941.
33. Wang, Z.X., B.E. Tan, I. Hussain, N. Schaeffer, M.F. Wyatt, M. Brust, A.I. Cooper, Langmuir, 2007. **23**(2): p. 885-895.
34. Hostetler, M.J., A.C. Templeton, and R.W. Murray, Langmuir, 1999. **15**(11): p. 3782-3789.
35. Guo, R., Y. Song, G.L. Wang, R.W. Murray, J. Am. Chem. Soc., 2005. **127**(8): p. 2752-2757.
36. El-Sayed, M.A., *Nanoscience.* Abstracts of Papers of the American Chemical Society, 2005. **229**: p. U469-U469.
37. Daniel, M.C. and D. Astruc, Chem. Rev., 2004. **104**(1): p. 293-346.
38. Alivisatos, A.P., Science, 1996. **271**(5251): p. 933-937.

39. Manninen, M., J. Mansikka-aho, and E. Hammarén, Zeitschrift für Physik D Atoms, Molecules and Clusters, 1993. **26**(1-4).

40. Brust, M. and C.J. Kiely, Colloids and Surfaces a-Physicochem. Eng. Aspects, 2002. **202**(2-3): p. 175-186.

41. Henglein, A., J. Phys. Chem., 1993. **97**(21): p. 5457-5471.

42. Fendler, J.H., Chem. Mater., 1996. **8**(8): p. 1616-1624.

43. [cited 2007; Available from: http://www.chemistry.helsinki.fi/polylab/research/content/gold?lang=fi.

44. Kanaras, A.G., Z.X. Wang, I. Hussain, M. Brust, R. Costick, A.D. Bates, Small, 2007. **3**(1): p. 67-70.

45. Alivisatos, A.P., K.P. Johnsson, X.G. Peng, T.E. Wilson, C.J. Loweth, M.P. Bruchez, P.G. Schultz, Nature, 1996. **382**(6592): p. 609-611.

46. Brennan, J.L., N.S Hatzakis, T.R. Tshikhudo, N. Dirvianskyte, V. Razumas, S. Patkar, J. Vind, A. Svendsen, R.J. M Nolte, A.E. Rowan, M. Brust, Bioconj. Chem., 2006. **17**(6): p. 1373-1375.

47. El-Sayed, M.A., Abstracts of Papers of the Am. Chem. Soc., 2001. **222**: p. U213-U213.

48. Anand, M., M.C. Mcleod, P.W. Bell, C.B Roberts, J. Phys. Chem. B, 2005. **109**(48): p. 22852-22859.

49. Shah, P.S., J.D. Holmes, K.P. Johnston, B.A. Korgel J. Phys. Chem. B, 2002. **106**(10): p. 2545-2551.

50. Lee, J.S., S.I. Stoeva, and C.A. Mirkin, J. Am. Chem. Soc., 2006. **128**(27): p. 8899-8903.

51. Sweeney, S.F., G.H. Woehrle, and J.E. Hutchison, J. Am. Chem. Soc, 2006. **128**(10): p. 3190-3197.

52. Akthakul, A., A.I. Hochbaum, F. Stellacci, A.M Mayes, Adv. Mater., 2005. **17**(5): p. 532-+.

53. Jimenez, V.L., D.G. Georganopoulou, R.J. White, A.S. Harper, A.J. Mills, D.I. Lee, R.W. Murray, Langmuir, 2004. **20**(16): p. 6864-6870.

54. Wilcoxon, J.P., J.E. Martin, and P. Provencio, Langmuir, 2000. **16**(25): p. 9912-9920.

55. Al-Somali, A.M., K.M Krueger, J.C. Falkner, V.L. Colvin, Anal.Chem., 2004. **76**(19): p. 5903-5910.

56. Siebrands, T., M. Giersig, P. Mulvaney, C.H. Fischer , Langmuir, 1993. **9**(9): p. 2297-2300.

57. Hussain, I., S. Graham, Z.X. Wang, B. Tan, D.C. Sherrington, S.P. Rannard,

A.I Cooper, M. Brust, J. Am. Chem. Soc., 2005. **127**(47): p. 16398-16399.

58. Shimmin, R.G., A.B. Schoch, and P.V. Braun, Langmuir, 2004. **20**(13): p. 5613-5620.
59. Cagniard de la Tour, C., Ann. Chim. Phys., 1822. **127**: p. 178.
60. Shah, P.S., J.D. Holmes, R.C. Doty, K.P. Johnston, B.A. Korgel, J. Am. Chem. Soc., 2000. **122**(17): p. 4245-4246.
61. Pierotti, R.A., Chem. Rev., 1976. **76**(6): p. 717-726.
62. Hunter, R.J., *Zeta Potential in Colloid Science: Principles and Applications*. 1988: Academic Press.
63. Stenkamp, V.S. and J.C. Berg, Langmuir, 1997. **13**(14): p. 3827-3832.
64. Everett, D.H., *Basic principles of Colloid Science*. 1994, London: Royal Society of Chemistry.
65. Christenson, H.K., J. Chem. Soc., Faraday Trans. I, 1984. **80**: p. 1933-1946.
66. Hermansson, M., Coll. Surf. B Biointerfaces, 1999. **14**(1-4): p. 105-119.
67. Ogwu, A.A., et al.,Metallurgical and Materials Transactions a-Physical Metallurgy and Materials Science, 2005. **36A**(9): p. 2435-2439.
68. McBride, M.B. and P. Baveye, Soil Sci. Soc. Am. J., 2002. **66**(4): p. 1207-1217.
69. Azeredo, J., J. Visser, and R. Oliveira, Coll. Surf. B Biointerfaces, 1999. **14**(1-4): p. 141-148.
70. Laaksonen, T., P. Ahonen, C. Johans, K. Kontturi, Chemphyschem, 2006. **7**(10): p. 2143-2149.
71. Chechik, V., J. Am. Chem. Soc., 2004. **126**(25): p. 7780-7781.
72. Waters, C.A., A.J. Mills, K.A. Johnson, D.J. Schiffrin, Chem. Commun., 2003(4): p. 540-541.
73. Balasubramanian, R., R. Guo, A.J. Mills, R.W. Murray, J. Am. Chem. Soc., 2005. **127**(22): p. 8126-8132.
74. Templeton, A.C., M.J. Hostetler, C.T. Craft, R.W. Murray, J. Am. Chem. Soc., 1998. **120**(8): p. 1906-1911.
75. Templeton, A.C., M.J. Hosteteler, E.K. Warmoth, S.W. Chen, M.D.E. Forbes, R.W. Murray, Abstracts of Papers of the Am. Chem. Soc., 1998. **215**: p. U456-U456.
76. Wellsted, H., E. Sitsen, A. Caragheorgheopol, V. Chechik, Anal. Chem.. 2004. **76** p. 2010-2016.
77. Helcher, H.H., 1718, Breslau and Leipzig: J. Herbord Klossen.

78. Wuelfing, W.P., S.M. Gross, D.T. Miles, R.W. Murray, J. Am. Chem. Soc., 1998. **120**(48): p. 12696-12697.

79. Wuelfing, W.P., A.C. Templeton, J.J. Pietron, R.W. Murray Abstracts of Papers of the Am. Chem. Soc., 1998. **215**: p. U456-U456.

80. Corbierre, M.K., N.S. Cameron, M. Sutton, S.G.J. Mochrie, L.B. Lurio, A. Ruhm, R.B. Lennox, J. Am. Chem. Soc., 2001. **123**(42): p. 10411-10412.

81. Marinakos, S.M., D.A. Shultz, and D.L. Feldheim, Adv. Mater., 1999(250): p. 142-148.

82. Liang, Z., A. Susha, and F. Caruso, Chem. Mater., 2003. **15**(16): p. 3176-3183.

83. Chah, S., D.A. Fendler, and J. Yi, J. Colloid Interface Sci., 2002(250): p. 142-148.

84. Kamata, K., Y. Lu, and Y. Xia, J. Am. Chem. Soc. 2003. **125**: p. 2384-2385.

85. Creighton, J.A. and D.G. Eadon, J. Chem. Soc., Faraday Trans., 1991. **87**: p. 3881-3891.

86. Malinsky, M.D., K.L. Kelly, G.C. Schatz, R.P. Van Duyne, J. Am. Chem. Soc., 2001. **123**(7): p. 1471-1482.

87. Kashiwagi, Y., M. Yamamoto, and M. Nakamoto, J. Coll. Int. Sci., 2006. **300**(1): p. 169-175.

88. Yamamoto, M., Y. Kashiwagi, and M. Nakamoto, Langmuir, 2006. **22**(20): p. 8581-8586.

89. Zhang, W.Z., X.L. Qiao, and J.G. Chen, J. Chem. Phys., 2006. **330**(3): p. 495-500.

90. Mallick, K., M.J. Witcomb, and M.S. Scurrell, J. Mater. Sci., 2004. **39**(14): p. 4459-4463.

91. Gao, J., J. Fu, C. Lin, J. Lin, Y. Han, X. Yu, and C. Pan Langmuir, 2004. **20**(22): p. 9775-9779.

92. Bao, H., G. Chumanov, R. Cazerw, D.L. Carroll, and S.H. Foulger, Colloid Polym. Sci., 2005. **283**(6): p. 653-661.

93. Quaroni, L. and G. Chumanov, J. Am. Chem. Soc., 1999. **121**(45): p. 10642-10643.

94. Xu, X.Y., M.S. Han, and C.A. Mirkin, Angew. Chemie Int. Ed., 2007. **46**(19): p. 3468-3470.

95. Hurst, S.J., A.K.R. Lytton-Jean, and C.A. Mirkin, Anal. Chem., 2006. **78**(24): p. 8313-8318.

96. Huo, F.W., A.K.R. Lytton-Jean, and C.A. Mirkin, Adv. Mater., 2006. **18**(17): p. 2304-+.

97. Storhofff, J.J., R. Elghanian, C.A. Mirkin, and R.L. Letsinger, Langmuir, 2002. **18**(17): p. 6666-6670.

98. Li, Z., R.C. Jin, C.A. Mirkin, R.L. Letsinger, Nucl. Acids Res., 2002. **30**(7): p. 1558-1562.

99. Reynolds, R.A., C.A. Mirkin, and R.L. Letsinger, Pure Appl. Chem., 2000. **72**(1-2): p. 229-235.

100. Storhoff, J.J., A.A. Lazarides, R.C. Mucic, C.A. Mirkin, R.L Letsinger, and G.C. Schatz, J. Am. Chem. Soc., 2000. **122**(19): p. 4640-4650.

101. Reynolds, R.A., C.A. Mirkin, and R.L. Letsinger, J. Am. Chem. Soc., 2000. **122**(15): p. 3795-3796.

102. Letsinger, R.L., C.A. Mirkin, R. Elghanian, R.C. Mucic, J.J. Storhoff, Phos. Sul. Sil., 1999. **146**: p. 359-362.

103. Viswanadham, G., R. Elghanian, C.A. Mirkin, and R.L. Letsinger, Abstracts of Papers of the American Chemical Society, 1999. **218**: p. U123-U123.

104. Mirkin, C.A., R.L. Letsinger, R. Elghanian, R.C. Mucic, J.J. Storhoff, Abstracts of Papers of the American Chemical Society, 1997. **214**: p. 17-MTLS.

105. Elghanian, R., J.J. Storhoff, R.C. Mucic, R.L. Letsinger, and C.A. Mirkin, Science, 1997. **277**(5329): p. 1078-1081.

106. Leong, W.L., P.S. Lee, S.G. Mhaisalkar, T.P. Chen, and A. Dodabalapur, Appl. Phys. Lett., 2007. **90**(4).

107. Pasquato, L., F. Rancan, P. Scrimin, F. Mancin, and F. Cesare, Chem. Commun., 2000(22): p. 2253.

108. Raible, I., M. Burghard, U. Schlecht, A. Yasuda, and T. Vossmeyer, Sens. Actuators B Chem., 2005. **106**(2): p. 730-735.

109. Lu, A.H., G.H. Lu, A.M. Kessinger, and C.A. Foss, J. Phys. Chem. B, 1997: p. 9139.

110. Lee, P.C. and D. Meisel, J. Phys. Chem., 1982. **86**(17): p. 3391-3395.

111. Link, S. and M.A. El-Sayed, J. Phys. Chem. B, 1999. **103**(21): p. 4212-4217.

112. von Soxhlet, F., Polytechnisches J. (Dingler's) 1879 **232**: p. 461.

113. Bloor, W.R., J. Biol. Chem., 1914. **17**: p. 377-384.

114. Fisher, J.A., M.J. Scarlett, and A.D. Stott, Environ. Sci. Technol., 1997. **31**(4): p. 1120-1127.

115. Frank, M.D., *Soxhlet Extraction and Analysis of a Soil or Sediment Sample Contaminated with <I>n</I>-Pentadecane*, in *Environmental Laboratory Exercises for Instrumental Analysis and Environmental Chemistry*. 2004. p. 178-189.

116. Li, W., C. Ye, J. Feng, and K. Xie, Chinese J. Anal. Chem., 2006. **34**(7): p. 905-910.

117. Shah, V.K.G., H. Dunstan, and W. Taylor, J. Chromatogr. A, 2006. **1108**(1): p. 111-115.

118. Murray, C.B., C.R. Kagan, and M.G. Bawendi, Ann. Rev. Mater. Sci., 2000. **30**: p. 545-610.

119. Pajkossy, T., T. Wandlowski, and D. Kolb, J. Electroanal. Chem., 1996(414): p. 209.

120. Badia, A., L. Cuccia, L. Demers, F. Morin, R.B. Lennox, J. Am. Chem. Soc., 1997(119): p. 2682-2692.

121. Pankau, W.M., K. Verbist, and G. von Kiedrowski, Chem. Commun., 2001(6) :p.519-520

122. Miles, D.T. and R.W. Murray, Anal. Chem., 2003. **75**(6): p. 1251-1257.

123. Yu-Ju Chen, S-H.Chen., Y-Y.Chien., Y-W. Chang, H-K. Liao, C-Y. Chang, M-D Jan, K-T Wang, C-C. Lin, ChemBioChem, 2005. **6**(7): p. 1169-1173.

124. Schaaff, T.G., et al., J. Phys. Chem. B, 2001. **105**(37): p. 8785-8796.

125. Whetten, R.L., M.N. Shafigullin, J.T. Khoury, I. Vezmar, R.L. Whetten, Adv. Mater., 1996. **8**(5): p. 428-&.

126. Abramoff, M.D., P.J. Magelhaes, and S.J. Ram, Biophot. Int., 2004. **11**(7): p. 36-42.

127. *Liverpool EM Unit*. 2004 cited; Available from: http://www.liv.ac.uk/emunit/tem.htm.

128. cited; Available from: http://astronomy.nmsu.edu/jlevans/seminarSpr07/transmission_electron_microscope.png.

129. Martin, J.E., J.P. Wilcoson, J. Odinek, and P. Provinencio, J. Phys. Chem. B, 2000(104): p. 9475.

130. Prasad, B.L.V., S.I. Stova, C.M. Sorensen, and K.J Klabunde, Langmuir, 2002(18): p. 7515.

131. Rasband, W.S., *ImageJ*. 1997-2005, U. S. National Institutes of Health, Bethesda, Maryland, USA. http://rsb.info.nih.gov/ij/.

132. Henglein, A. and M. Giersig, J. Phys. Chem. B, 1999, **103**(44): p. 9533-9539.

133. Cecere, D., A. Bruno, P. Minutolo, and A. D'Alessio, Synth. Metals, 2003. **139**(3): p. 653-656.

134. El-Sayed, M.A., Abstracts of Papers of the American Chemcal Society, 2002, (223), C49.

135. Shah, P.S., S. Husain, K.P. Johnston, and B.A. Korgel, 2001, **105**(39): p.9433-9440.

136. Shah, P.S., S. Husain, K.P. Johnston, and B.A. Korgel, 2002, **106**(47): p.12178-12185.

137. Alvarez, M.M., J.T. Khoury, T.G. Schaaf, M.N. Schafigullin, I. Vezmar, and R.L. Whetten, J. Phys. Chem. B, 1997, **101**(19): p.3706-3712

138. Link, S. and M.A. El-Sayed, J. Phys. Chem. B, 1999. **103**(40): p. 8410-8426.

139. Liu, X., M. Atwater, J. Wang, Q. Huo, Coll. Surf. B-Biointerf., 2007. **58**(1): p. 3-7.

140. Henglein, A. and D. Meisel, J. Phys. Chem. B, 1998, **102**(43): p.8364-8366.

141. Lin, S.Y., Y.T. Tsai, C.C. Chen, C.M. Lin, and C.H. Chen, J. Phys. Chem. B, 2004, **108**(7): P.2134-2139.

142. Hostetler, M.J., J.J. Stokes, and R.W. Murray, Langmuir, 1996, **12**(15): p.3604-3612.

143. Harvey, A.H., J. Phys. Chem., 1990. **94**(22): p. 8403-8406.

144. Ewald, A.H., W.B. Jepson, and J.S. Rowlinson, Discuss. Faraday Soc., 1953. **15**: p. 238 - 243.